NASA Contractor Report 4299

# Subsonic Sting Interference on the Aerodynamic Characteristics of a Family of Slanted-Base Ogive-Cylinders

Colin P. Britcher, Charles W. Alcorn,
and W. Allen Kilgore

GRANT NAG1-716
JUNE 1990

NASA

NASA Contractor Report 4299

# Subsonic Sting Interference on the Aerodynamic Characteristics of a Family of Slanted-Base Ogive-Cylinders

Colin P. Britcher, Charles W. Alcorn,
and W. Allen Kilgore
*Old Dominion University Research Foundation*
*Norfolk, Virginia*

Prepared for
Langley Research Center
under Grant NAG1-716

National Aeronautics and
Space Administration
Office of Management
Scientific and Technical
Information Division

**1990**

## ABSTRACT

Support interference free drag, lift and pitching moment measurements on a range of slanted-base ogive-cylinders have been made using the NASA Langley 13 inch Magnetic Suspension and Balance System. Typical test Mach numbers were in the range 0.04 to 0.2. Drag results are shown to be in broad agreement with previous tests with this configuration. Measurements were repeated with a dummy sting support installed in the wind tunnel. Significant support interferences were found at all test conditions and are quantified. Further comparison is made between interference free base pressures, obtained using remote telemetry, and sting cavity pressures.

## TABLE OF CONTENTS

## TABLE OF CONTENTS (Continued)

## LIST OF TABLES



## LIST OF FIGURES

## TABLE OF CONTENTS (Continued)

## LIST OF FIGURES (Continued)

## TABLE OF CONTENTS (Concluded)

## LIST OF FIGURES (Concluded)

## NOMENCLATURE

| Symbol | Meaning |
|---|---|
| A | Area, $m^2$ |
| $a_1$- $a_{10}$ | Calibration coefficients, $N/A^2$ or $Nm/A^2$ |
| $C_D$ | Drag coefficient, based on frontal area |
| $C_L$ | Lift coefficient, based on frontal area |
| $C_{LR}$ | Lift coefficient of rear portion of vehicle, based on frontal area |
| $C_{P_b}$ | Base pressure coefficient |
| D | Drag, N |
| $F_x$ | Force in x direction (-Drag), N |
| $F_z$ | Force in z direction (-Lift), N |
| $I_1$- $I_5$ | Current in electromagnets 1-5 |
| $I_D$ | "Drag" current, $= I_5$ |
| $I_L$ | "Lift" current, $= I_1 + I_2 + I_3 + I_4$ |
| $I_p$ | "Pitch" current, $= I_1 - I_2 + I_3 - I_4$ |
| M | Mach number, also pitching moment, Nm |
| p | Pressure, $N/m^2$ |
| $Re_L$ | Reynolds number, based on length of zero degree base model (11.193 inches) |
| $\beta$ | $\sqrt{(1-M^2)}$ |
| MSBS | Magnetic Suspension and Balance System |

# 1. INTRODUCTION

Support interference is a significant problem in wind tunnel testing. The majority of test results are influenced to some extent by the intrusion of mechanical supports into the flow. Numerous variations of support design are in use, encompassing many types of testing over a wide speed range. The principal type of support used in the transonic, supersonic and hypersonic speed regimes, and the primary focus of this report, is the rear mounted sting.

Some information concerning the magnitude of sting interference on drag and base pressures is available for axisymmetric (generally cylindrical or truncated boat-tail) bases. Data for non-axisymmetric bases is rather sparse. The slanted-base models chosen here provide an opportunity to assess sting interference effects over a family of geometries, ranging from axisymmetric to highly non-axisymmetric.

The original interest in slanted-base models was as an analogy to the flow over the sloping rear windows of hatchback and fastback automobiles (Figure 1). For the work reported here, the model is conceptually "inverted" and argued to be an analogy to the flow under the upswept rear fuselage of a transport aircraft. Design constraints are similar in both cases - namely minimum drag and maximum utilization of enclosed volume. The former tends to suggest slender, tapering base geometries while the latter suggest rather blunt geometries. Rather perversely, automobiles frequently show minimum drag with a blunt base. This is due to the formation of intense trailing vortices from the corners of the sloping rear window of fastback designs, leading to high induced drag.

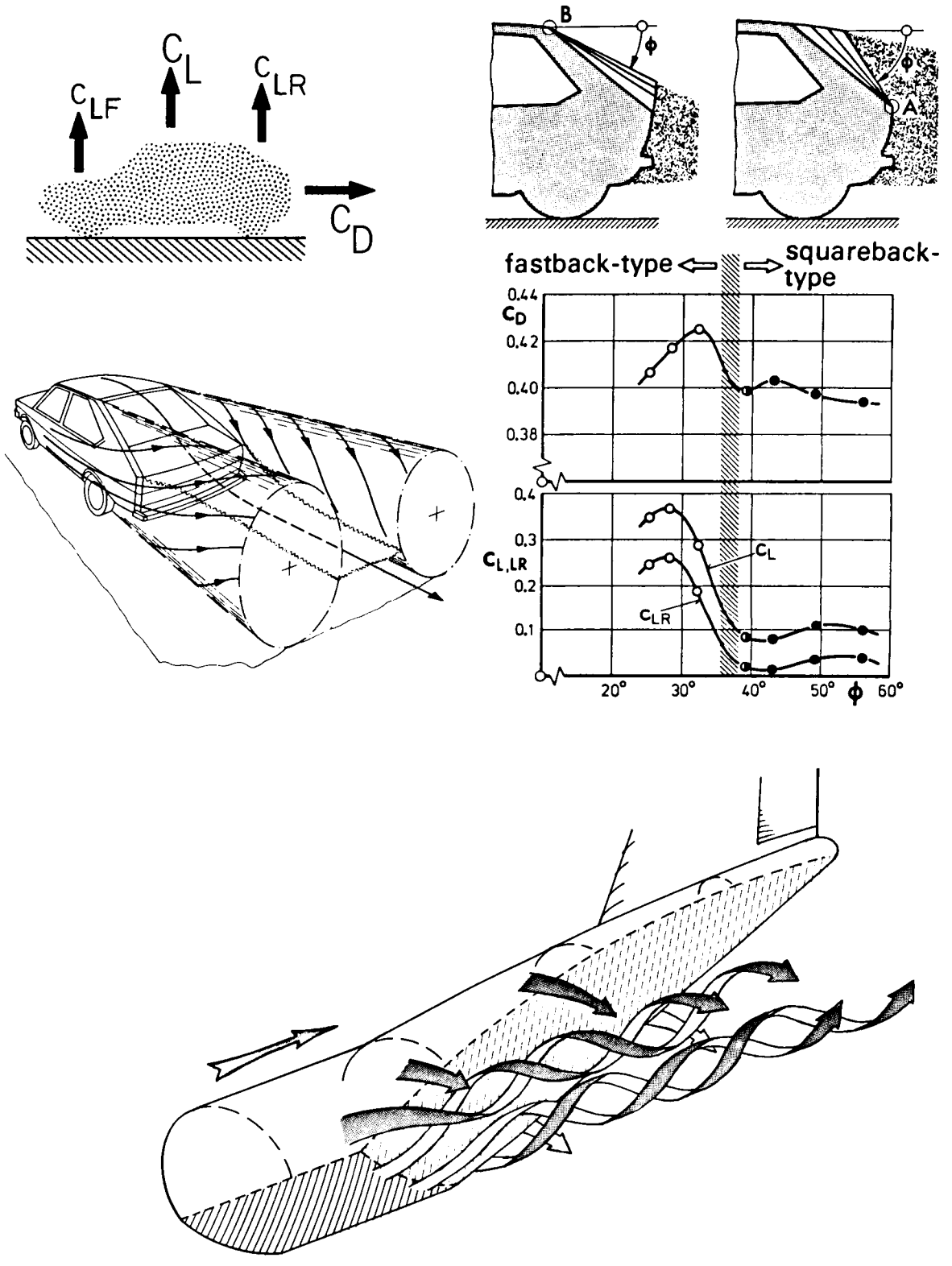


FIGURE 1 - Slanted-Base Aerodynamics. Automobile (upper) and aircraft (lower)

## 2. AERODYNAMIC STING INTERFERENCE

For the purposes of this report, the aerodynamic interference of the sting on the model is divided into three components (Figure 2):

(a) "Overall" flow disturbance. Physical blockage downstream of the model introduces a pressure gradient into the flow in the region of the model. If the sting is at angle-of-attack or if the model's wake flow involves strong crossflow velocities (relative to the sting) then flow inclinations will also be induced in the region of the model.

(b) "Local" flow disturbance. Boundary layer development, particularly on the aft regions of the model will be affected by the presence of the sting, partly due to (a) above. The wake geometry and structure are likely to be substantially affected, due to the physical presence of the sting within, or close to, the wake.

(c) Geometrical distortion of the model. In every case, the geometry of the aft region of the model is corrupted to accomodate the sting. This corruption includes, but is not limited to, truncation of the base and/or creation of a sting cavity.

### 2.1 STING INTERFERENCE CORRECTION TECHNIQUES

Aerodynamic data must be adjusted or corrected for sting interferences. Repeat testing, with alternative sting arrangements and metric divisions of the model, is a viable and apparently the most common method of extracting the interferences [1]. This approach can unfortunately lead to considerable complexity, with several test sequences required to extract the interference terms, due to the fact that no support system has zero overall interference [2,3]. It should be noted that some model geometries, particularly slender vehicles, may not lend themselves to alternative support arrangements. Further, if the alternative support is of the blade type, then testing is restricted to a small range of sideslip angles.

Analytic or empirical correction of test results is often attempted, though is fraught with its own difficulties. Overall flow disturbances ((a) above) can be corrected for, at least approximately, by estimating the far-field of the support system's flow using linearized methods, then correcting the model's angle of attack, drag due to longitudinal buoyancy and so on. Straightforward calculations may be possible where the support is slender and aligned with the flow [4]. There is increasing evidence of rather elaborate analysis being undertaken, involving panel methods and the like, particularly where the support is of a more complex geometry [5]. The reliability of all these corrections rests entirely on the model and sting flows being weakly interacting, that is to say, the support-induced flows must represent a small perturbation of the overall flowfield around the model.

When considering local flow disturbances, ((b) above), this assumption is invalid. If important details of the model's flow are strongly affected by the presence of the support, then simple "corrections" in the traditional sense are impossible. Rather, a "calculation" of at least part of the flowfield is necessary, sometimes carried out implicitly by subtracting out the experimental base drag, then adding a predicted base drag term [6]. Empirical data to assist in predicting or adjusting measured base pressures is rather scarce.

If aerodynamic results correspond to significantly incorrect model contours ((c) above), then traditional corrections may again be impossible. Some concern is evident on this point, particularly in high dynamic-pressure facilites [7].

Contemporary test data reduction therefore generally relies on geometrical distortions and/or local flow disturbances being small or of negligable influence. Overall flow disturbances are minimized with correct support design, permitting reliable correction for residual interferences in this category.

## 2.2 BASE PRESSURE CORRECTIONS

Corrections could be applied to sting cavity or model base pressures from conventional tests, if adequate reference data was available. However, a modest literature review indicates that, even for axisymmetric bases, substantial differences exist between experimental measurements from different sources. Similar comments apply to analytic or numerical predictions. A selection of results is assembled in the Table below. Whilst it is freely admitted that the model geometry and test Reynolds and Mach numbers cover a wide range, no coherent pattern can be recognized. Presuming that all experiments were conducted properly, the conclusion must be drawn that base pressure is at least somewhat sensitive to factors such as forebody geometry, test Reynolds and Mach numbers, boundary layer state, tunnel turbulence and so on. Thus, in order to reliably correct base pressures from conventional tests, specific base pressure evaluation tests might be required. Analytic or numerical methods do not yet seem to accurately reproduce existing reference data, therefore cannot be generally applied.

Little literature has been found dealing with non-axisymmetric geometries, by any means, apart from those tests specific to the slanted base problem.

TABLE A - Ogive-cylinder base pressure coefficients (zero base slant)

| $-C_{p_b}$ | Ref. | $Re_L$ | M | Comments |
|---|---|---|---|---|
| 0.15 | 8 | $\simeq$900k | Low | Wire supports, centerline |
| 0.13 | 8 | " | | 91.5% radial station |
| 0.21 | 9 | $\simeq$200k | Low | Strut supports, centerline |
| 0.23 | 9 | " | | 45% radial station |
| 0.12 | 10 | Range | Low | Empirical, various data |
| 0.12 | 11 | 800k | 0.6 | Blade support |
| 0.13 | 12 | Range | Low | Empirical, various data |
| 0.33 | 13 | Range | Low | True predictive method, depends on boundary layer $\theta$ |

## 2.3 STING INTERFERENCE WITH SLANTED-BASE MODELS

For the tests reported herein, the geometrical distortion of the base is limited to the creation of a simple sting cavity. The sting is aligned with the tunnel axis and the models are non- or weakly lifting, so the overall flow disturbance caused by the sting is principally a weak longitudinal pressure gradient. The effects of the local flow disturbances, particularly disturbance of the model's wake, are thus highlighted.

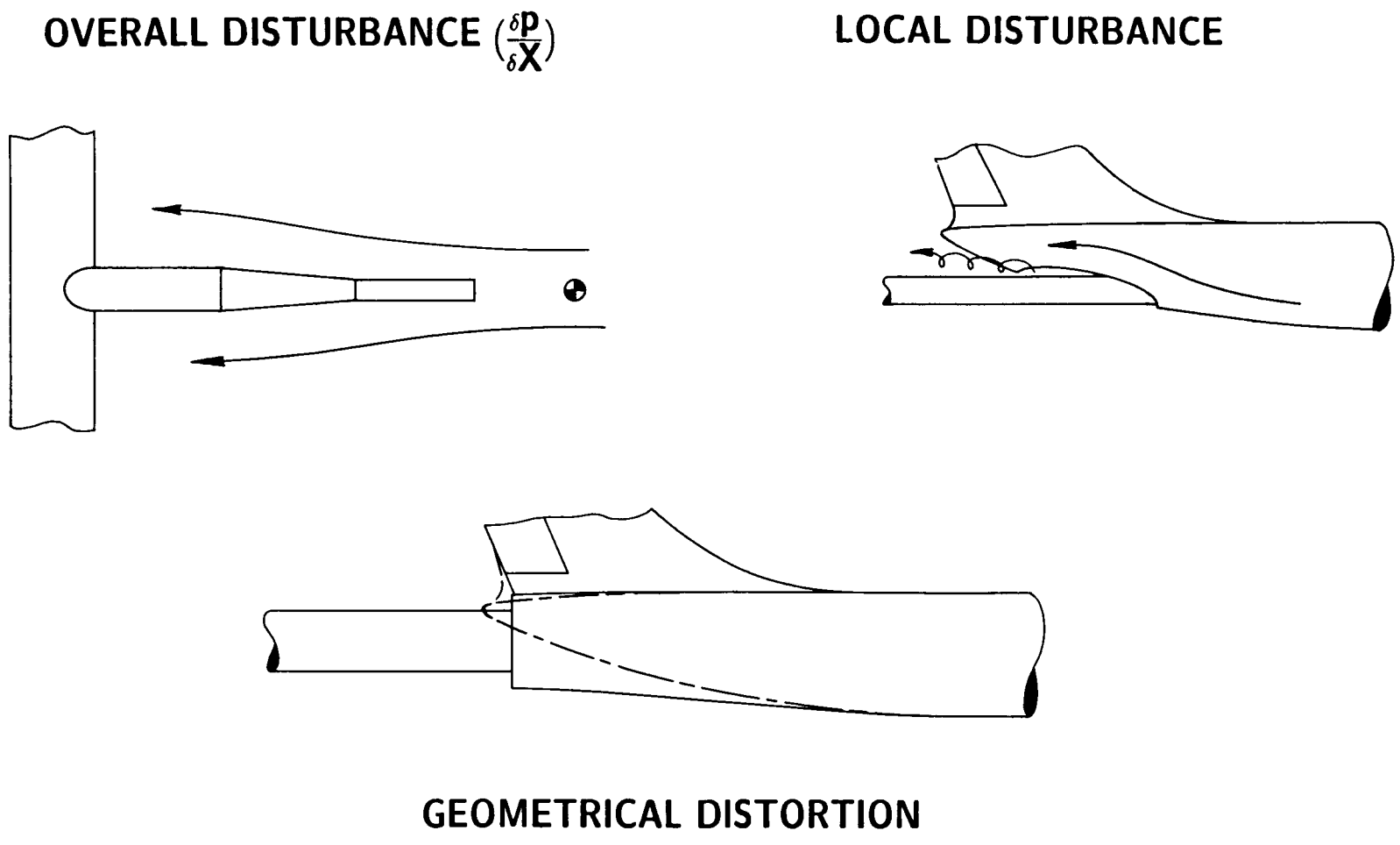


FIGURE 2 - Classification of Aerodynamic Sting Interference

# 3. EXPERIMENTAL DETAILS

## 3.1 MODELS

Slanted-base ogive-cylinder models have been extensively tested by Morel [8] and others [9,14]. The principal interest in this geometry is the sudden change of wake structure, with corresponding large change in drag coefficient, occurring for small changes of base slant angle, around 45 degrees slant. A summary of important previous results is shown in Figure 3. The models used for this research correspond to Morel's geometry and are illustrated in Figure 4. Additional details can be found in Appendix A. The models are manufactured from aluminum alloy, with enclosed low-carbon iron cores. Considerable care was taken to ensure geometric fidelity and high quality of surface finish. Interchangeable bases permit a range of base slant angles to be tested. One model is used exclusively for force and moment tests, while an alternate, of nominally identical aerodynamic lines, is equipped for direct measurement of base pressures. For all tests, the models are suspended magnetically with no mechanical support of any kind. Previous experiments with these models (magnetically suspended) have established their basic aerodynamic characteristics and are fully reported elsewhere [15,16].

## 3.2 NASA LANGLEY 13 INCH MSBS

The NASA Langley Research Center (LaRC) 13 inch Magnetic Suspension and Balance System (MSBS) has been developed from a system constructed at the Arnold Engineering Development Center in the 1960's [17], though little of the original hardware remains in use. The position and attitude of the model is detected optically [18], position signals are fed to a digital control system [19] with the electromagnet currents supplied by SCR power amplifiers. The wind tunnel is a low speed, open circuit design [20], illustrated in Figure 5, with a maximum Mach number of 0.5. An aluminum alloy dummy sting and support strut, shown in Figure 6, can be installed downstream.

## 3.3 PRESSURE TELEMETRY

A single channel onboard pressure telemetry system had been developed previously [16,21] to permit measurement of interference-free base pressures. Due to the low dynamic pressures encountered in these tests, this proved to be a quite challenging measurement. That is to say, freestream static pressure and model base pressure are both roughly atmospheric and the difference between them is small. With no direct connection between the model and the outside world, great care must be taken to

overcome the "subtraction of elephants" problem. In the original configuration, a sensitive differential pressure transducer was installed in the model with the backside vent tube filled with inert gas and sealed. The gas reservoir served as the pressure reference. Unfortunately, the temperature of the gas chamber could not be adequately stabilized in normal testing, leading to acute temperature sensitivity.

For the slanted-base tests, a similar differential transducer was installed with the backside vented to a total pressure tap in the extreme nose of the model. This tap is just visible in Figure 4. Temperature sensitivity was much improved, although the electronics package is still noticeably deficient in this regard. Base pressures are now derived by subtraction of two smaller elephants, namely the difference between base static and tunnel total pressure compared to the difference between local static and tunnel total.

Details of the design and installation of the telemetry system are given in Figure 7. It has been found that a fresh battery pack (5 E41 cells) will give well over 2 hours of valid data. As the batteries near the end of their discharge, the rapid drop in terminal voltage causes a relatively rapid drift of the wind-off (zero differential pressure) frequency. Wind-off zeros are therefore taken before and after each "run" as a precautionary measure.

### 3.4 TEST SEQUENCES

Three separate test sequences, illustrated in Figure 8, permit complete identification of interference effects:

(a) Magnetically suspended. With no mechanical intrusion into the flow, true support interference free data is obtained. These measurements are taken to be the "reference" data in this case, since all further tests involve the same model and test section set-up. The results shown in this paper are all-new tests, though essentially repeats of previous MSBS data [16]. It should be noted that some discrepancies between MSBS results and previous mechanically-supported data have been identified and examined [16].

(b) Magnetically suspended with dummy sting. The rear portion of the model is modified to provide a representative sting cavity. The model is then magnetically suspended with a dummy sting protruding into the cavity, but not in contact with any portion of the model. Sting cavity pressure is measured via a tapping through the dummy sting.

(c) Magnetically suspended with base pressure telemetry. A model equipped with onboard telemetry, with no dummy support, establishes interference free base pressures.

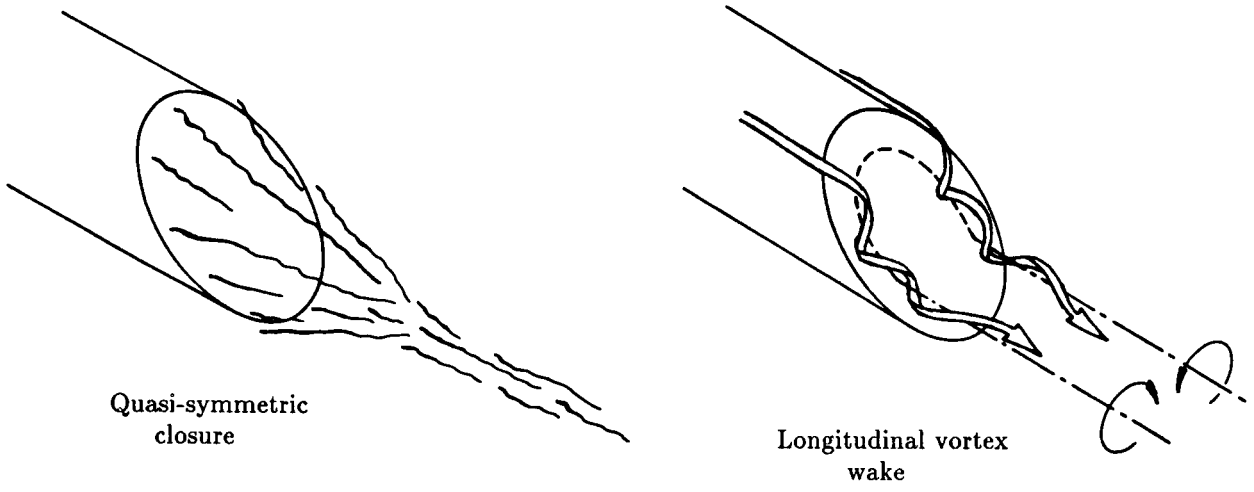


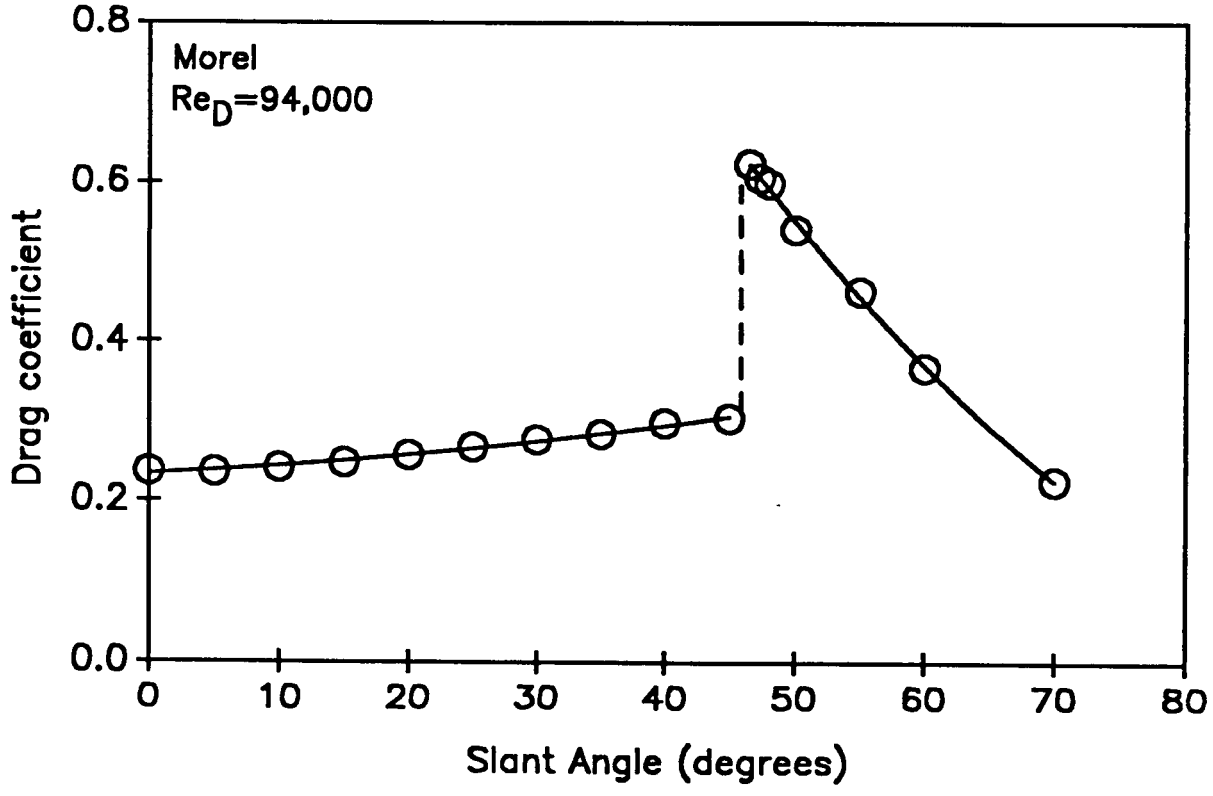


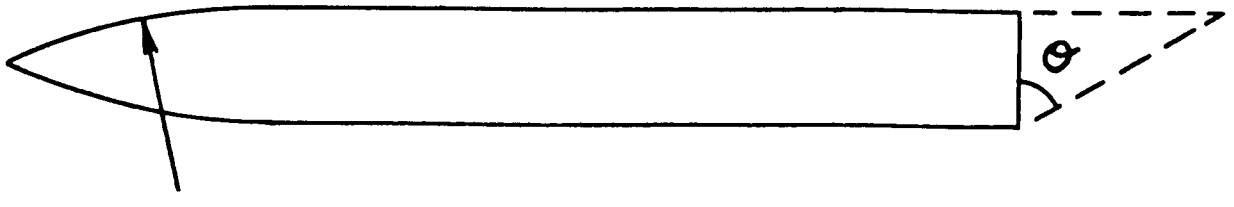

FIGURE 3 - Slanted-Base Ogive-Cylinder Aerodynamics

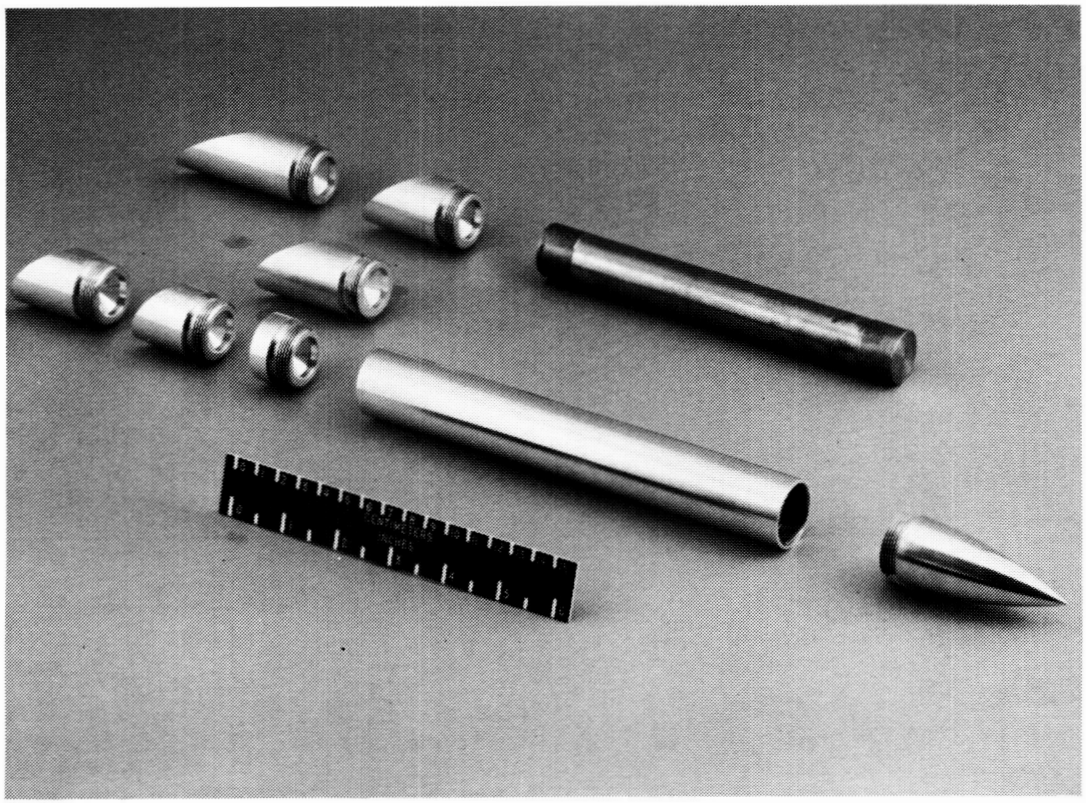

Force Model

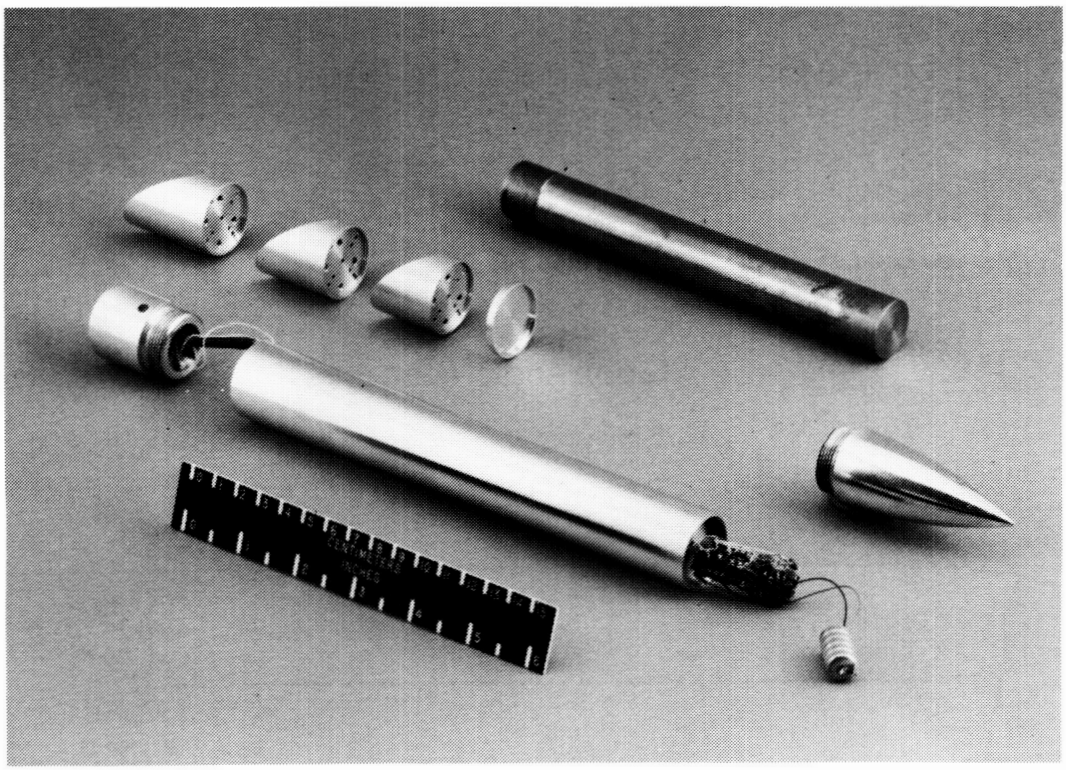

Pressure Model

FIGURE 4 - Slanted-Base Ogive-Cylinder MSBS Models

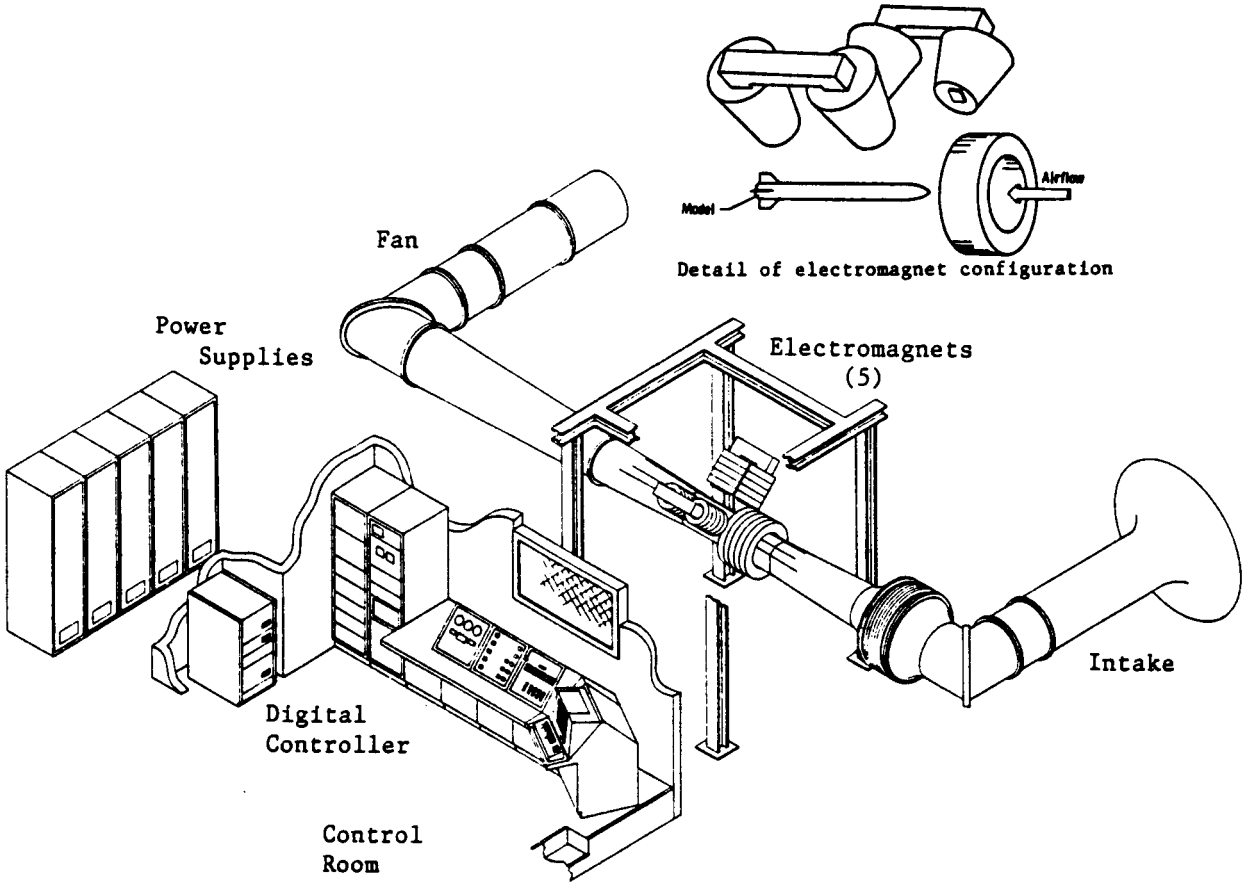


FIGURE 5 - NASA Langley 13 inch Magnetic Suspension and Balance System Laboratory

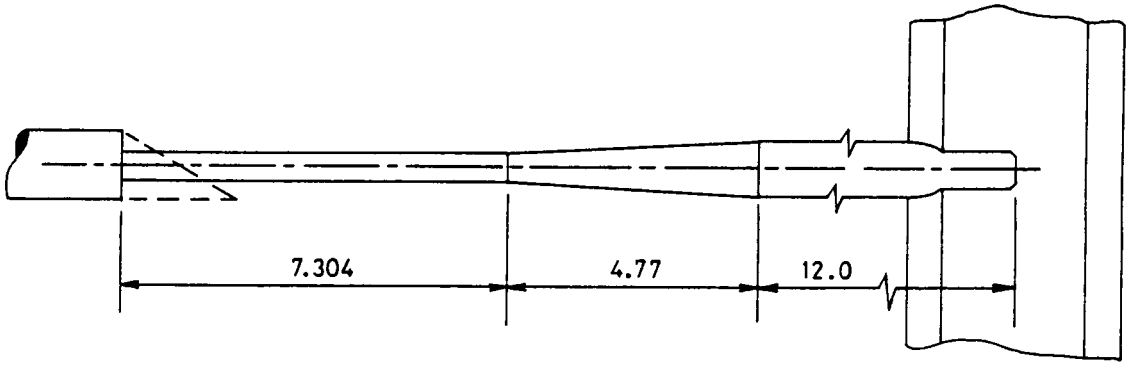


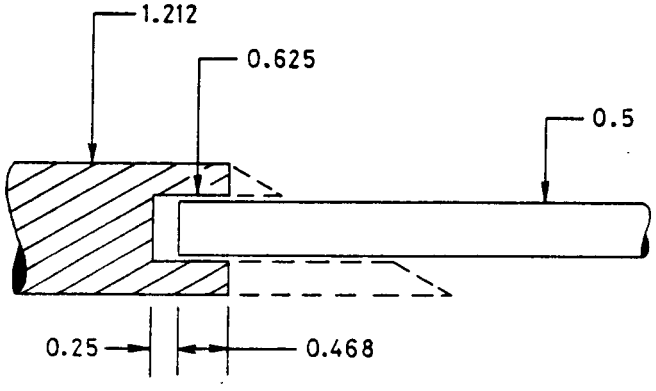


FIGURE 6 - Dummy Sting and Strut Geometry

Dimensions
in inches

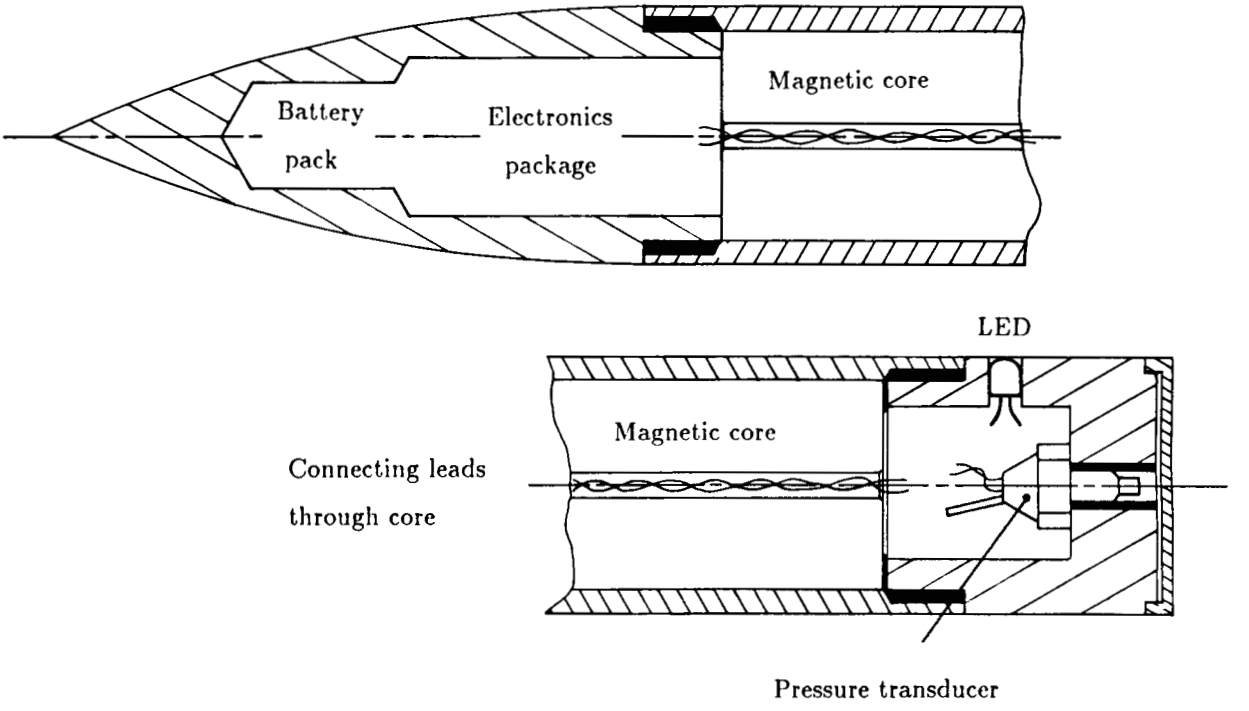


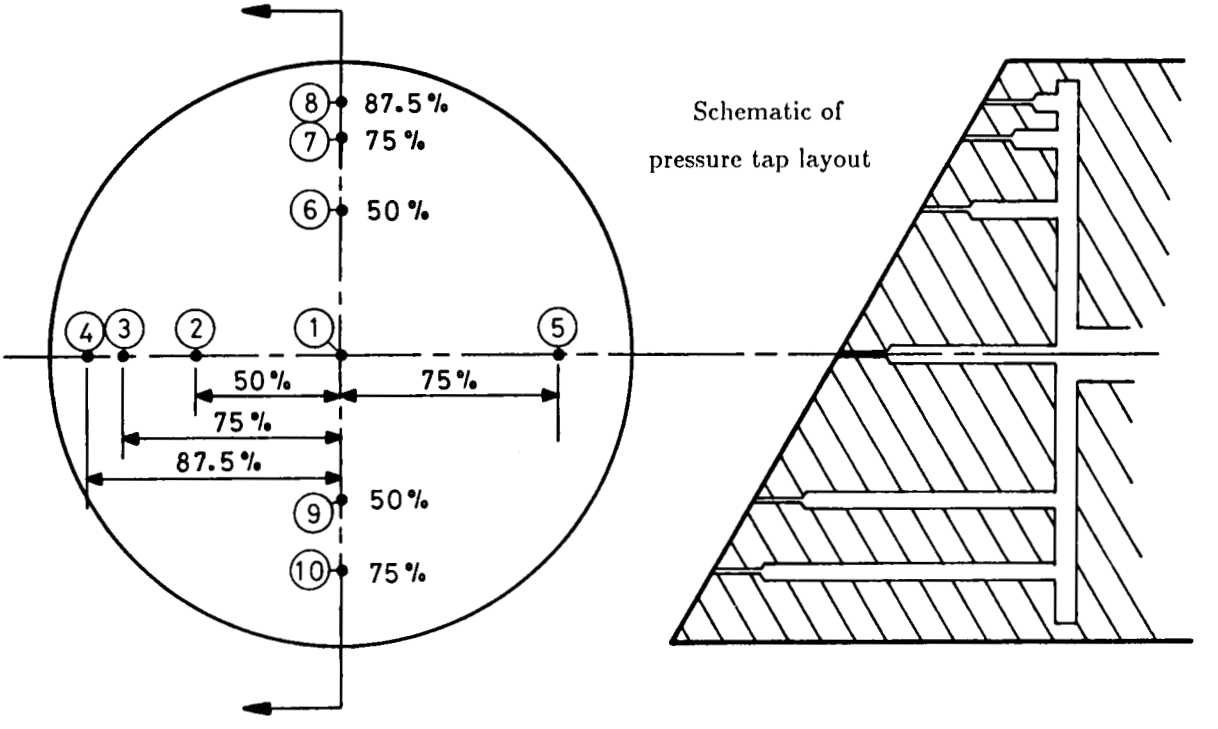


FIGURE 7 - Onboard Pressure Telemetry System

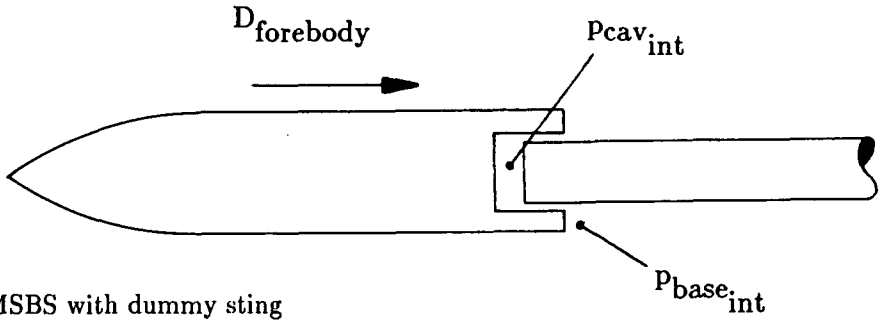


MSBS with dummy sting

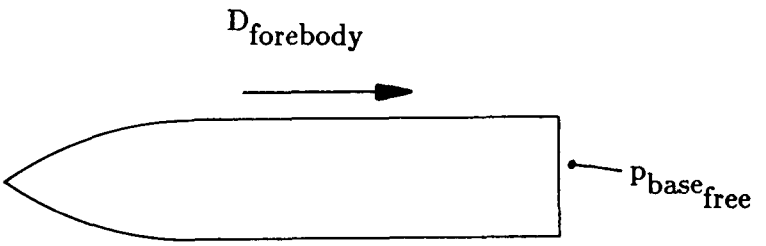


MSBS interference free

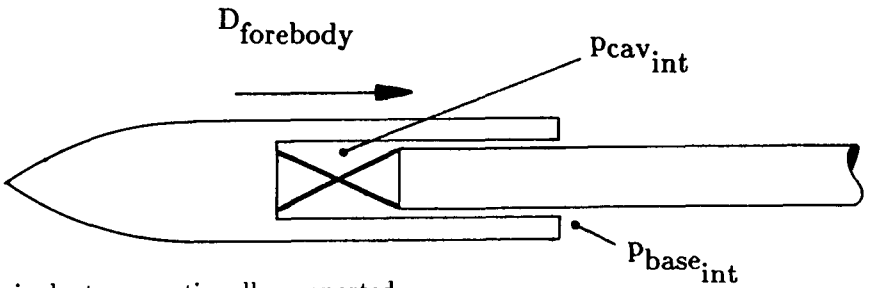


Equivalent conventionally supported

FIGURE 8 - Test Sequences used for Support Interference Evaluation

# 4. DATA REDUCTION

## 4.1 FORCE AND MOMENT CALIBRATION OF MSBS

Previous analysis [16] has indicated that the drag and lift forces and pitching moment for a model at zero angles of attack and sideslip in the 13 inch MSBS can be expressed as follows:

$$F_x = a_1 I_L^2 + a_2 I_L I_D + a_3 I_D^2 + a_4 I_P I_L$$

$$F_z = a_5 I_L^2 + a_6 I_L I_D + a_7 I_P^2 + a_8 I_P I_D$$

$$M = a_9 I_P I_L + a_{10} I_P I_D \qquad (1)$$

where $I_L = I_1 + I_2 + I_3 + I_4$ ; $I_P = I_1 - I_2 + I_3 - I_4$ (2)

The numbering sequence for the electromagnet currents is shown in Figure 9. Coefficients $a_1$ through $a_{10}$ are constants found by multiple regression fitting of calibration data. A linear method is used, in the dummy variables $\{I_L^2\}$, $\{I_L I_D\}$ etc. (Supercalc 5© routine). This may not be the best approach since the equations are fundamentally non-linear in nature, but appears to function satisfactorily for the ranges of variables so far encountered.

In practice the electromagnet current "zeros" do not repeat exactly from run to run, for a variety of reasons, including slight position and attitude shifts. All current measurements are therefore corrected as follows:

$$I_{D_{corrected}} = I_{D_{measured}} + (I_{D_{calibration\ zero}} - I_{D_{wind\text{-}off}})$$

$$I_{L_{corrected}} = I_{L_{measured}} + (I_{L_{calibration\ zero}} - I_{L_{wind\text{-}off}})$$

$$I_{P_{corrected}} = I_{P_{measured}} + (I_{P_{calibration\ zero}} - I_{P_{wind\text{-}off}}) \qquad (3)$$

Again, this may not be the best procedure but appears to function quite satisfactorily at the present time.

A representative model (zero degree base) was suspended and loaded at three stations, as shown in Figure 10. Forces and moments encompassed the range of magnitudes encountered in aerodynamic testing. However, pitching moments of both signs were applied during calibration (only nose-down in aerodynamic testing) and only downforces were applied (upforces in aerodynamic testing). Nevertheless,

the resulting calibration is thought to be reasonable, especially since drag is the most important degree of freedom in this case.

TABLE B - Calibration ranges

| Force/moment component | Approximate range | Comments |
|---|---|---|
| Drag | 0-0.75N | Positive downstream |
| Lift | 0-1.25N | Applied downwards |
| Pitching moment | ±0.06Nm | Nose up and nose down |

Results of the calibration are as follows:

$$F_X = 0.0879 + 19.405*10^{-6}I_L{}^2 + 841.578*10^{-6}I_L I_D + 331.855*10^{-6}I_D{}^2 + 103.266*10^{-6}I_L I_P \qquad (4)$$

- where currents are in Amps and force in Newtons. The principal term during normal testing is $I_L I_D$. Typical values of current during aerodynamic testing were:

$$I_L \simeq 80 \text{ (weak variable)}$$
$$-3 \text{ (wind off)} < I_D < 10 \text{ (high q cases)}$$
$$-10 \text{ (wind off)} < I_P < -15 \text{ (high slant angles, high q)}$$

The leading constant in Equation 4 represents an accumulation of zeroing errors during calibration, imperfect modelling of MSBS behaviour by Equation 1 and so on. The wind off drag forces predicted by direct application of Equation 4 tend to be non-zero but small. Other drag forces are corrected by the wind off measurement :

$$D_{corrected} = D_{predicted} - D_{predicted_{wind\text{-}off}}$$

Calibration equations for lift force and pitching moment are deduced and handled similarly :

$$F_Z = -7.062 + 1135.7*10^{-6}I_L{}^2 + 561.887*10^{-6}I_L I_D - 185.100*10^{-6}I_P{}^2 - 7.062*10^{-6}I_P I_D$$

The $I_L{}^2$ term is dominant. The leading constant is primarily due to the deadweight of the model; also residual errors as discussed above.

$$M = 1.227*10^{-3} + 128.908*10^{-6}I_P I_L + 17.578*10^{-6}I_P I_D$$

The $I_P I_L$ term is dominant. Again, the leading constant is related to the mass distribution of the model, its fore-and-aft location in the wind tunnel and other effects. Moment is expressed in Newton-meters.

## 4.2 CORRECTIONS TO AERODYNAMIC DATA

Again following [16], various corrections are applied to the tunnel conditions and drag forces. No corrections are made to lift forces or pitching moments.

Buoyancy

$$\Delta D_{\text{buoyancy}} = V' \frac{dp_s}{dx}$$

where $V'$ is an effective model volume, found to be 1.3% greater than the actual volume, using the integral expressions in [22]. The static pressure gradient in the wind tunnel has been carefully measured with the test section empty and is expressed as follows:

$$\frac{dp_s}{dx} \simeq (2379.0\ M^3 + 2477.81\ M^2 + 110.954\ M)\ \text{Pa/m}$$

Blockage

A solid body blockage factor is calculated using formulae in [23], as detailed in [16]:

$$\epsilon_s = 7.576 \times 10^{-3}\ \beta^{-3}$$

A wake blockage factor is similarly found from [24]:

$$\epsilon_w = 0.25 \times \frac{A_{\text{model}}}{A_{\text{test section}}} \left(\frac{1+0.4M^2}{\beta^2}\right) C_D$$

A corrected Mach number is derived as follows:

$$M_{\text{corrected}} = M_{\text{uncorrected}} \left(1+(1+\frac{\gamma-1}{2}M^2)(\epsilon_s+\epsilon_w)\right)$$

An appreciation of the magnitudes of the corrections is given in the following Table:

TABLE C - Approximate magnitude of drag coefficient corrections

| Base | Nominal $C_D$ | Nominal Mach | $\%C_{D_{buoy}}$ | $\%C_{D_{block}}$ |
|---|---|---|---|---|
| $0^o$ | 0.2 | 0.04 | 8% | 2% |
| | 0.2 | 0.2 | 6% | 2% |
| $45^o$ | 0.3 | 0.04 | 5% | 2% |
| | 0.6 | 0.18 | 2% | 2% |
| | 0.6 | 0.04 | 3% | 2% |

All corrections relative to uncorrected measurement, all subtractive

## 4.3 BASE PRESSURES

A static calibration of the transducer/telemetry package is performed prior to magnetically suspending the model. No shift of calibration due to magnetic fields has been detected. Typical results are:

$$\text{Frequency} = 10{,}849 - 1.123\Delta p \text{ Hz} \qquad (\Delta p \text{ in Pa})$$

The model must be removed from the tunnel to change active pressure taps. Unused taps are taped over in the conventional manner. The problem of transducer zero shifts with temperature is minimized by operating only when the (outside) ambient air temperature is in the range $70^o$-$80^o$F. This results in minimal model temperature change during removal from the tunnel for change of pressure taps.

The on-board transducer is referenced to $p_{total}$, which is assumed constant through the test section. Thus:

$$p_{base} = p_{total} - \Delta p_{transducer}$$

The static pressure in the test section is derived from the tunnel total and a static pressure ring just upstream of the test section. A correction is made to the latter reading based on previous empty tunnel calibrations.

$$p_{test\ section} = p_{static\ ring} - 0.1269024*(p_{total}-p_{st.\ ring})-0.0272046*(p_{total}-p_{st.\ ring})^2$$

A further correction is made to account for the longitudinal pressure gradient in the test section, detailed earlier. Thus the numerator of the base pressure coefficient is calculated as the difference between actual base pressure and tunnel empty local freestream static. The denominator carries a

blockage correction via the corrected Mach number. Further refinement of this pressure correction technique is possible.

Sting cavity pressure is measured via the central tap and a Datametrics 572 Barocell. This measurement is reduced to a pressure coefficient in the same manner as discussed above.

## 4.4 DATA ACCURACY

All electromagnet currents can be measured to an accuracy of around ±10mA (1mA instrument resolution). Measurements are an average of one hundred samples, taken under quasi steady-state conditions. This results in a typical uncertainty in drag force of less than 0.002N (using Equation 4). Resulting uncertainties in representative drag measurements are shown in the Table below :

TABLE D - Drag uncertainties

| Base | Nominal Mach | Drag (N) | ΔD | %uncertainty |
|---|---|---|---|---|
| $30^o$ | 0.1 | 0.138 | 0.002 | 1.4% |
| $30^o$ | 0.2 | 0.525 | 0.002 | 0.4% |
| $50^o$ | 0.1 | 0.326 | 0.002 | 0.6% |
| $50^o$ | 0.16 | 0.721 | 0.002 | 0.3% |

The principal items of wind tunnel data are the total and dynamic pressures, measured with Datametrics 572D Barocells. Typical quoted accuracy is of the order of 0.2%, all sources. This will result in a Mach number uncertainty of the order of 0.1%. Additional errors accumulate due to innacuracies in measurement of stagnation temperature, imperfect calibrations and so forth, but are generally rather small.

Analysis of the effects of inaccurate estimates of $a_1$-$a_{10}$ is very complex and is demanding of much further study. The correction of measured currents and predicted forces and moments by the wind-off zeros has the effect of cancelling some apparent error. Standard errors of the terms derived from the regression analysis are known and are recorded overleaf for reference :

| Parameter | $a_1$ | $a_2$ | $a_3$ | $a_4$ | $a_5$ |
|---|---|---|---|---|---|
| Value$*10^6$ | 19.405 | 841.578 | 331.855 | 103.266 | 1135.723 |
| Std. error$*10^6$ | 5.689 | 12.464 | 138.118 | 7.684 | 12.999 |

| Parameter | $a_6$ | $a_7$ | $a_8$ | $a_9$ | $a_{10}$ |
|---|---|---|---|---|---|
| Value$*10^6$ | 561.887 | -185.100 | -7.062 | 128.908 | 17.578 |
| Std. error$*10^6$ | 53.375 | -83.013 | -364.239 | 2.502 | 11.523 |

It is seen that the primary terms in each calibration equation ($a_2$, $a_5$, $a_9$) are relatively accurately known. The determination of some of the other terms is poor.

Error bars are <u>not</u> plotted on any of the accompanying graphs. This is due partly to the somewhat experimental nature of the MSBS calibration procedures employed. Further, examination of the figures in the context of the above analysis will indicate that the magnitudes of the aerodynamic effects being examined are so large that there can be no real doubt that the general trends are properly represented.

Considerable attention is also paid to the accuracy of drag measurements in the 13 inch MSBS in reference 24.

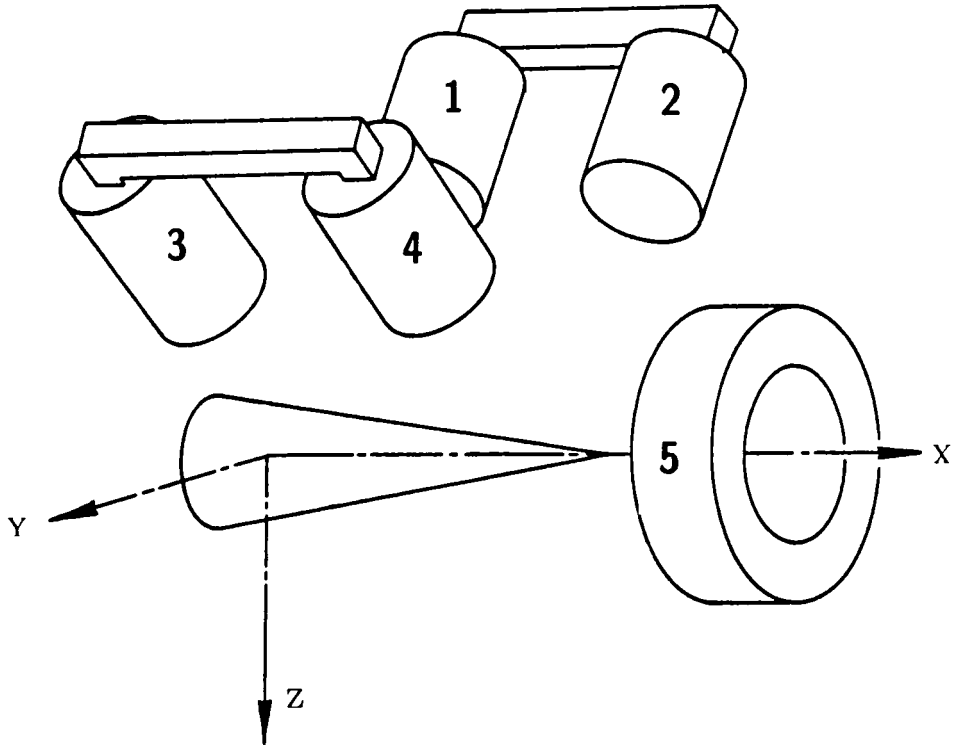


FIGURE 9 - 13 inch MSBS Electromagnet Numbering Sequence

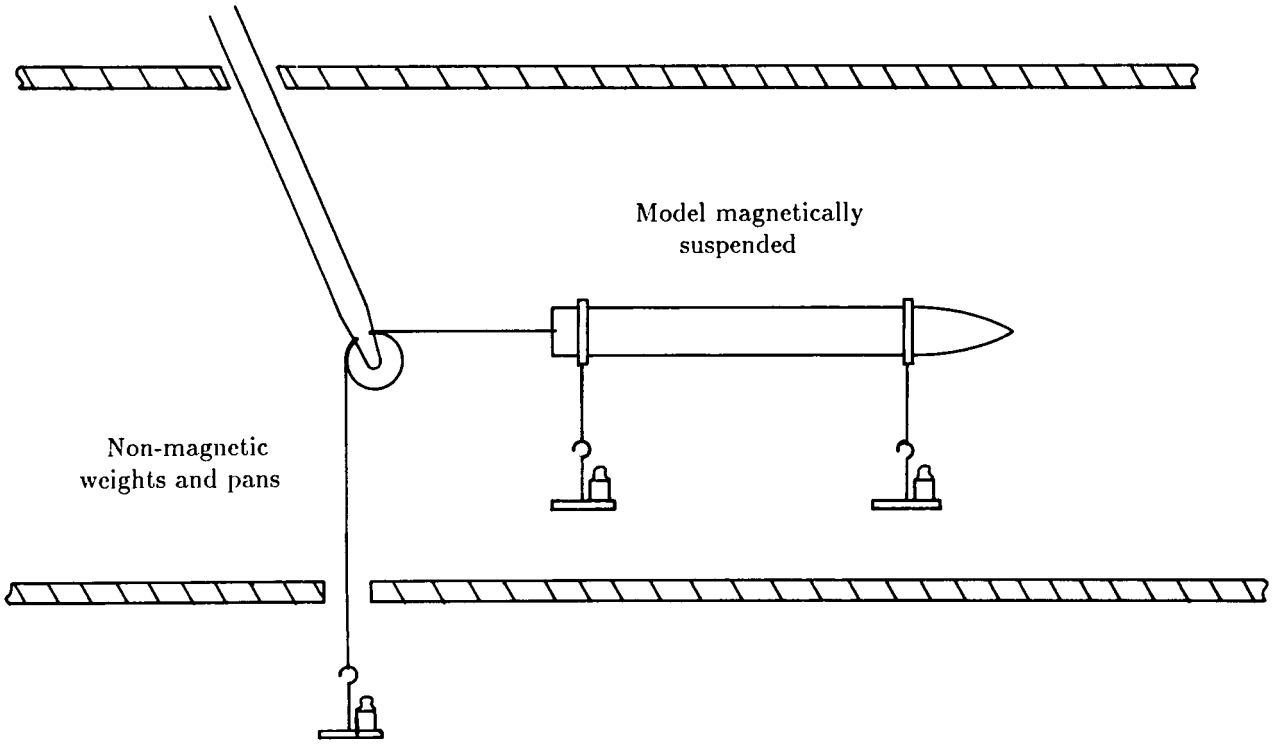


FIGURE 10 - Force and Moment Calibration

# 5. EXPERIMENTAL RESULTS

## 5.1 GENERAL REMARKS

Models were suspended close to the centerline of the wind tunnel, at nominally zero angles of attack and sideslip. The "clean" model is thought to exhibit principally laminar boundary layers, with transition just beginning to move forward from the base at the higher Reynolds numbers tested. The maximum Mach numbers (typically 0.2) were well below the tunnel limit (0.5), principally due to problems with the electromagnet power supplies. Most tests were repeated with transition fixed roughly 2cm downstream of the ogive-cylinder junction by a ring of No.60 grit. Some check runs were made with coarser grit to ensure tripping at lower Reynolds numbers. Corrections have been applied to account for model and wake blockage and longitudinal buoyancy, following the methods outlined in Section 4. Corrections for sting-induced buoyancy or blockage have not been applied, but would be extremely small. Base and sting cavity pressures have been corrected for model blockage and longitudinal pressure gradient effects.

## 5.2 DRAG RESULTS

Low base slant angles

Slight reductions in drag coefficients with increasing Reynold's number is noticeable, particularly for the fixed transition cases, consistent with usual boundary layer behaviour. Drag coefficients for the zero degree base, with and without the dummy sting present, are shown in Figure 11. The magnitudes of the discrepancies, presented in terms of required corrections to sting-supported results, are clarified in Figure 12. Similar data for the 30 and 40 degree bases are shown in Figures 13 through 16. It is clear that significant discrepancies exist between sting supported and interference free data. The signs and magnitudes are, however, broadly consistent with previous measurements for ogive-cylinders, that is, somewhat lower drag with sting on (for instance see [11]).

The mechanism for the drag reduction is thought to be the reduction in the required expansion of the flow surrounding the wake downstream of the base, since part of the flow area is occupied by the sting. This would result in slightly higher (less negative) base pressures in the sting-on case.

45 degree base

Previous MSBS tests [15,16] had revealed an unusual hysteretic behaviour of the wake for this base slant. As $Re_D$ for the "clean" model increased past 60,000 or so, the wake structure suddenly changed from a quasi-symmetric pattern, characteristic of low slant angles, to a longitudinal vortex

flow, characteristic of higher slant angles. The change in drag is dramatic, more than a doubling in value. Also, once the vortex flow is established, it persists even as $Re_D$ is reduced below the "critical" value. It is believed, though not yet experimentally confirmed, that this change in wake structure is linked with the onset of natural transition at the model's base or in the free shear layers developing just downstream. Further, the fact that the effect had not previously been detected is thought to be due to boundary layer tripping by upstream wire or strut attachments [16].

It had been found that tripping the boundary layer prevented this change in structure from occurring. Further testing has now revealed that the phenomena is sensitive to the grit size employed. It is known (see Section 6.1) that the No.60 grit normally used is too fine to ensure complete transition at the lowest Reynold's numbers. Repeat sweeps up and down through the "critical" Reynold's number with this size grit sometimes exhibited the wake flow change, sometimes not. A coarser grit size proved more consistently effective in inhibiting the formation of the vortical wake. Note that no change from one wake structure to another was ever observed above the critical Reynold's number, whereas spontaneous and random reorganization of the wake has been observed below the critical Reynold's number (Figures 17-19).

Not surprisingly, the introduction of a sting into the wake completely disrupts the changes in structure. With the sting present, the wake is always a quasi-symmetric closure, with no tendency to form a vortical wake under any condition tested. The discrepancies between sting supported and interference free data thus become strong variables with large peak magnitudes, illustrated in Figures 17-20. Drag is always lower with the sting present, due to the incorrect wake flow.

High slant angles

The interference free wake for these slant angles is a quasi-steady longitudinal vortex flow. This flow pattern produces low base pressures (see Section 5.3), high drag and significant lift forces and pitching moments (see Section 5.4). It is known that the behaviour of wake vortices can be strongly influenced by the presence of downstream obstructions [25]. This is reflected in the results for the 50 and 60 degree bases, shown in Figures 21-24. At low Reynolds numbers with the sting present, the drag coefficient of the "clean" 50 degree base model remains fairly low, indicating a quasi-symmetric wake closure. At some critical Reynolds number, the wake changes spontaneously to a longitudinal vortex flow, with corresponding increase in drag. No hysteresis has been detected. However, the drag increment in vastly less than that observed with the corresponding phenomena for the 45 degree base, interference free. Due to the rapid fall in drag coefficients for the interference free model beyond the critical angle, drag coefficients of the 60 degree base model are similar for all four cases tested.

It should be noted that the increment in drag between fixed and free transition, consistently observed for the lower slant angles, is not seen with the higher slant angles, particularly interference free. Since there must logically be an increment in forebody skin friction, suspicions are aroused as to

whether the base drag changes by a similar increment, but in the opposite sense. This point is resolved in Section 5.3.

A 70 degree base was fabricated late in the test program. Plexiglas was used instead of aluminum to reduce weight and consequent undesirable nose-up pitching moments. Limited results are shown in Figure 25.

## 5.3 BASE AND STING CAVITY PRESSURES

Base pressure data has only been taken for slant angles of $0^o$, $40^o$, $45^o$and $50^o$, due to the laborious testing procedure required with the single channel telemetry system. Sting cavity pressures were recorded for all base slants.

Zero degree base

Base pressures as a function of Reynold's number for the zero degree base are shown in Figure 26. No distinct trend is apparent. Examining the variation with radius, there is slight evidence of lowest base pressures (most negative $C_p$'s) in the center of the base, shown in Figure 27. No significant dependance on boundary layer state has been detected (Figure 28). Sting cavity pressures are noticeably higher than base pressures, corresponding to the observed drag differences between the two cases (Figure 29). The reader is cautioned against comparing the magnitudes of the pressure differences against the differences in drag, since the pressures on the annular region surrounding the sting cavity are not likely to be exactly equal to the cavity pressure.

40 degree base

Base pressures for the 40 degree base are substantially non-uniform, shown in Figures 30 and 31. There is some evidence that significant differences may exist with transition fixed, shown in Figures 31 and 32. Comparison between base and sting cavity pressures is shown in Figure 33, again corresponding to the observed drag differences.

45 degree base

The transition free base pressures for the 45 degree base, shown in Figure 34, dramatically illustrate the wake hysteresis observed in Section 5.2. The apparently steep variations of pressure coefficients with Reynold's number above the critical value are thought to be genuine, but may be due to slight shifts in the vortex locations, rather than actual changes in vortex strength or structure. Data below the critical Reynold's number should be considered unreliable, due to the very small pressure differences encountered. Figure 35 illustrates the distinctive pressure "footprint" of the vortices, with

very high suctions in the region of the vortex cores. Tripping of the boundary layers inhibits formation of the vortical wake, confimed by pressure measurements shown in Figure 36. Figure 37 nevertheless again shows a substantially non-uniform pressure distribution. Comparison to sting cavity pressures becomes meaningless, with no sensible similarity. Sting cavity pressures are thus shown separately in Figure 38, where differences between fixed and free transition cases are noticeable.

50 degree base

Base pressures for the 50 degree base are shown in Figures 39 and 40. A reduction in the strength of the trailing vortices (corresponding to a reduction in base drag) with transition fixed was suspected in Section 5.2 and is dramatically confirmed in Figure 41. Sting cavity pressures again bear no relation to base pressures, although Figure 42 again shows substantial differences between fixed and free transition runs. Spontaneous formation of some form of vortical wake for the free transition case is also noted. No hysteresis has been detected in this instance.

## 5.4 LIFT FORCES AND PITCHING MOMENTS

Lift forces are non-dimensionalized by the model cross-sectional area. Pitching moments are non-dimensionalized using the same reference area, also the half-length of the zero degree base model ($\frac{1}{2}$*11.193inches). For the purposes of presentation of results, upforce is considered positive lift, nose down moment is considered positive pitching moment, clarified in Figure 43.

The zero degree base should experience no lift or pitching moment. The residuals shown in Figure 44 are therefore an indication of limitations in the accuracy of the calibration procedures. The choice of reference area results in apparently large numeric values of $C_L$ and $C_M$, though it must be emphasized that the forces and moments involved are typically quite small. It is also noted that Figure 44 is a different "run" from those used for previous results.

Results for the 40 degree base, shown in Figure 45, indicate relatively constant values of $C_L$ and $C_M$, with consistently lower values sting-on. This corresponds to the drag variations shown earlier in Figure 15, presuming that the majority of all forces and moments arise due to base pressures. Figure 46 again shows the characteristic hysteretic behaviour of the wake for the 45 degree base, first noticed in Figure 17. Results for the 50 degree base, shown in Figure 47, also confirm the previously observed weakening of the wake vortices with transition fixed.

## 5.5 DISCUSSION OF RESULTS

Figure 48 shows a comparison of interference free drag coefficients to the original data by Morel([8], $Re_D$=94,000). MSBS points are obtained by interpolation for each base slant. Agreement for the interference free cases is quite good at the higher slant angles. At the lower slant angles, it is supposed that partial boundary layer tripping was induced by Morel's wire supports [16]. The critical slant angle was fractionally lower in the MSBS tests than had been previously reported. The apparent convergence of all results above the critical slant angle is again notable.

With sting-on, the drag is relatively constant for all base slants (Figure 49). For most angles the drag is too low, although at the highest angle tested the reverse is true. The data may appear somewhat scattered, but the reader is reminded that some form of vortex formation is quite likely around the 45 degree slant angle. Thus the points may lie on two or more distinct trend lines, as in the interference-free cases.

It is recognized that the use of a relatively massive sting support at subsonic speeds is rather unconventional. Thus the specific data presented herein might be regarded as unrepresentative of everyday interference problems. However, at transonic speeds, the use of some form of sting support is virtually universal and there is no reason to expect that interference phenomena should be confined to the subsonic regime.

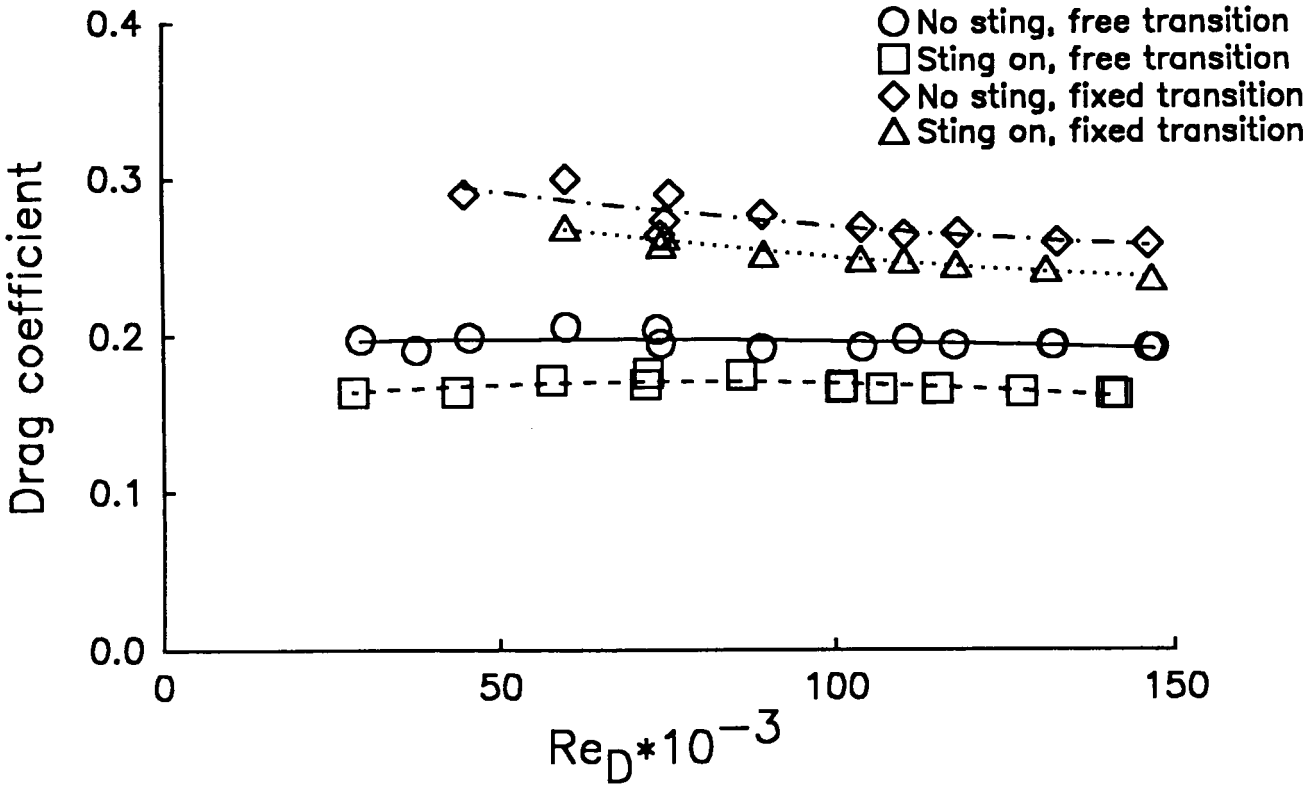


FIGURE 11 - Zero degree base: Drag Coefficients

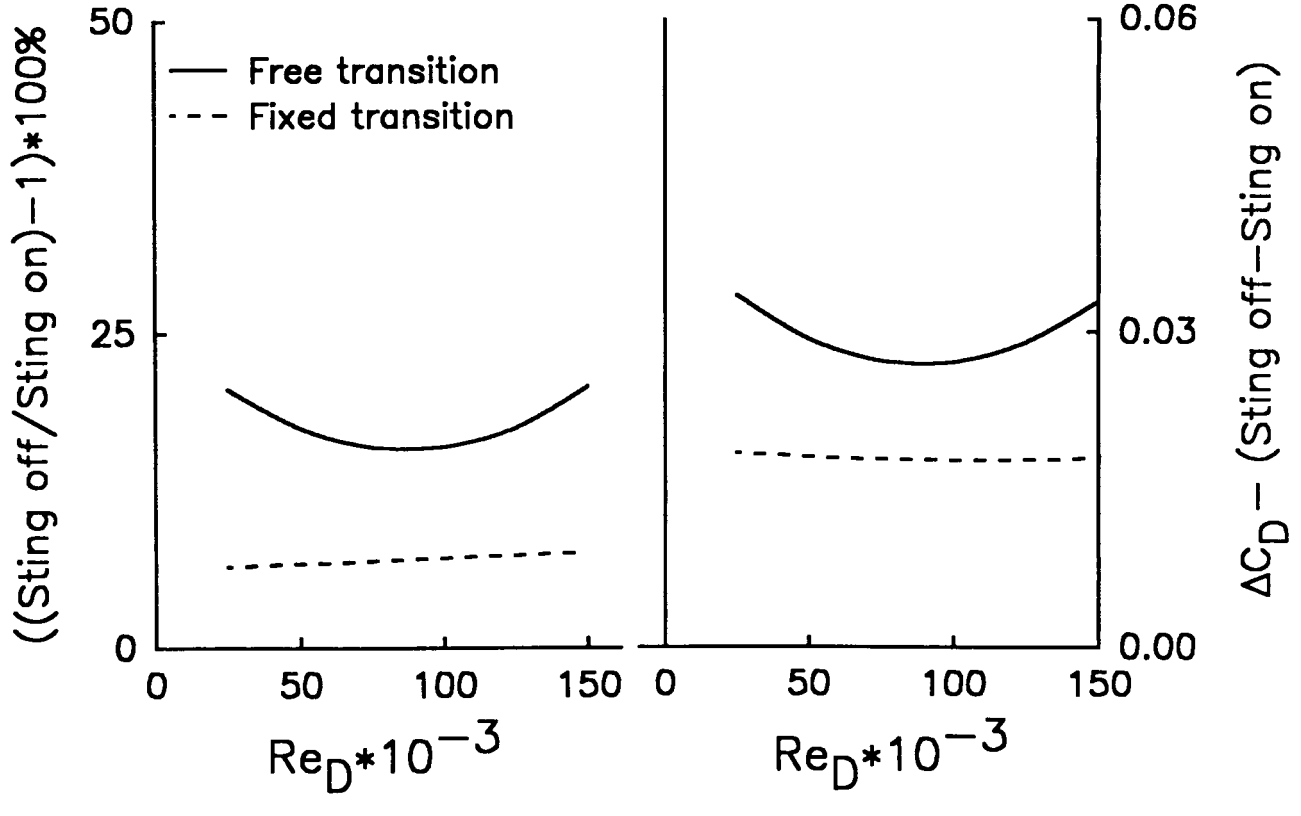


FIGURE 12 - Zero degree base: Sting Interference on Drag

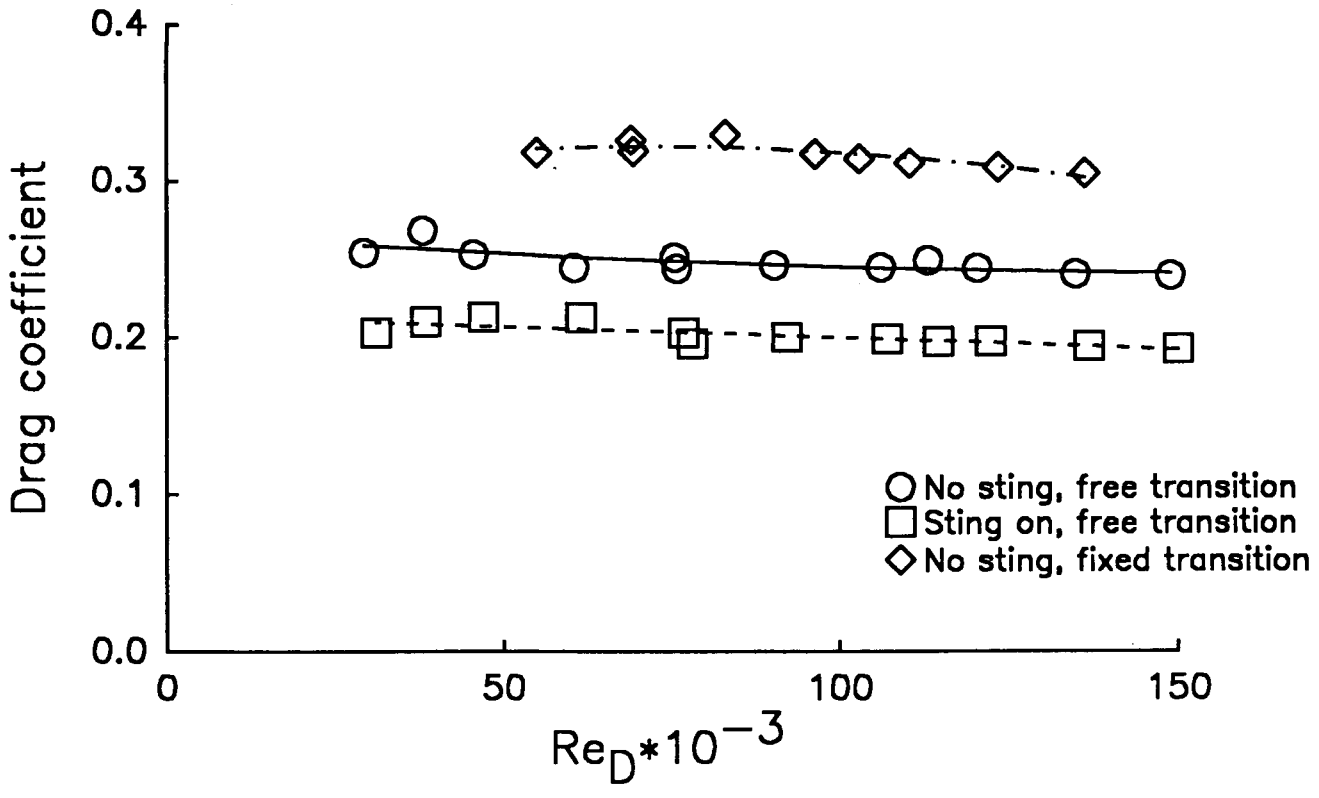


FIGURE 13 - 30 degree base: Drag Coefficients

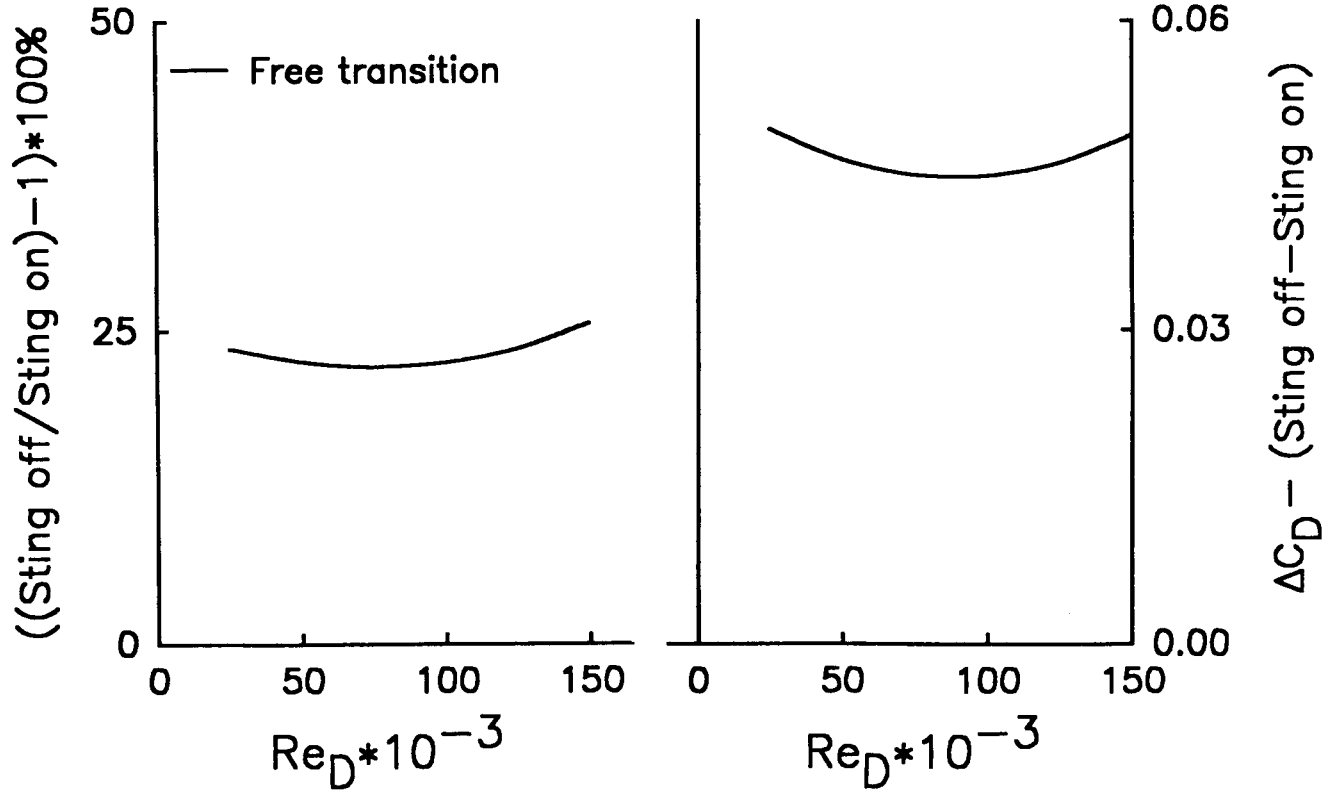


FIGURE 14 - 30 degree base: Sting Interference on Drag

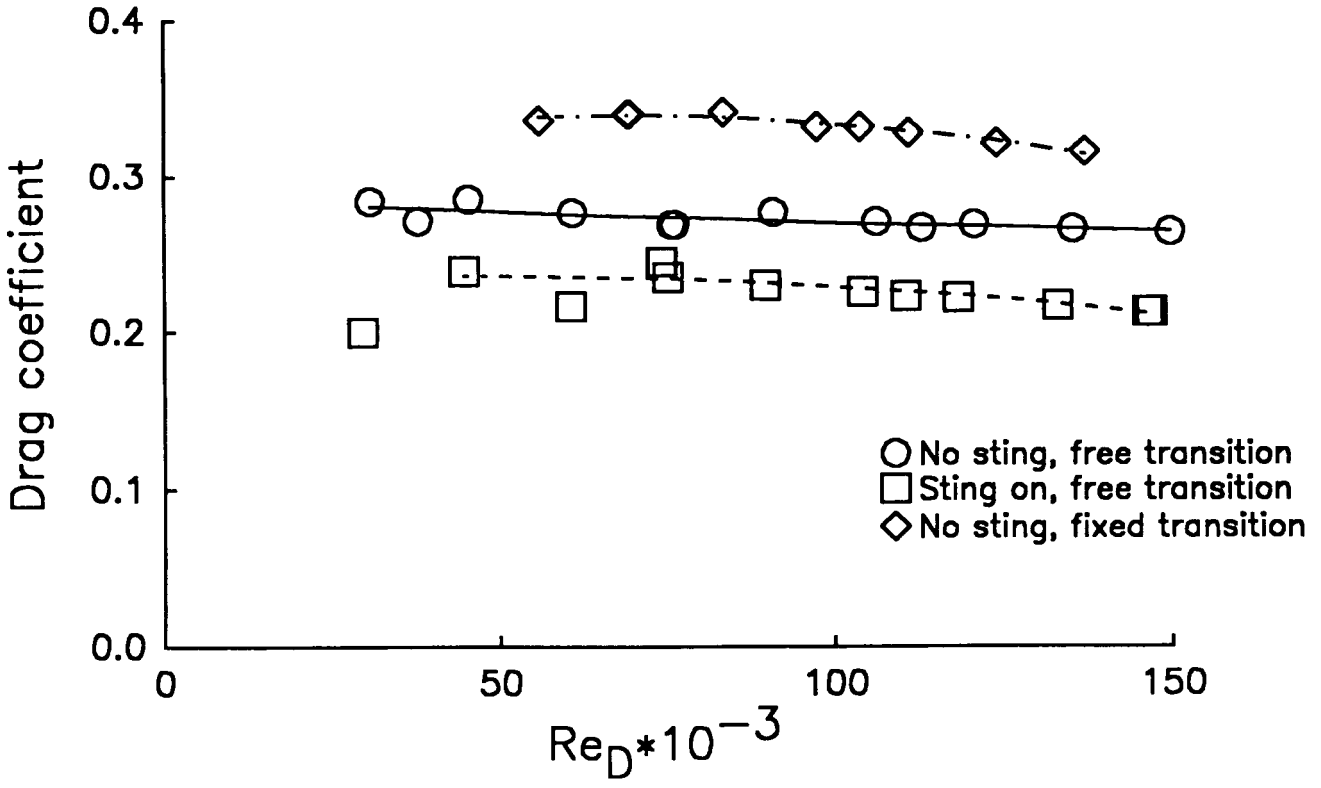


FIGURE 15 - 40 degree base: Drag Coefficients

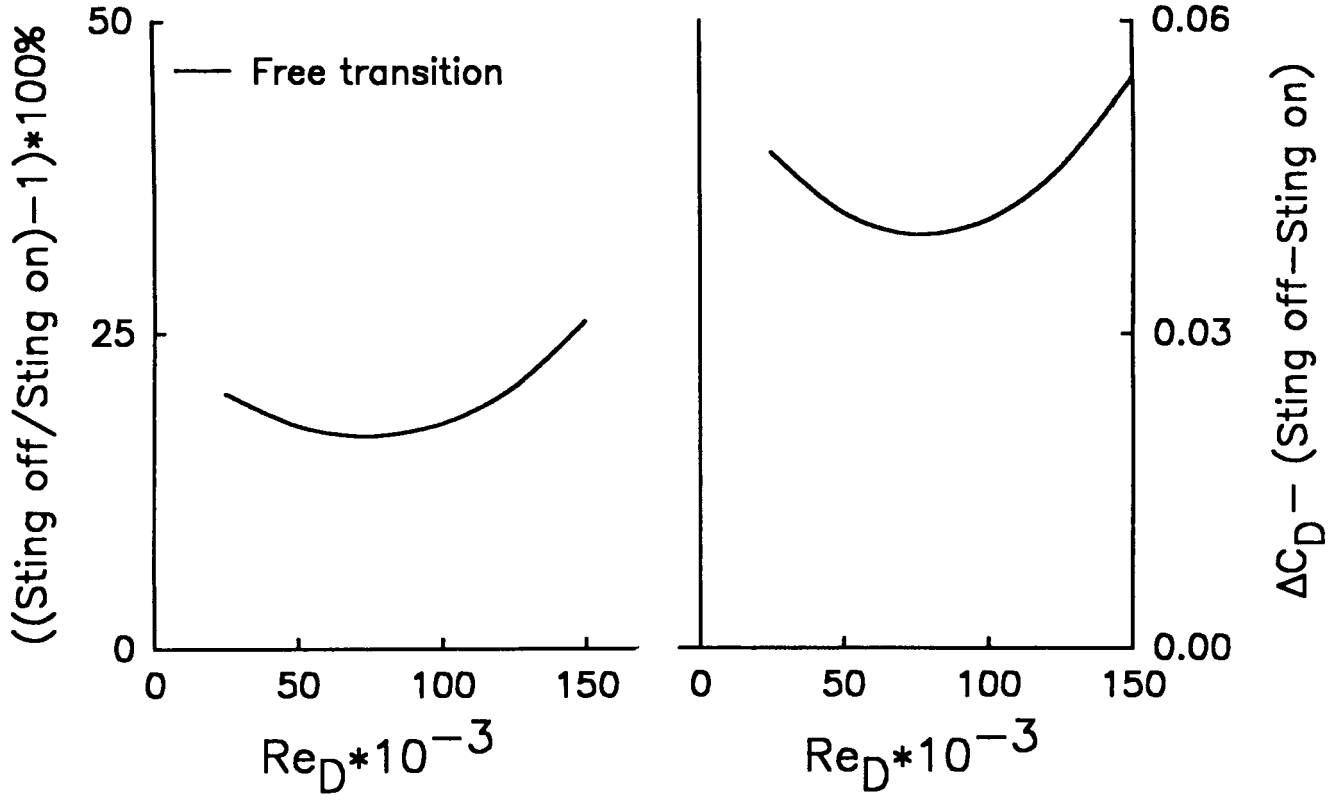


FIGURE 16 - 40 degree base: Sting Interference on Drag

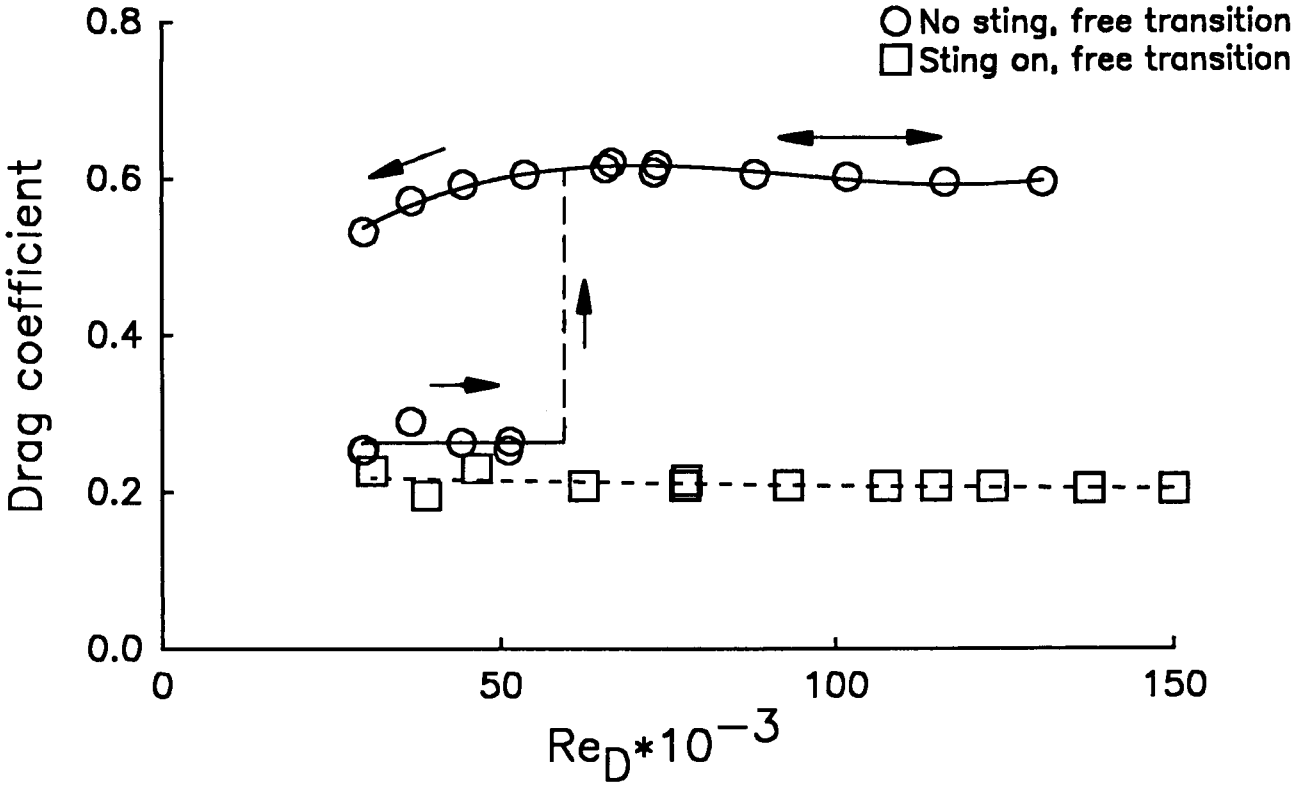


FIGURE 17 - 45 degree base: Drag Coefficients

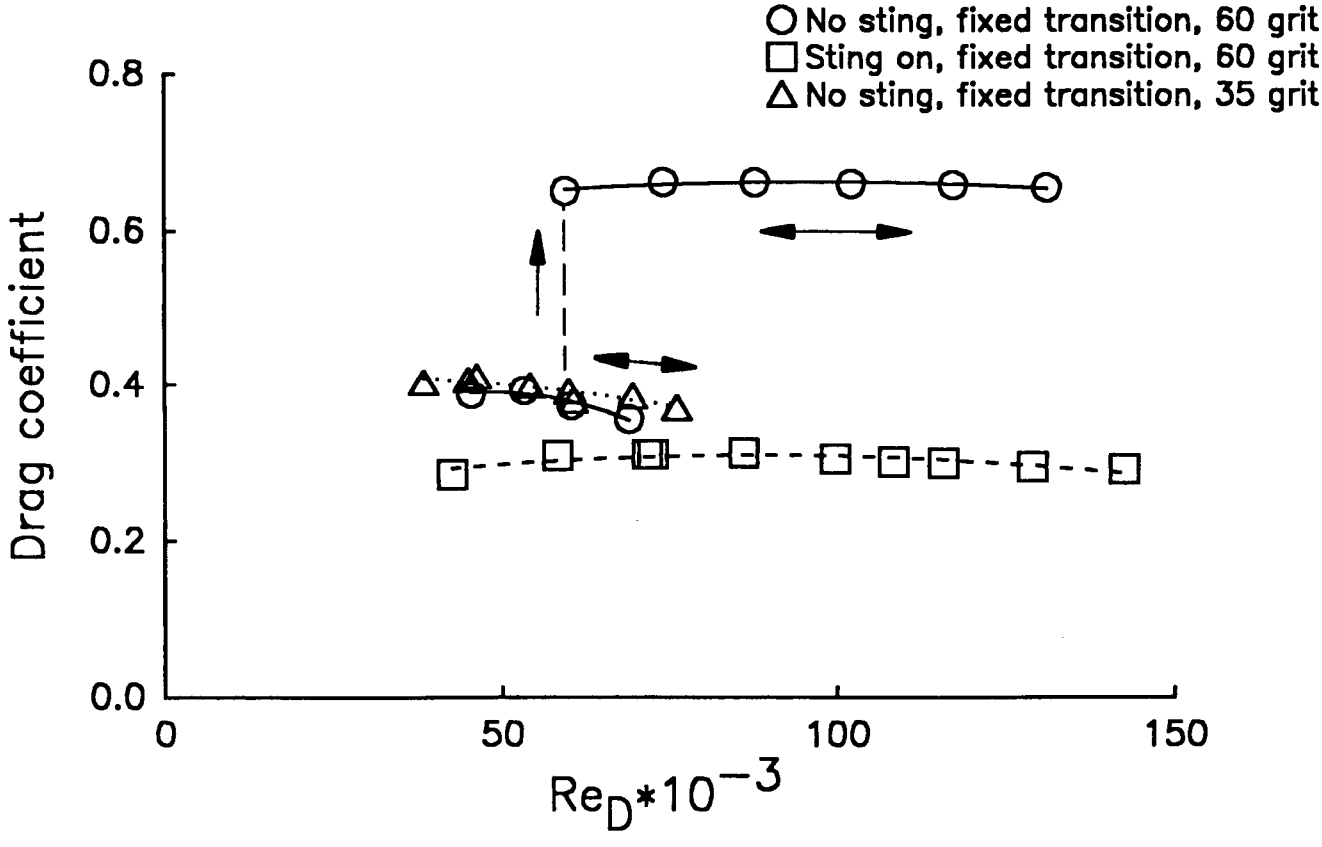


FIGURE 18 - 45 degree base: Drag Coefficients

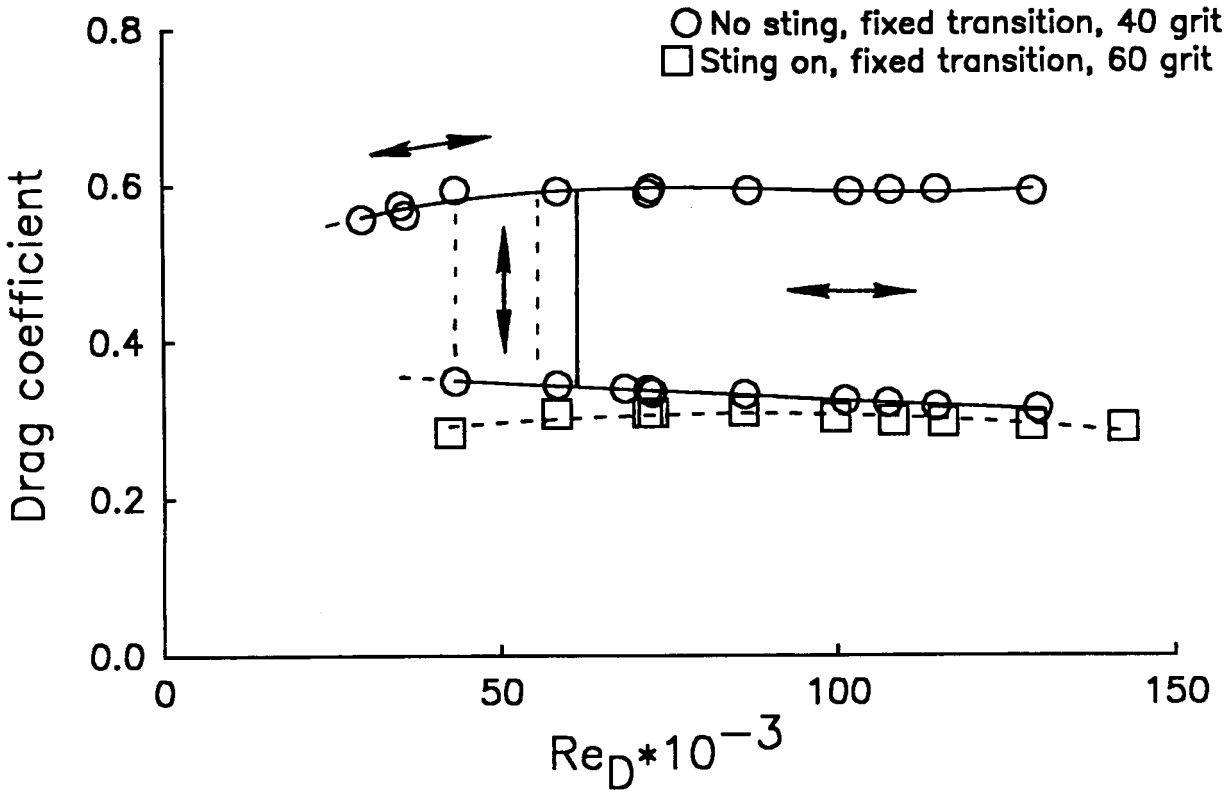


FIGURE 19 - 45 degree base: Drag Coefficients

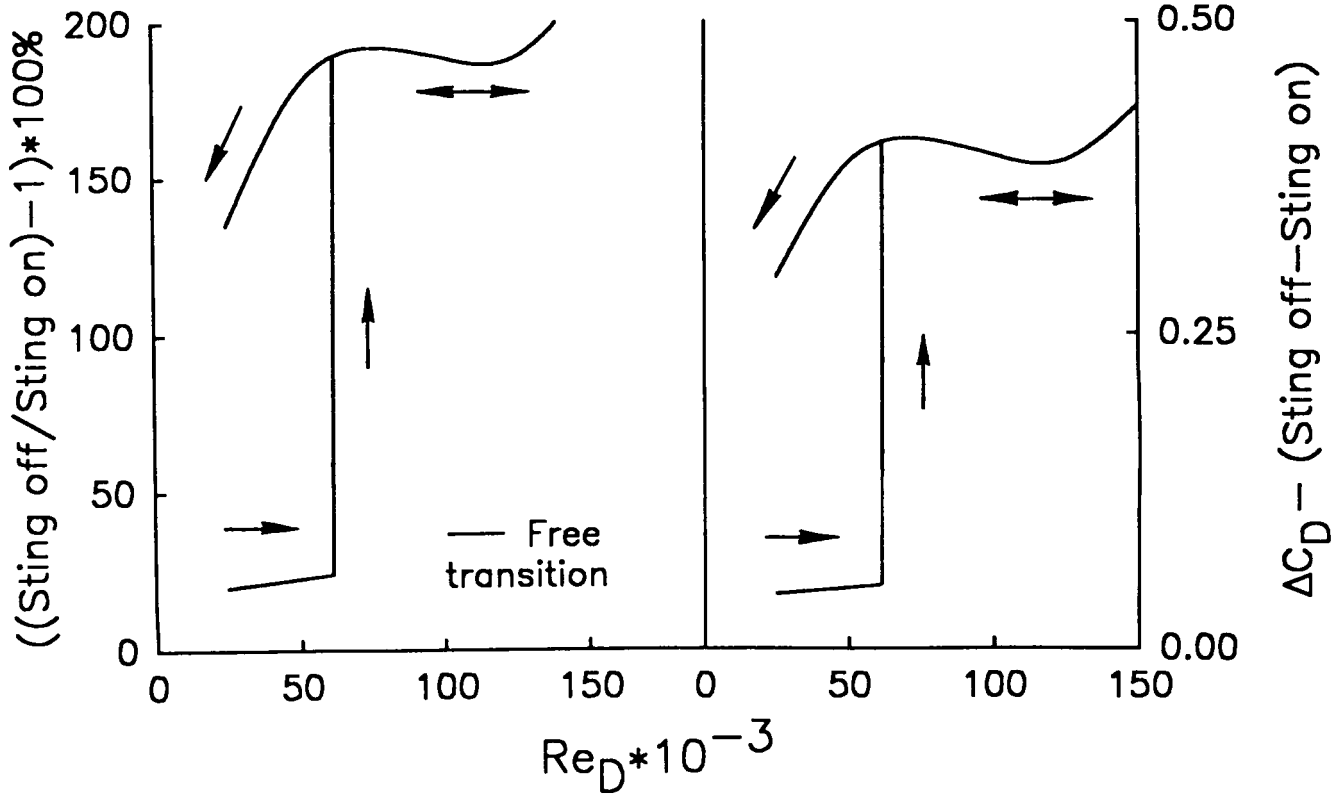


FIGURE 20 - 45 degree base: Sting Interference on Drag

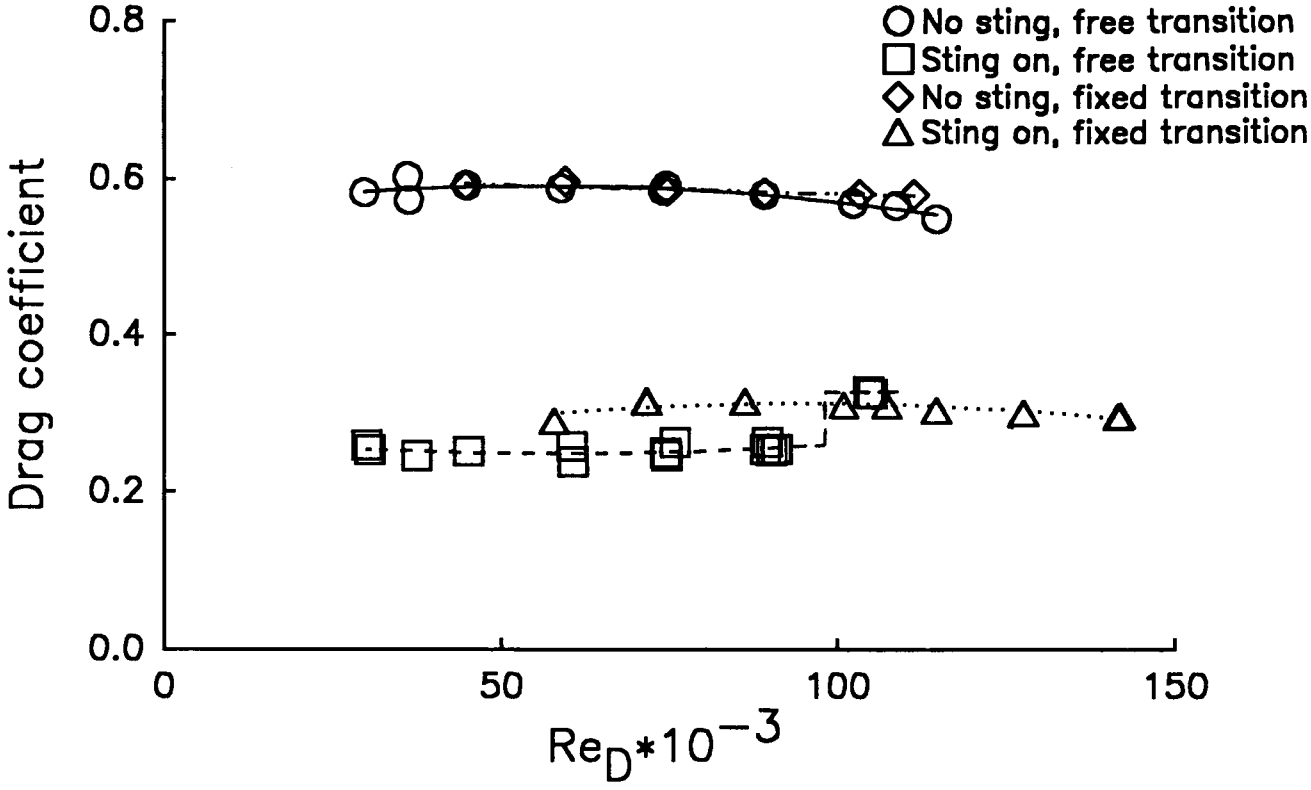


FIGURE 21 - 50 degree base: Drag Coefficients

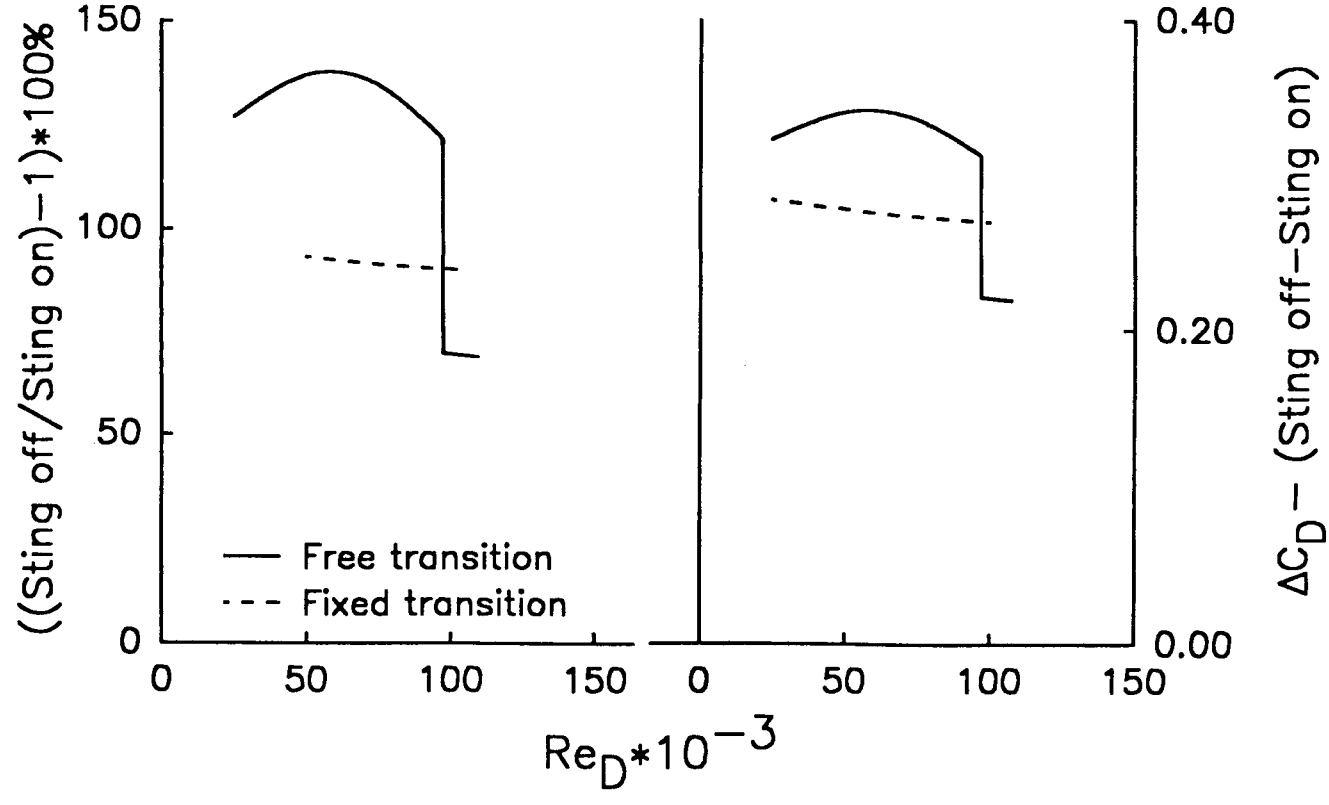


FIGURE 22 - 50 degree base: Sting Interference on Drag

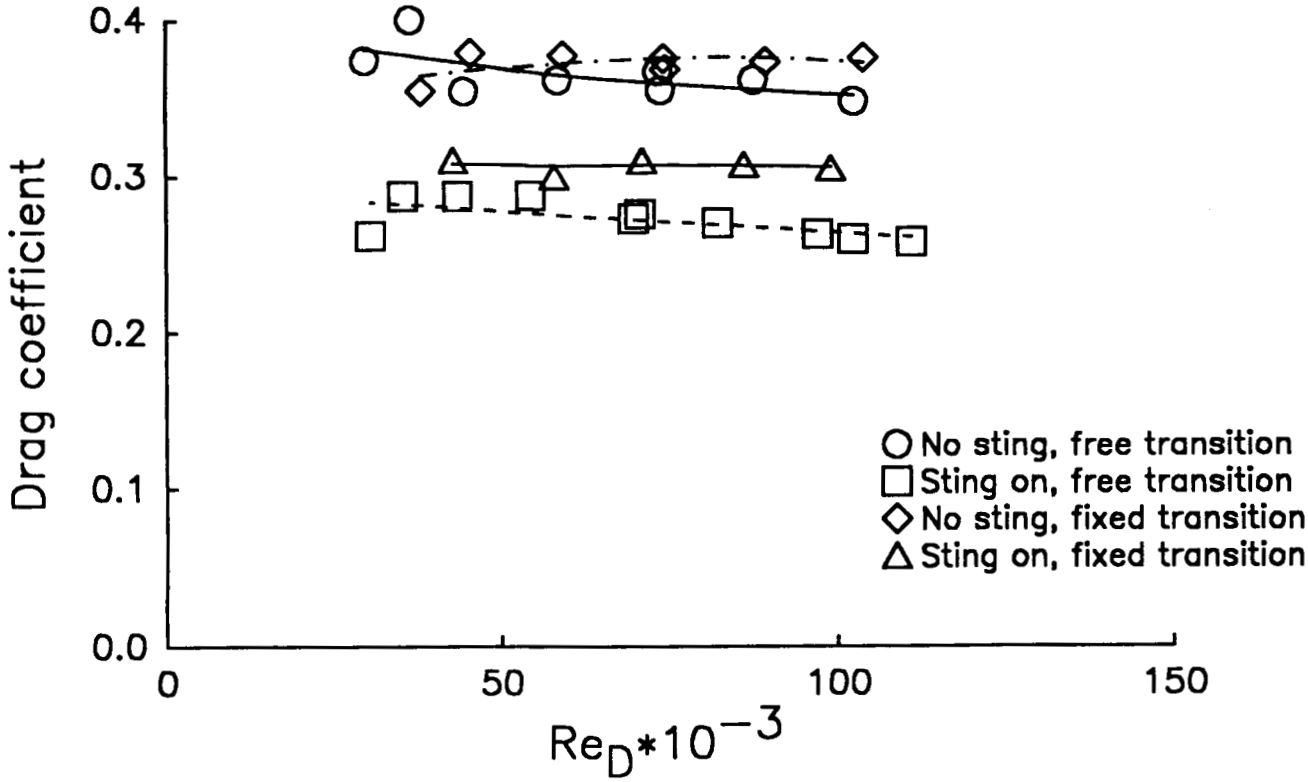


FIGURE 23 - 60 degree base: Drag Coefficients

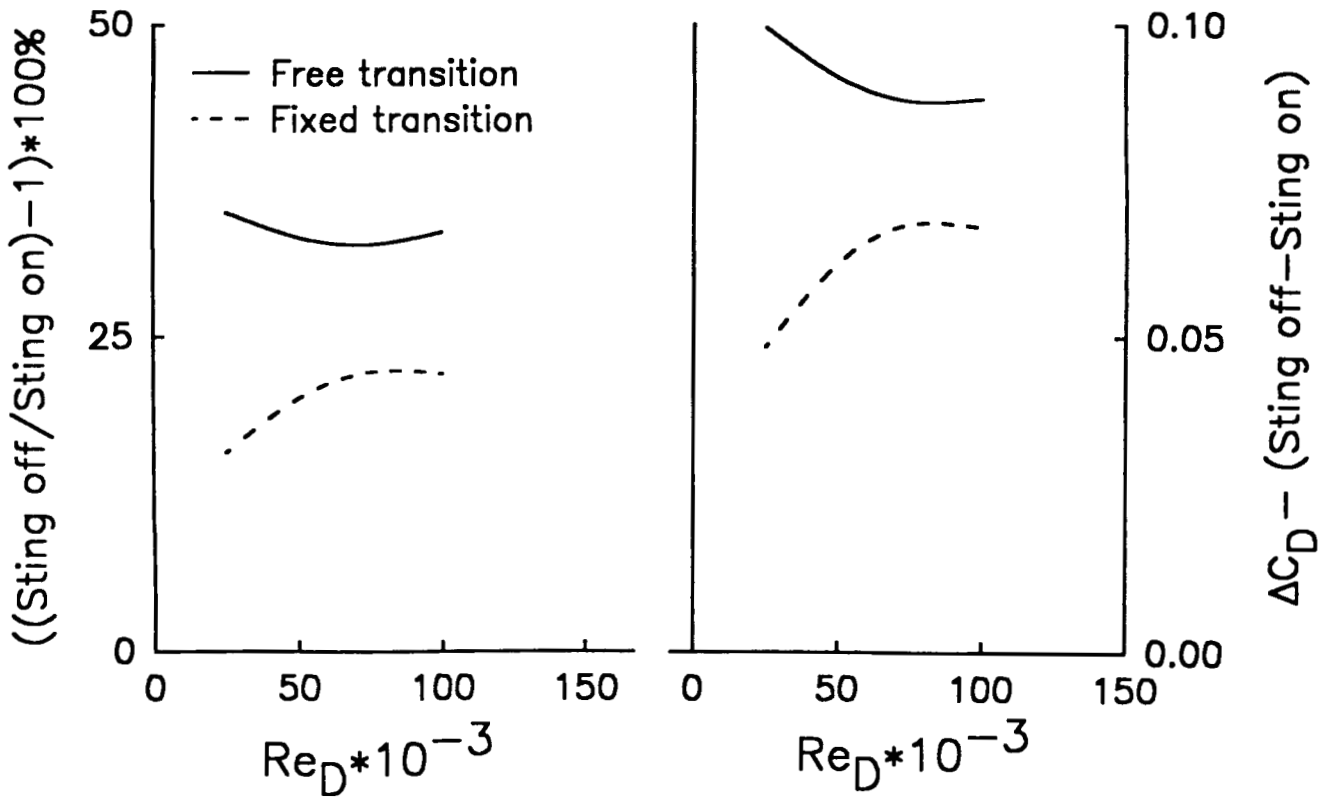


FIGURE 24 - 60 degree base: Sting Interference on Drag

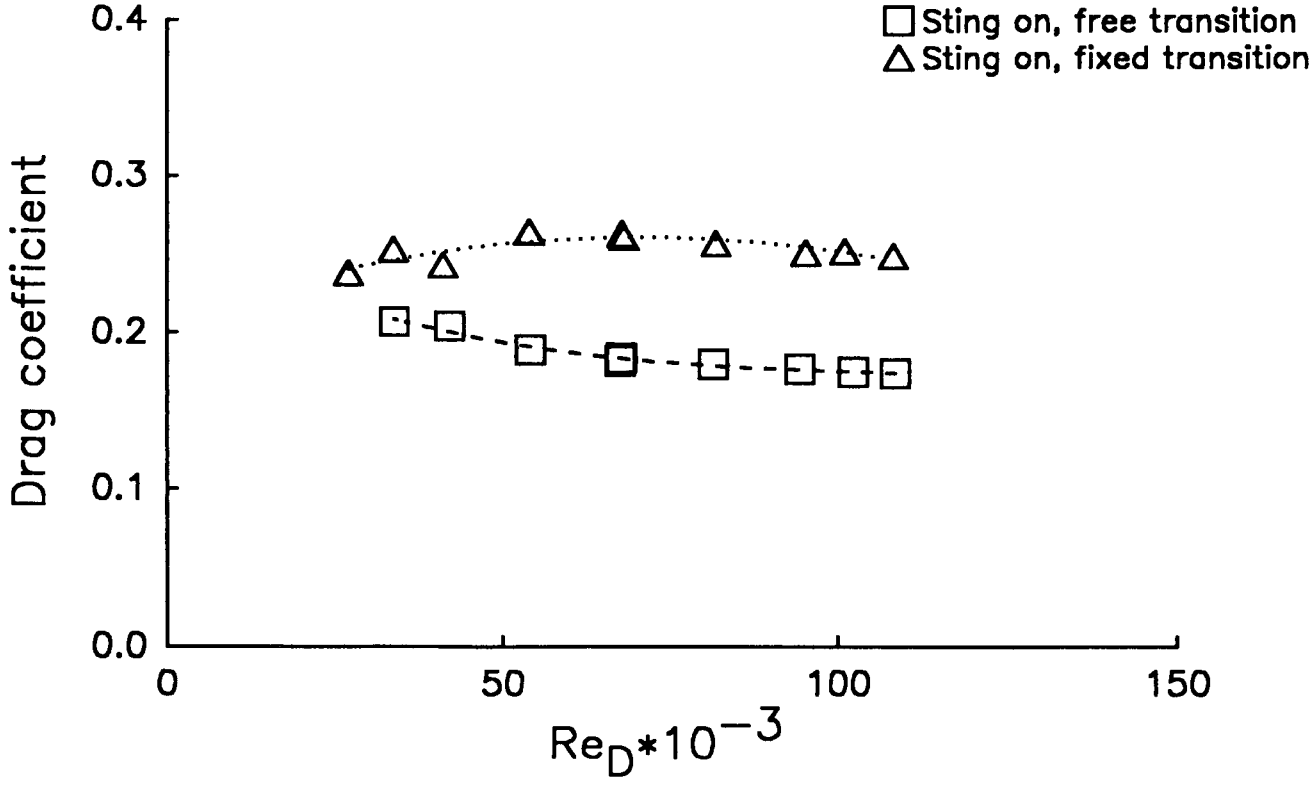


FIGURE 25 - 70 degree base: Drag Coefficients

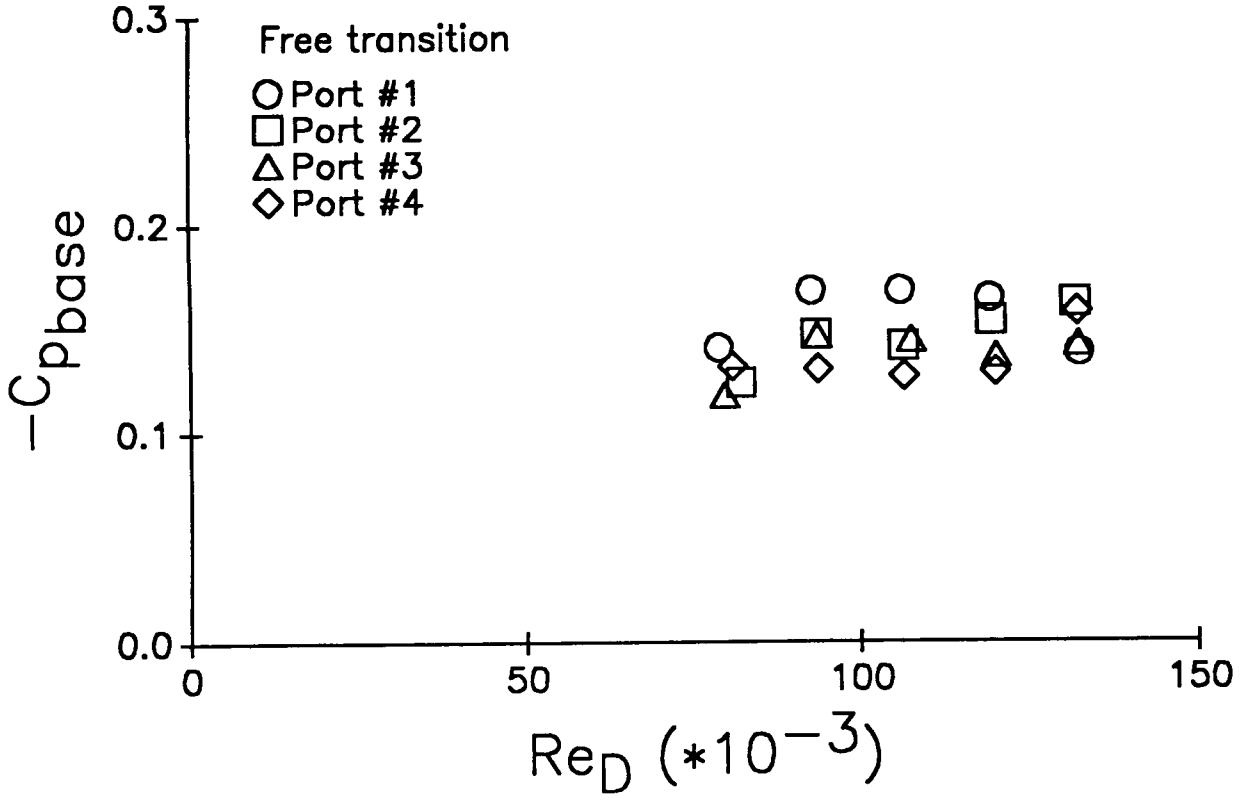


FIGURE 26 - Zero degree base: Base Pressure Coefficients

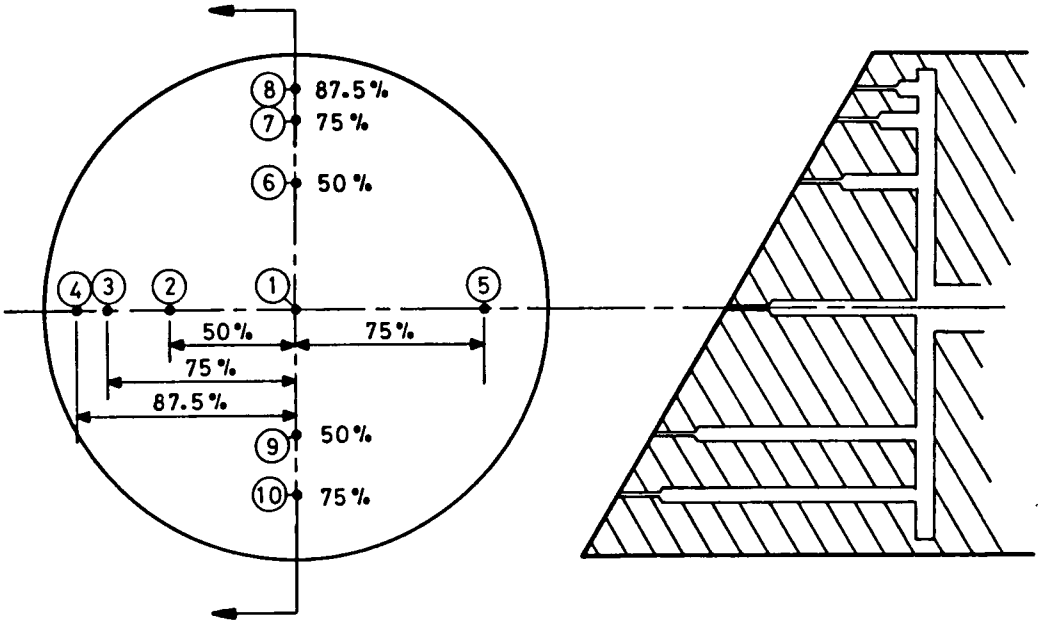

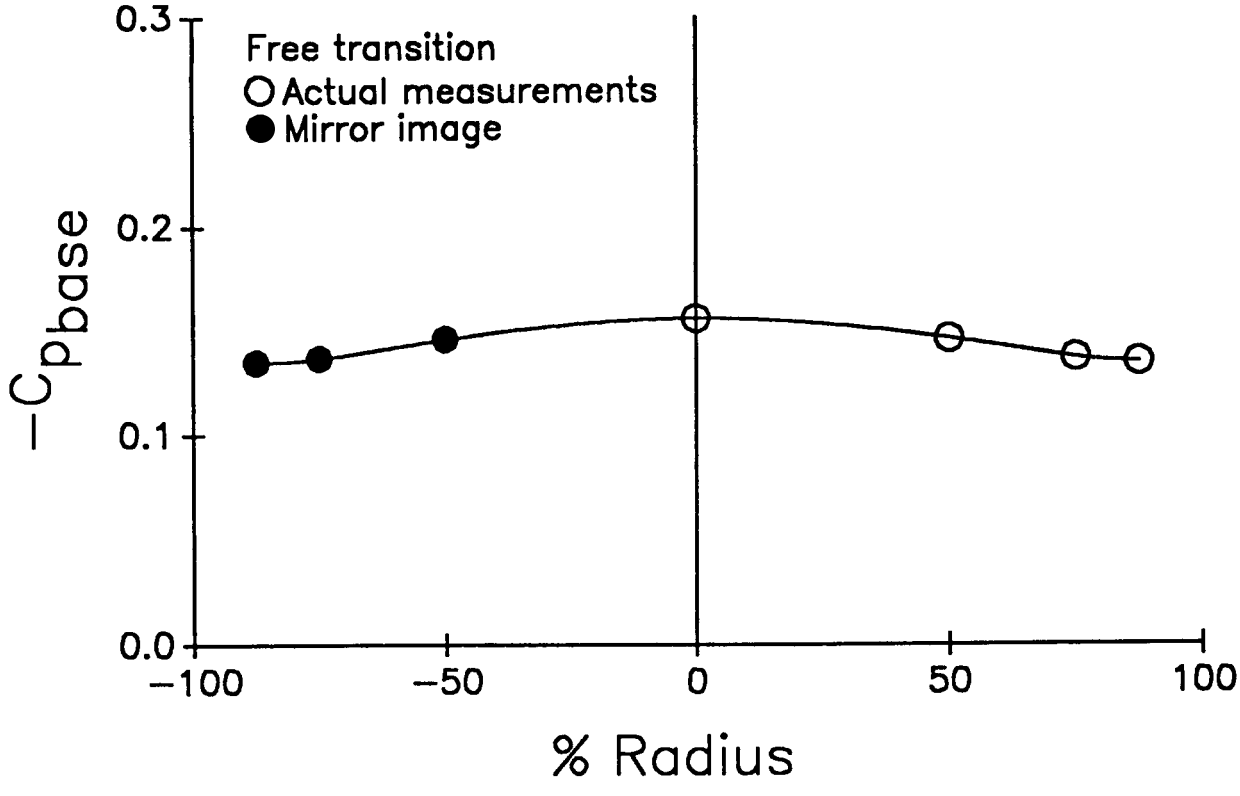


FIGURE 27 - Zero degree base: Base Pressure Coefficients, $Re_D$=94,000

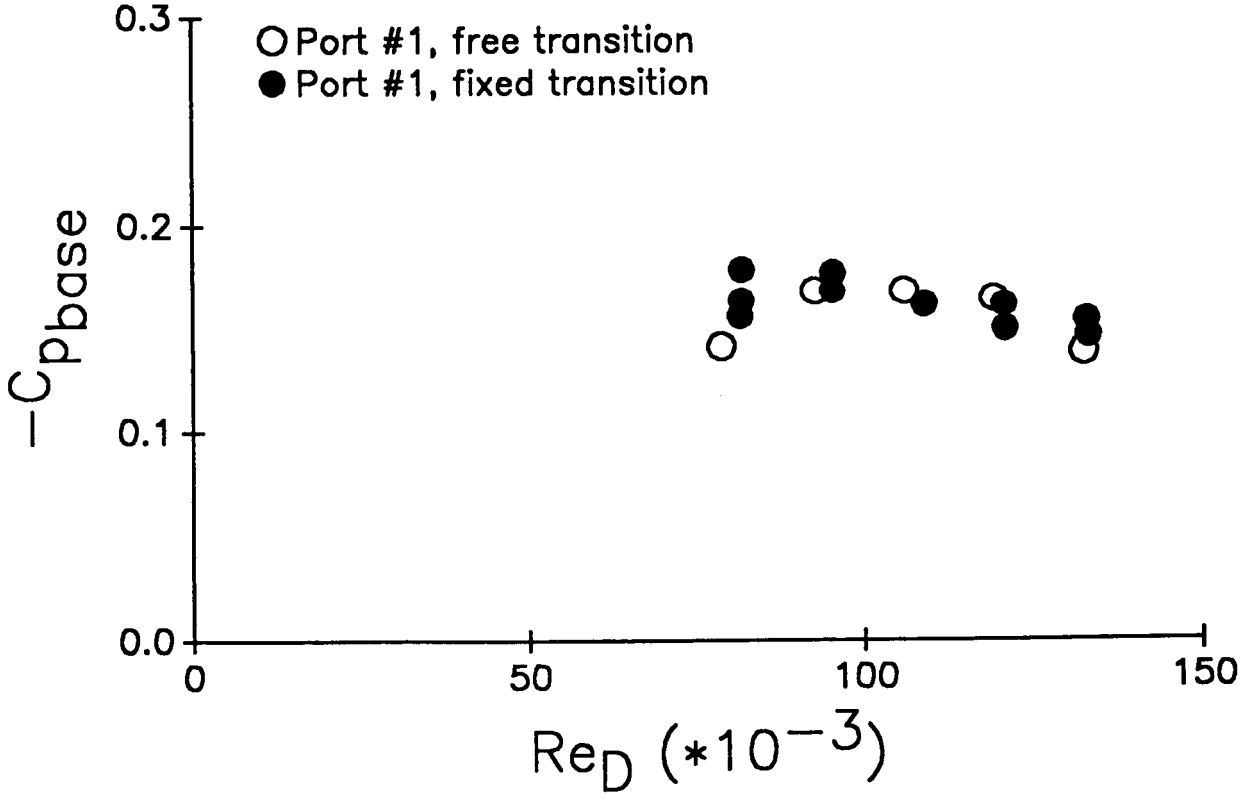


FIGURE 28 - Zero degree base: Base Pressure Coefficients

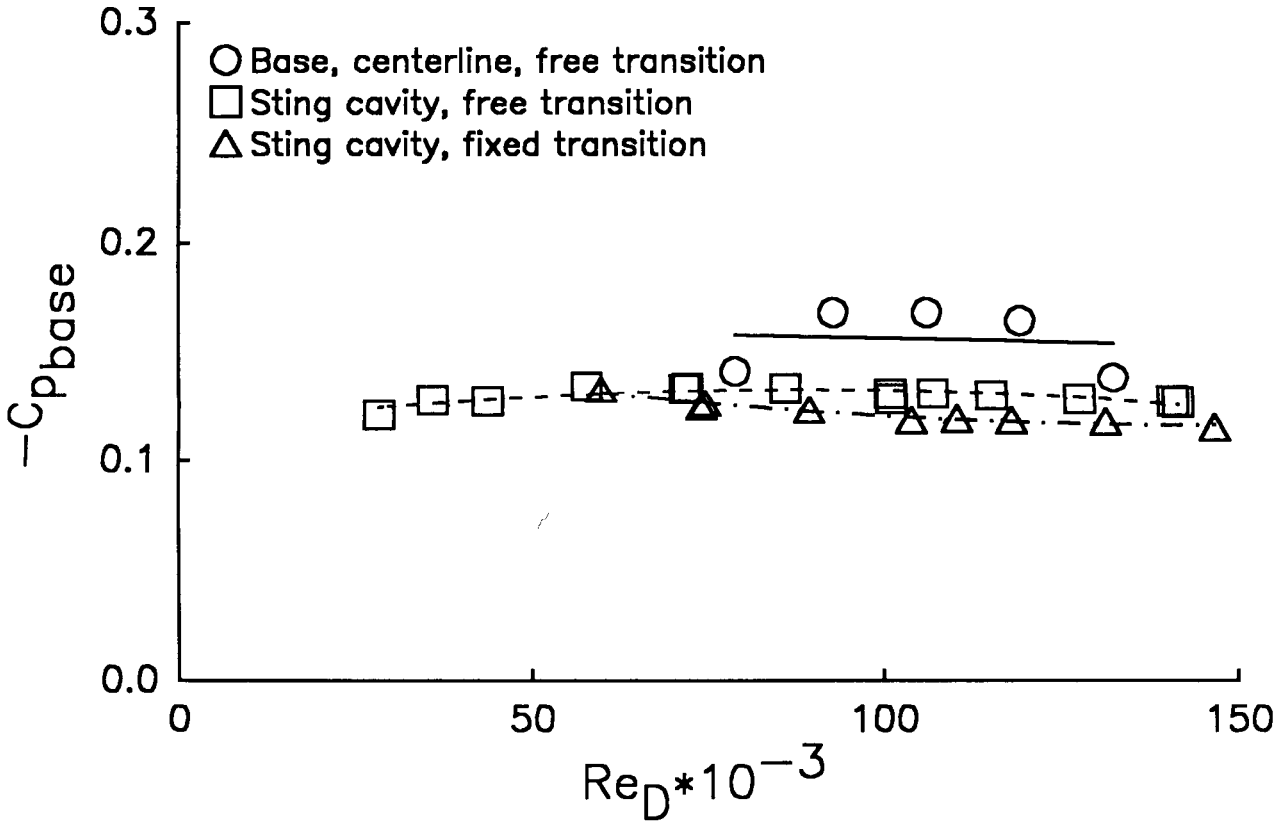


FIGURE 29 - Zero degree base: Comparison of Base and Sting Cavity Pressures

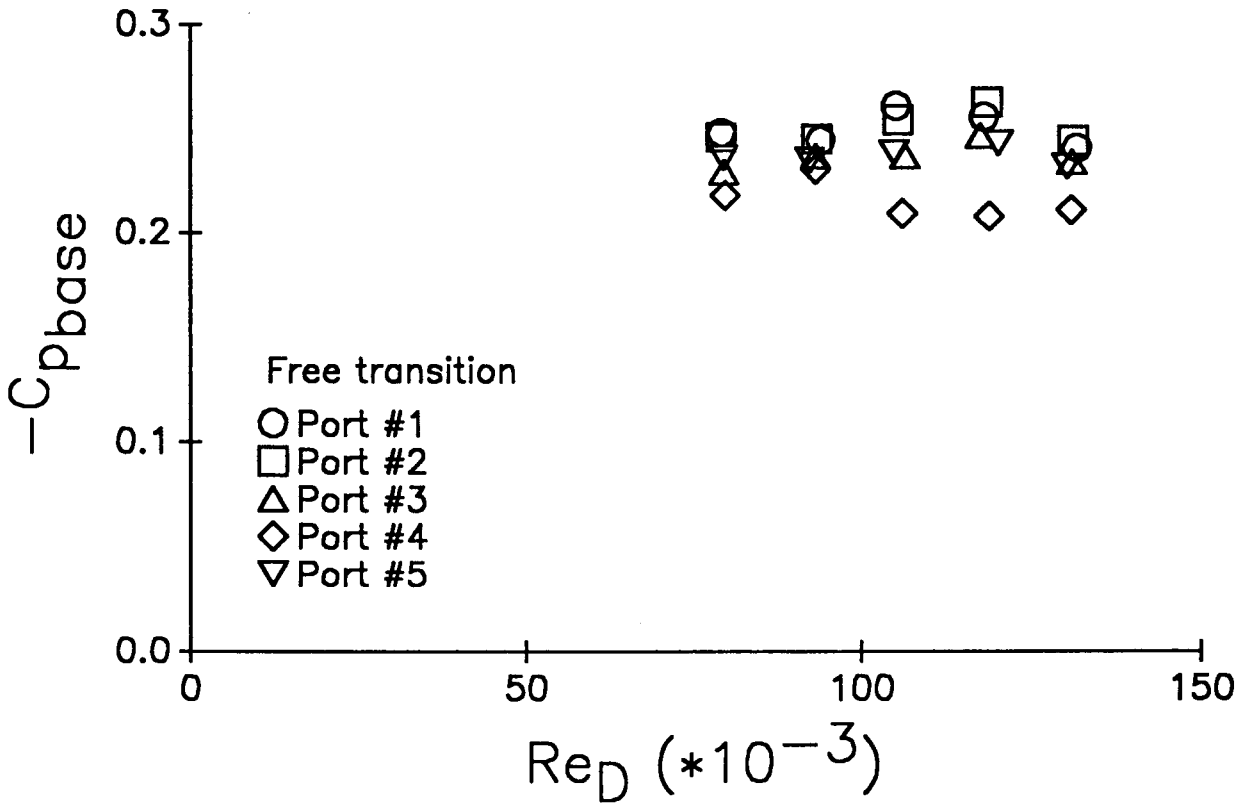


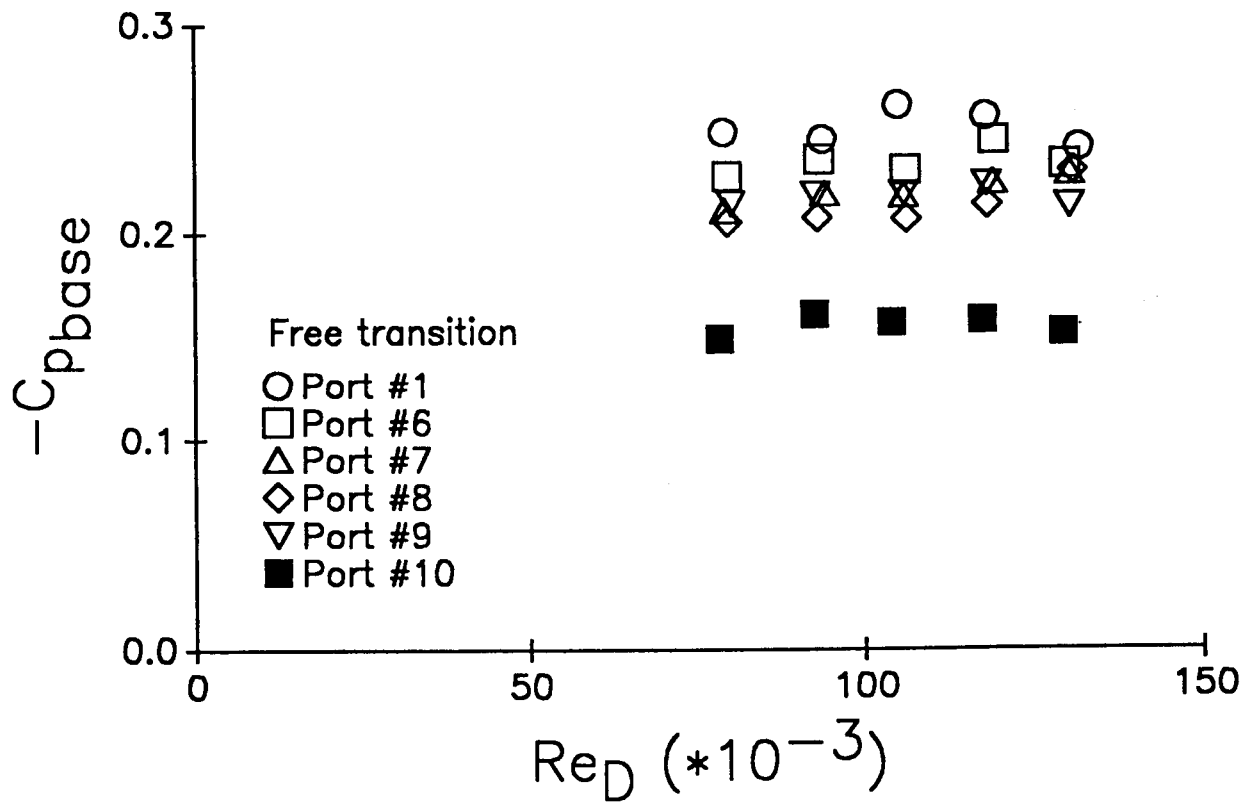


FIGURE 30 - 40 degree base: Base Pressure Coefficients

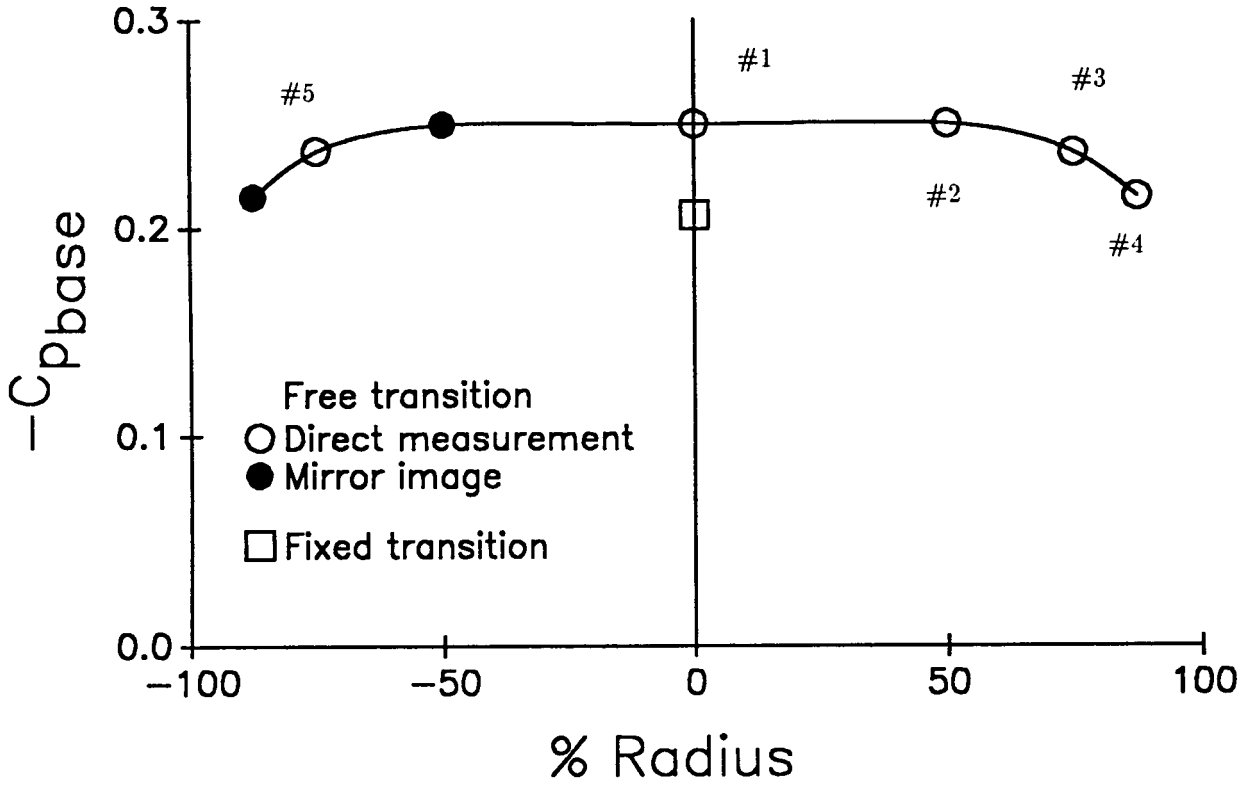


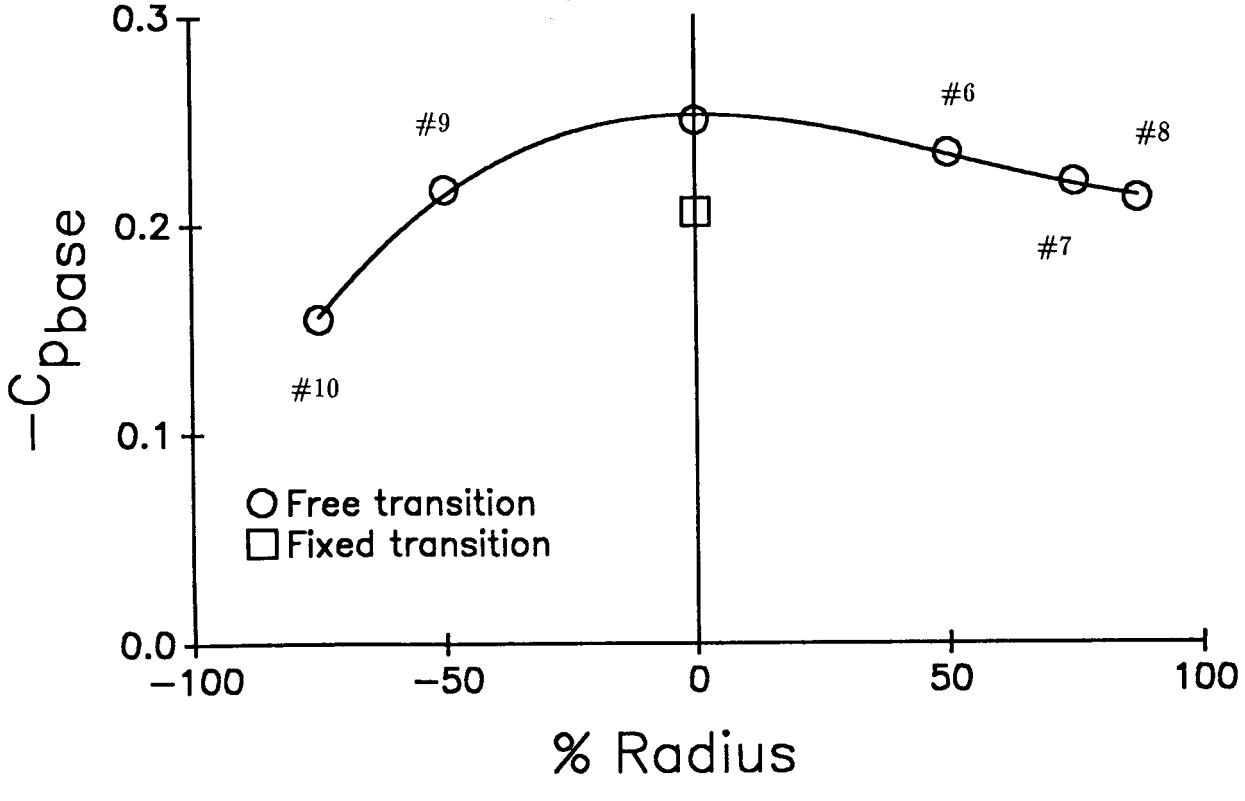


FIGURE 31 - 40 degree base: Base Pressure Coefficients, $Re_D$=94,000

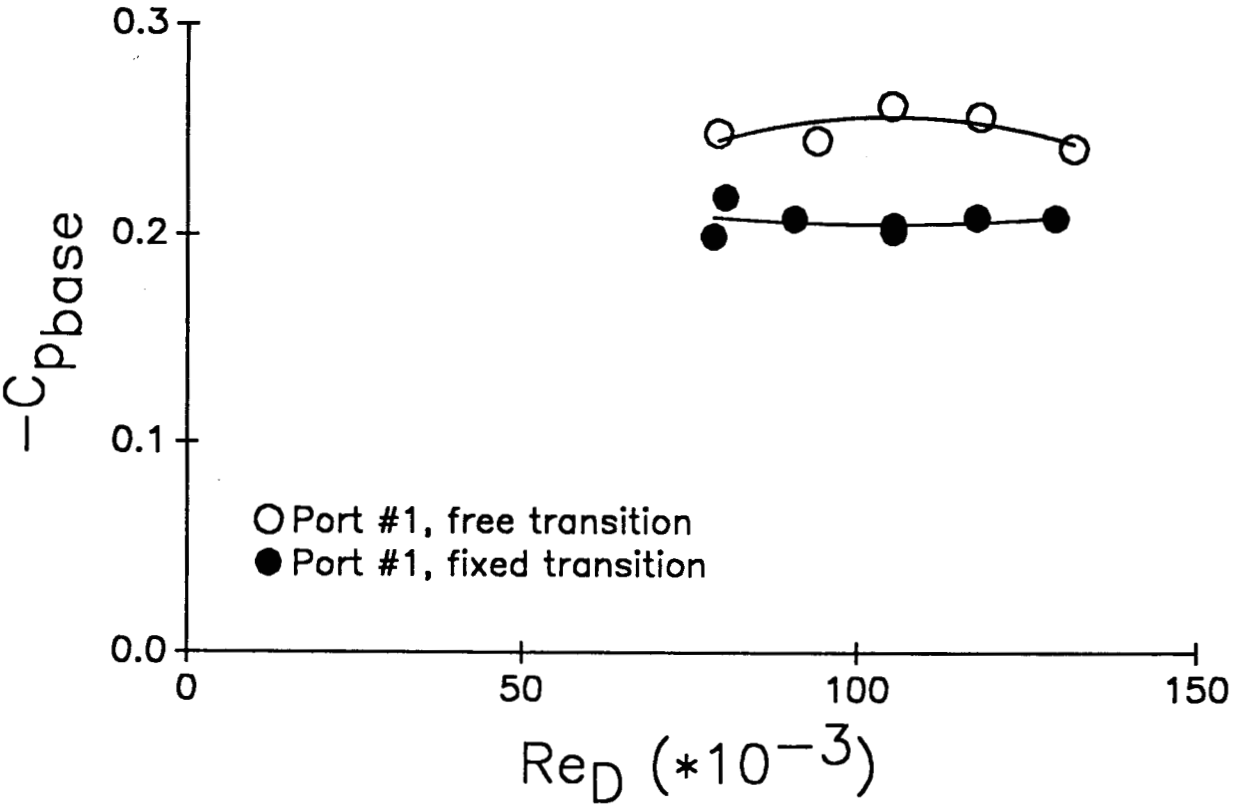


FIGURE 32 - 40 degree base: Base Pressure Coefficients

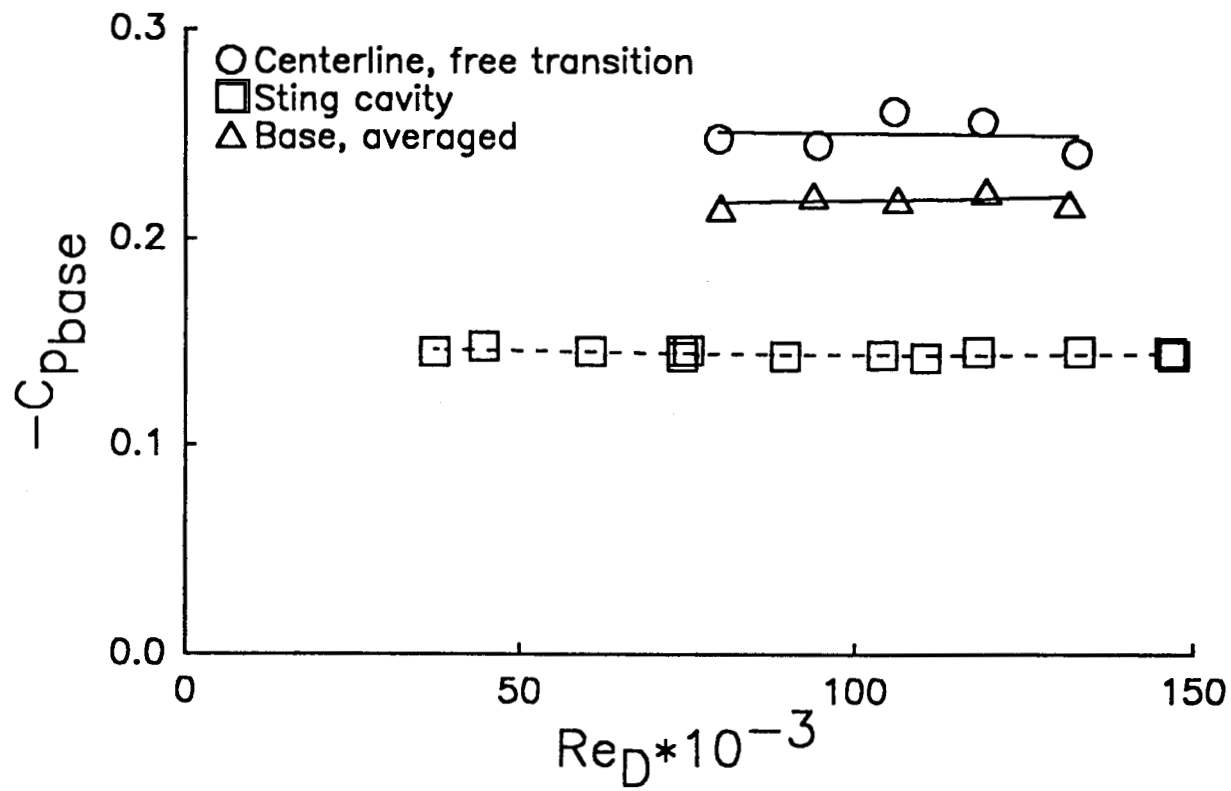


FIGURE 33 - 40 degree base: Comparison of Base and Sting Cavity Pressures

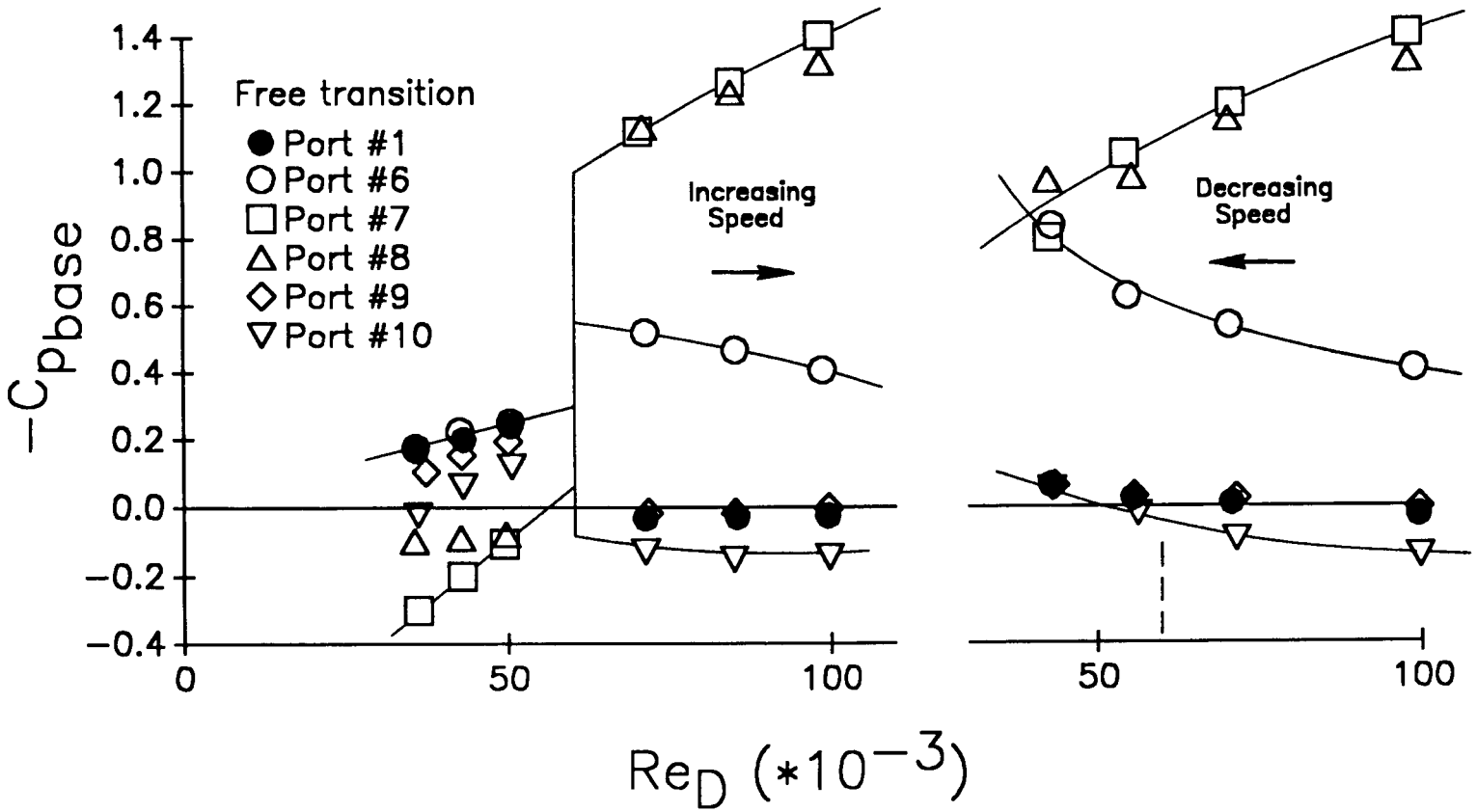


FIGURE 34 - 45 degree base: Base Pressure Coefficients

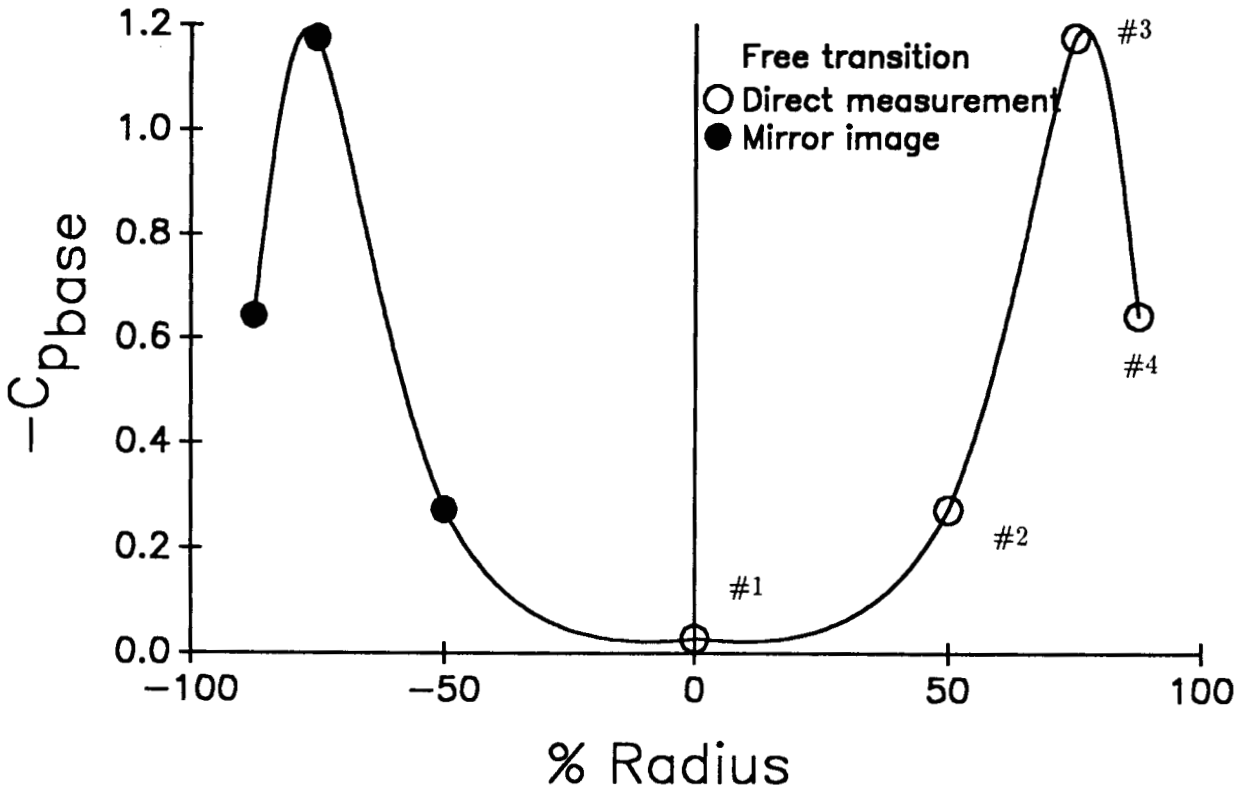


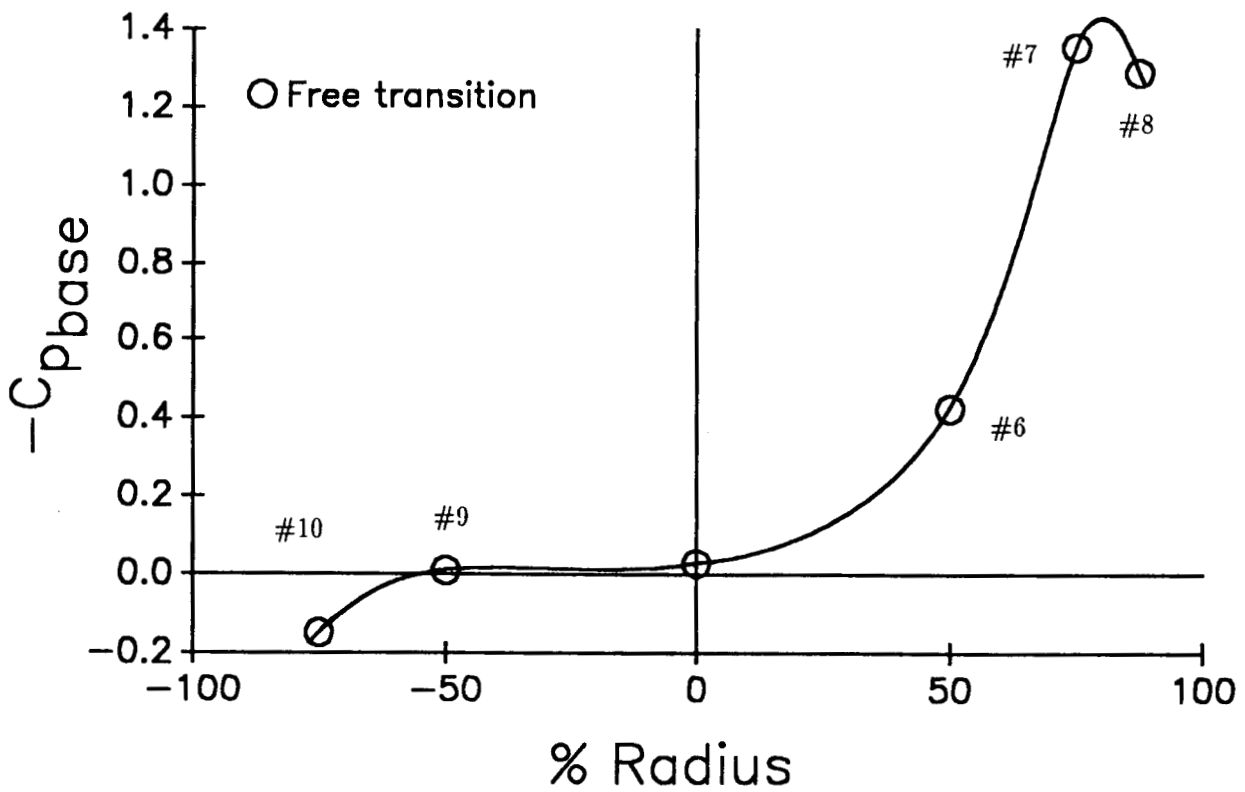


FIGURE 35 - 45 degree base: Base Pressure Coefficients, $Re_D$=94,000

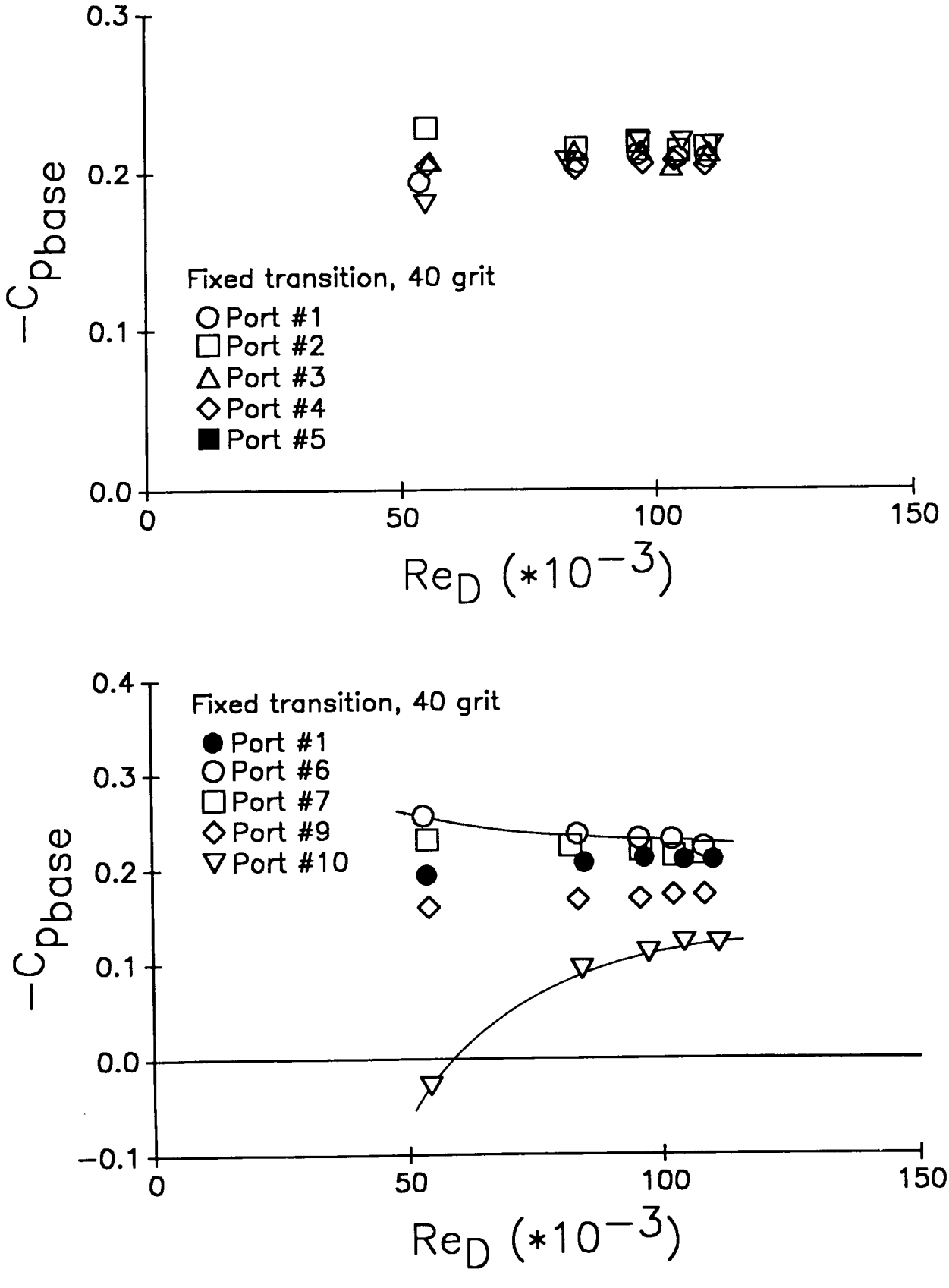


FIGURE 36 - 45 degree base: Base Pressure Coefficients

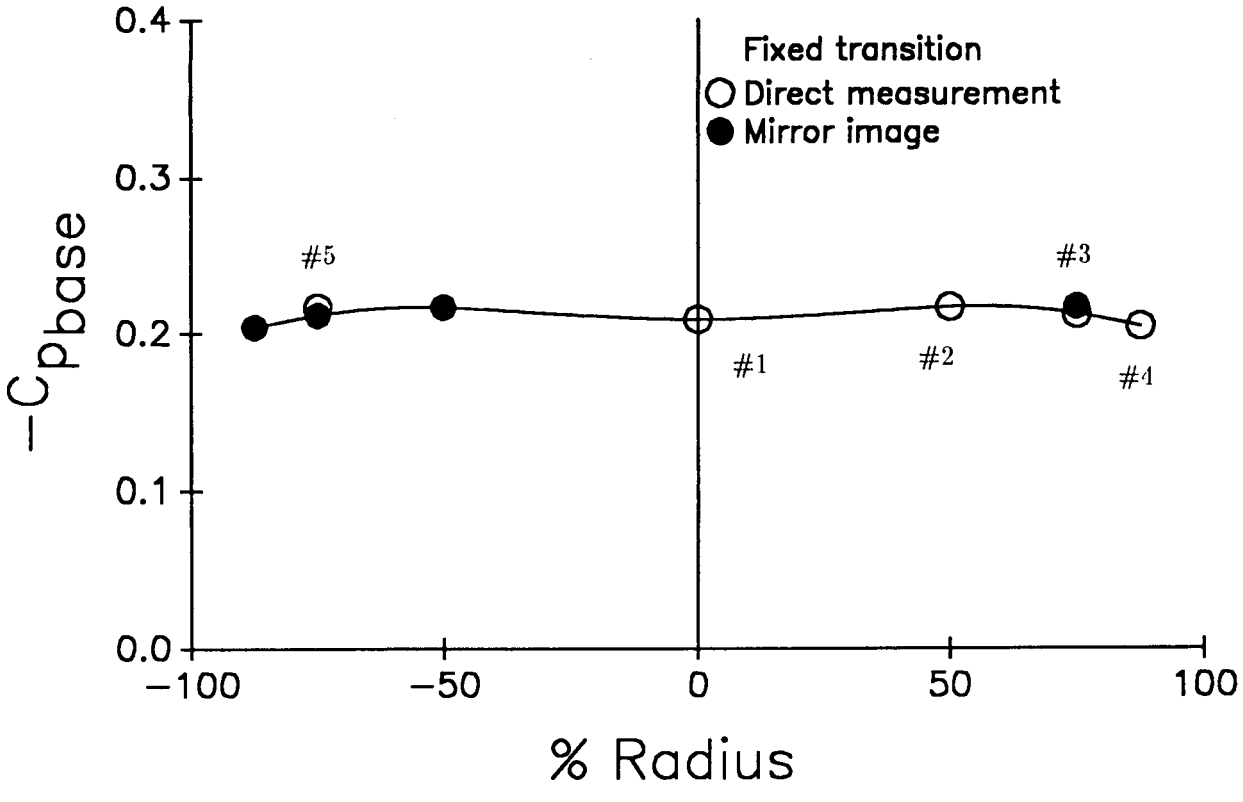


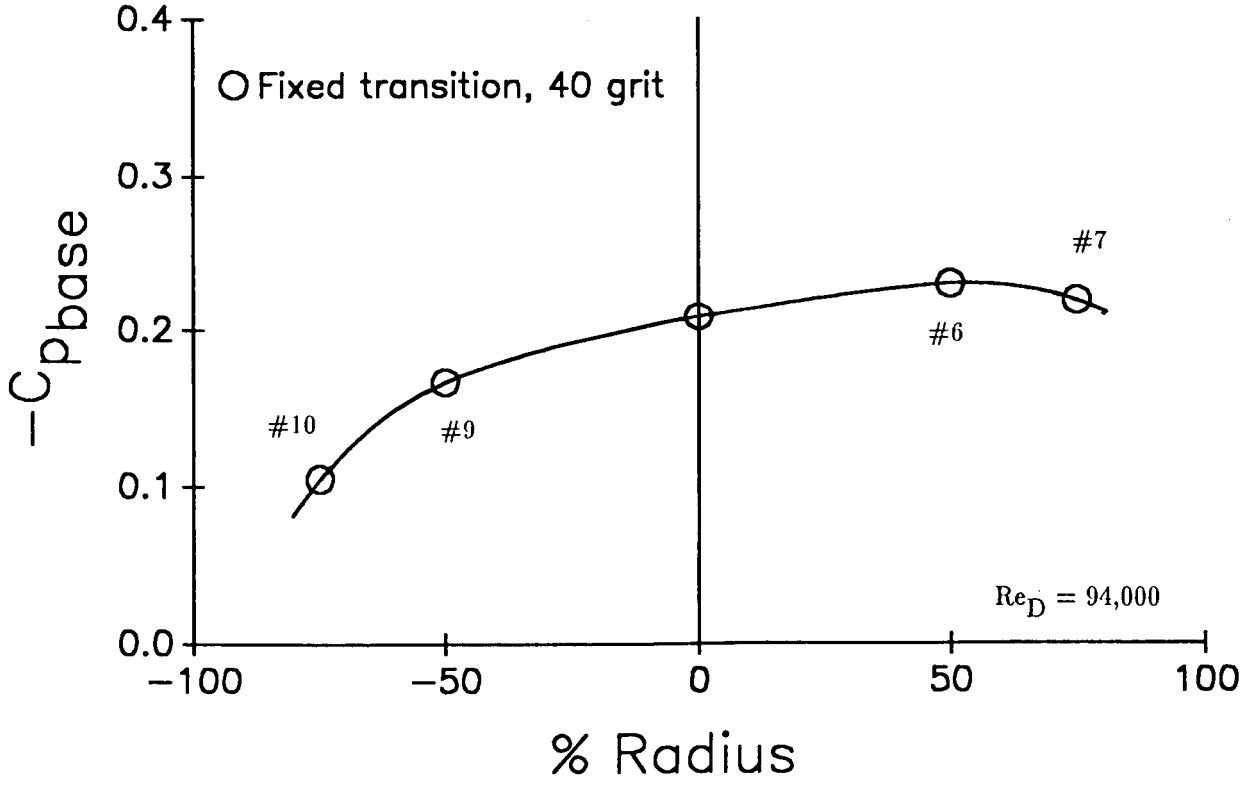


FIGURE 37 - 45 degree base: Base Pressure Coefficients

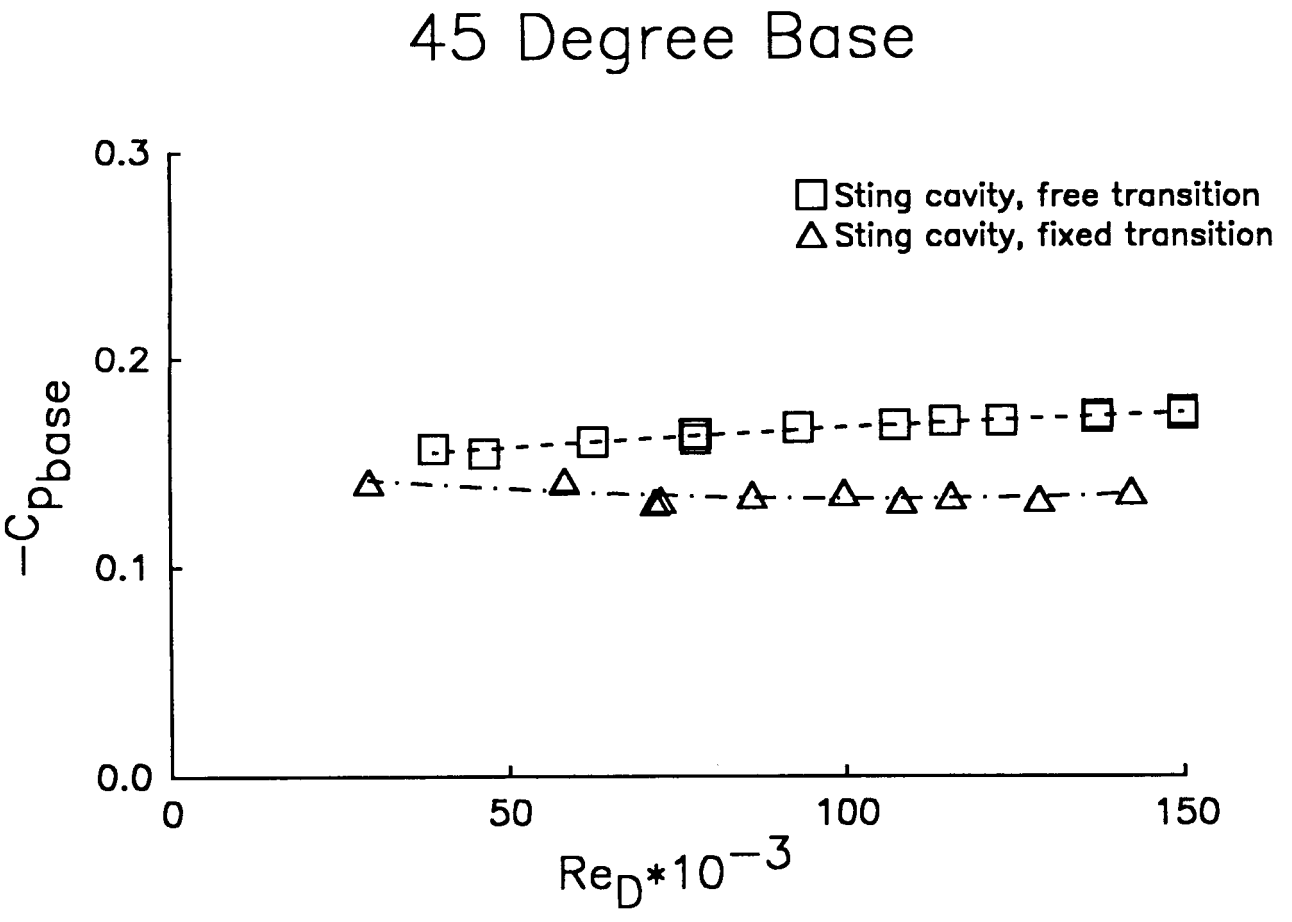


FIGURE 38 - 45 degree base: Sting Cavity Pressures

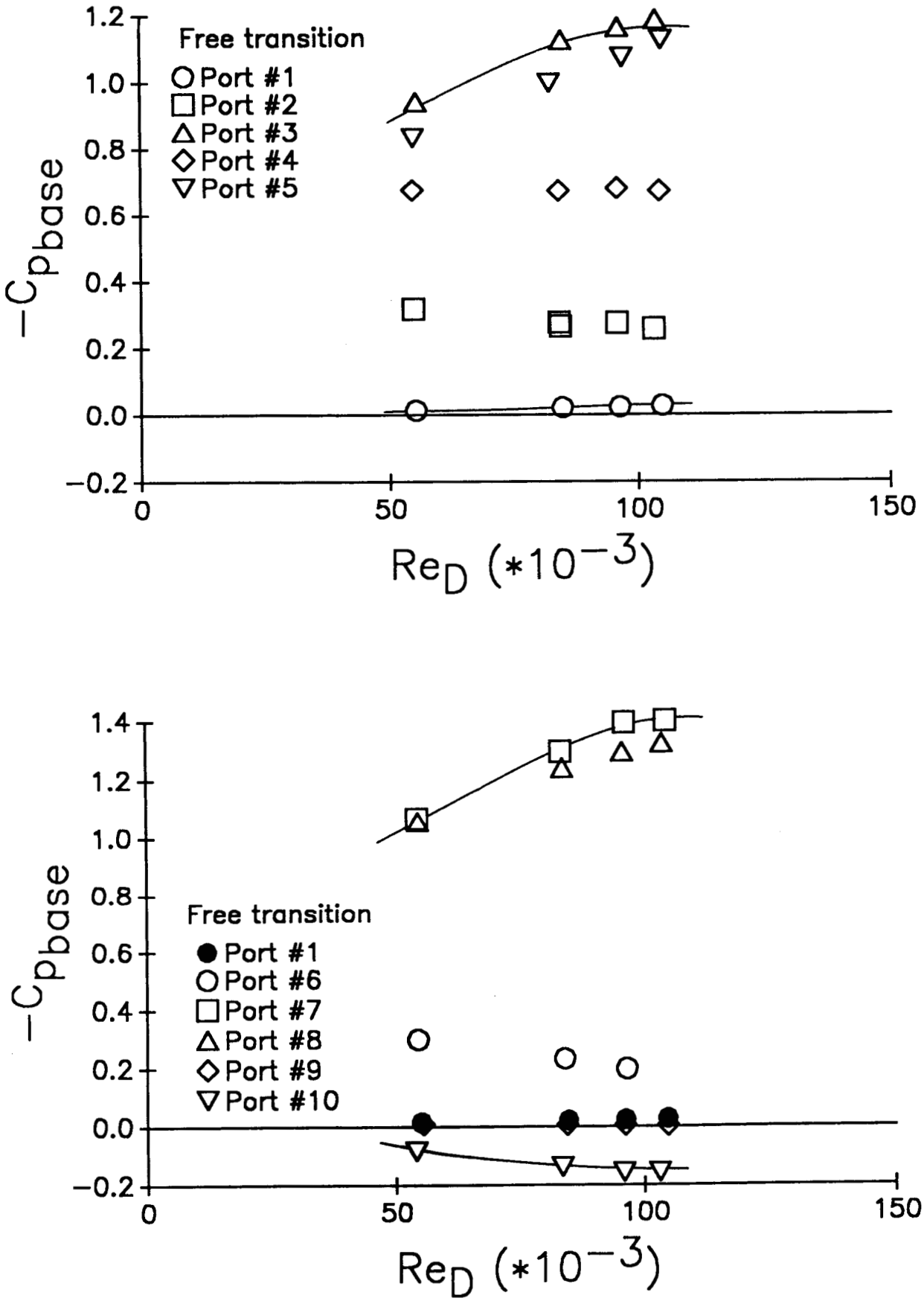


FIGURE 39 - 50 degree base: Base Pressure Coefficients

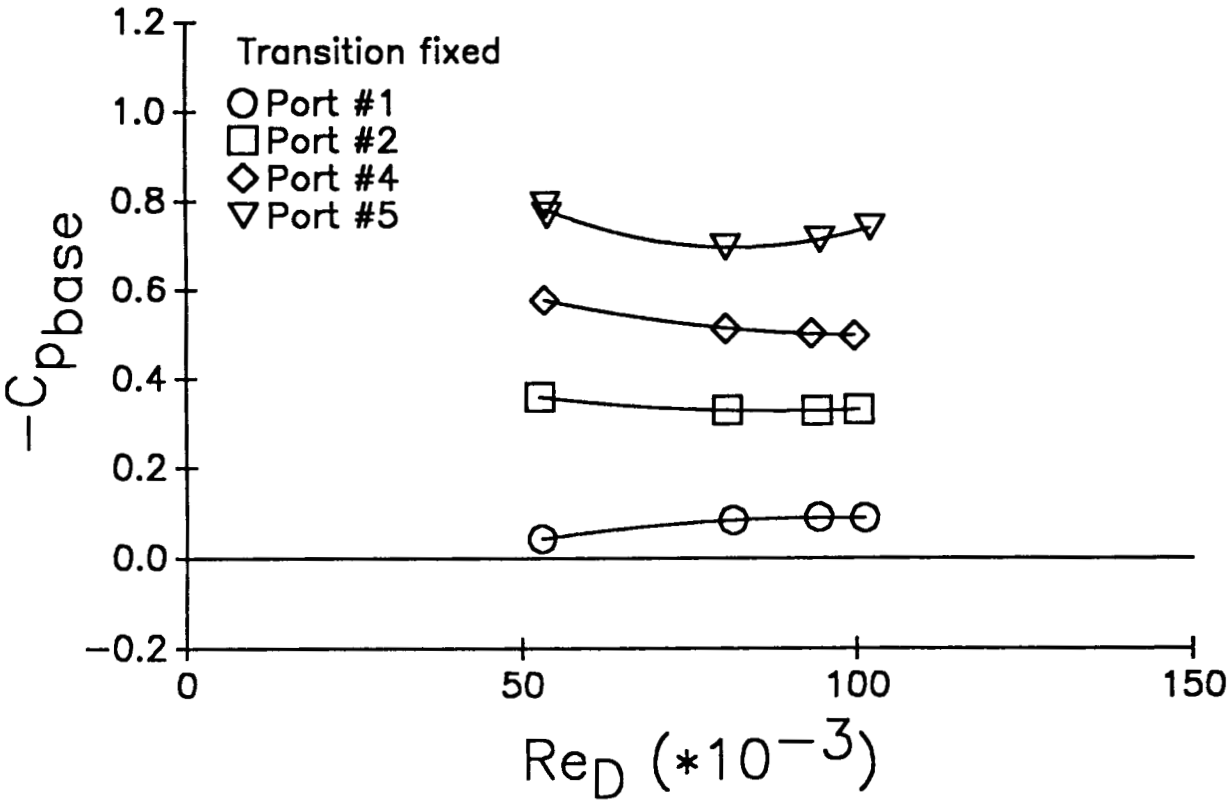


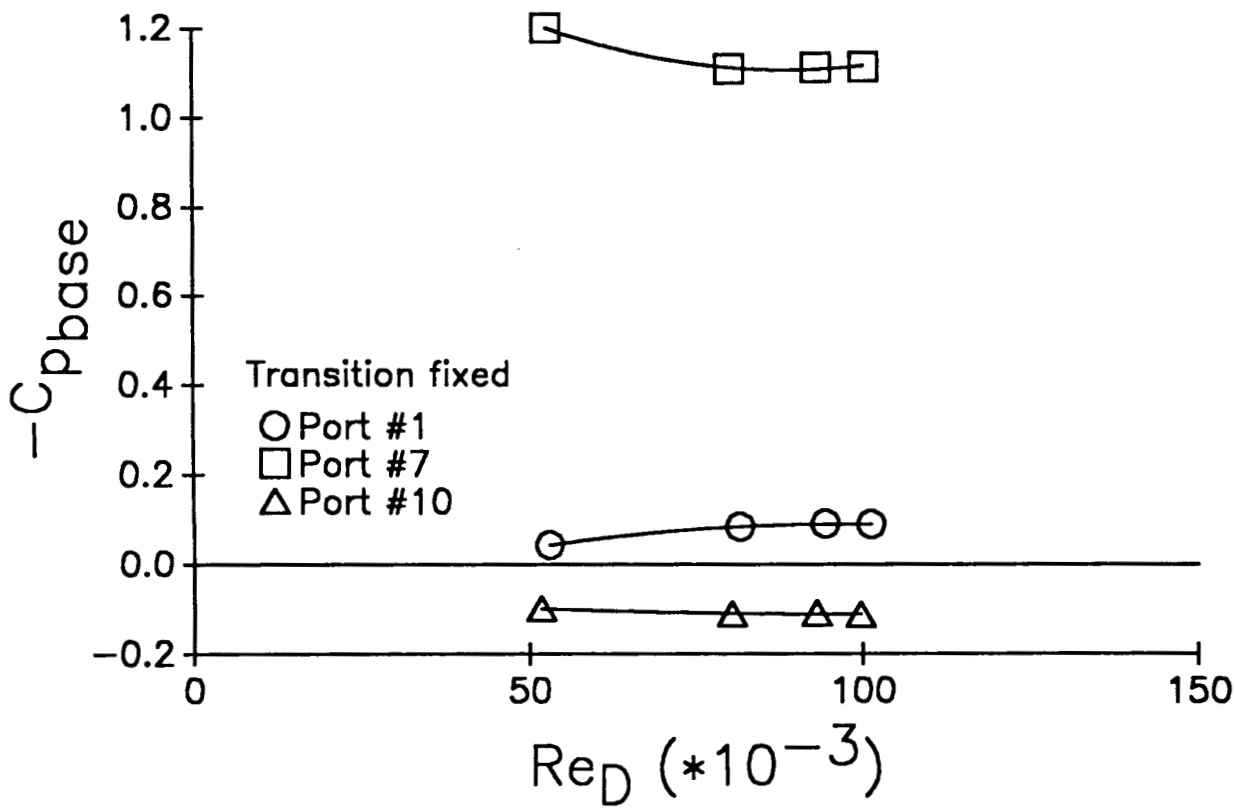


FIGURE 40 - 50 degree base: Base Pressure Coefficients

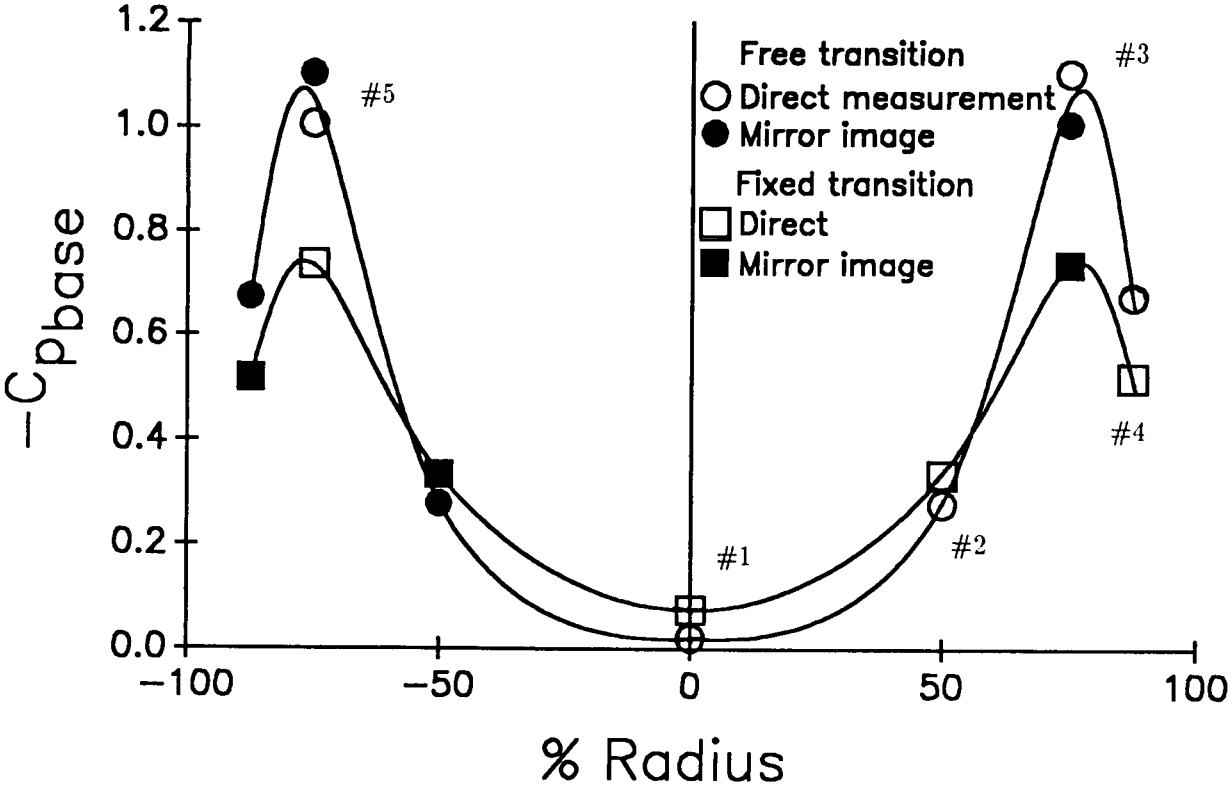


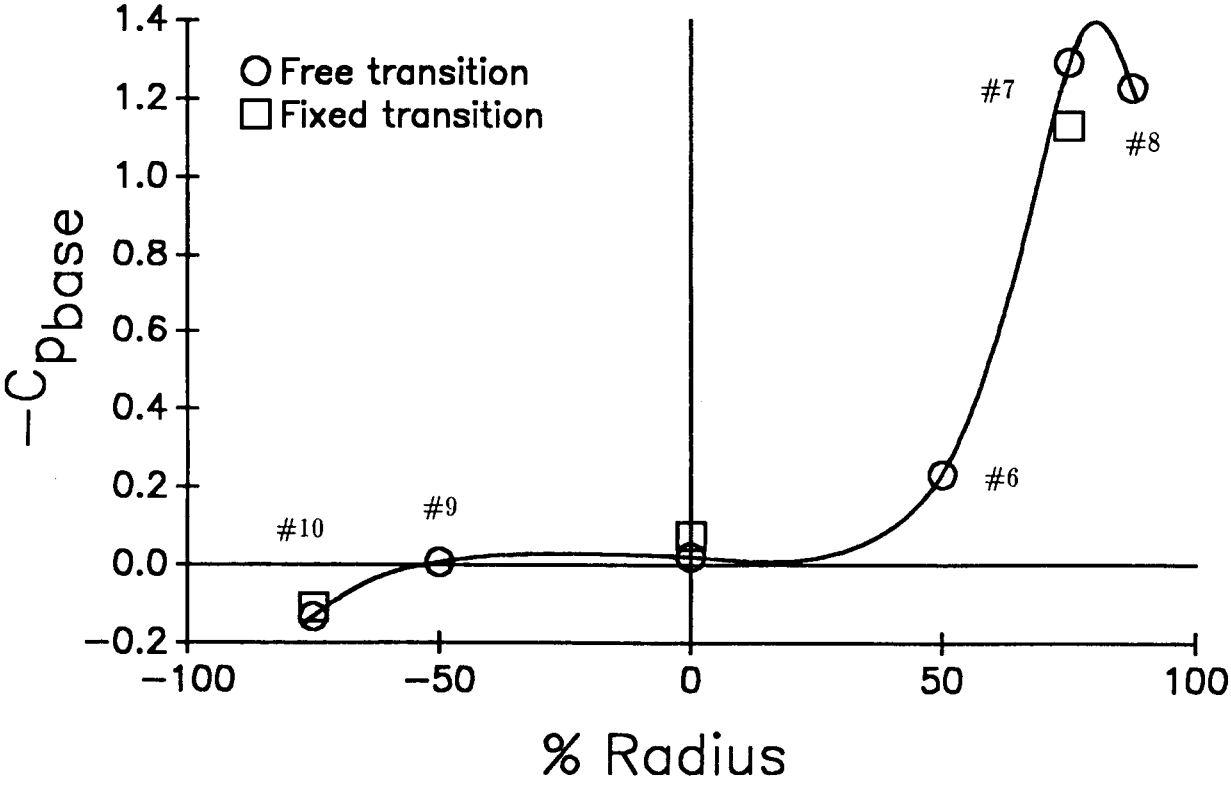


FIGURE 41 - 50 degree base: Base Pressure Coefficients, $Re_D$=94,000

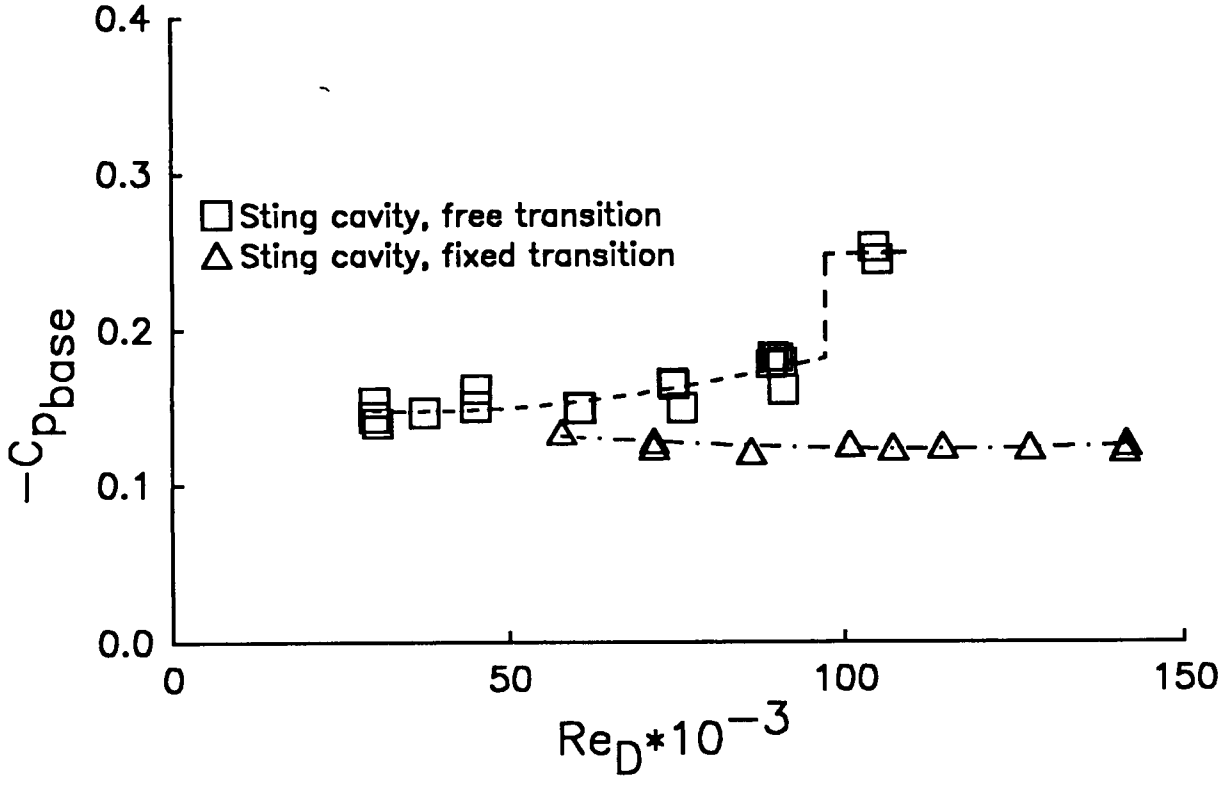


FIGURE 42 - 50 degree base: Sting Cavity Pressures

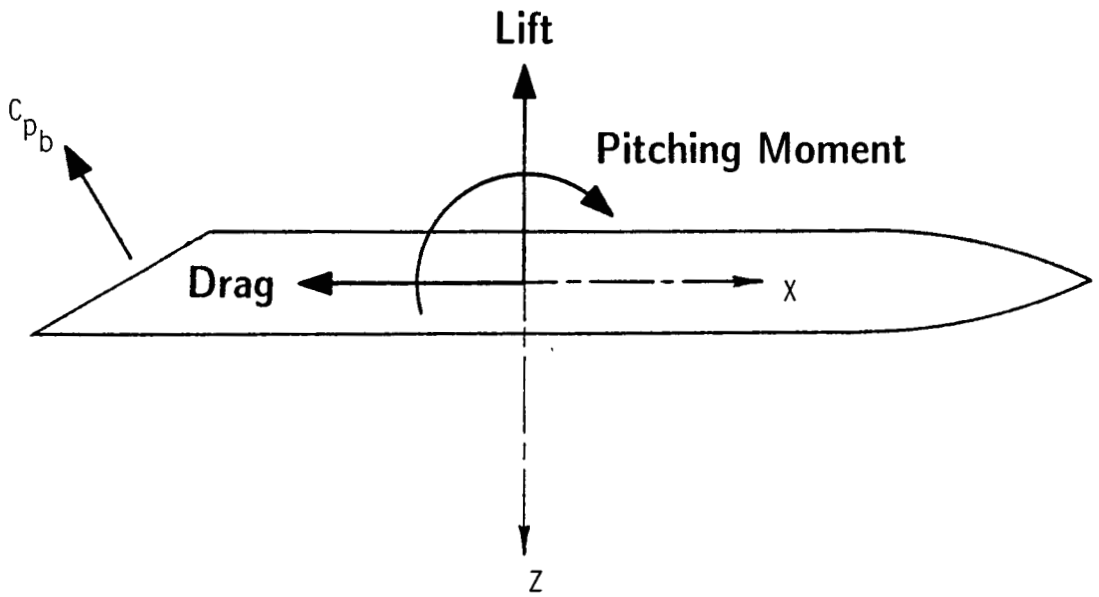


FIGURE 43 - Positive Directions for Lift Forces and Pitching Moments

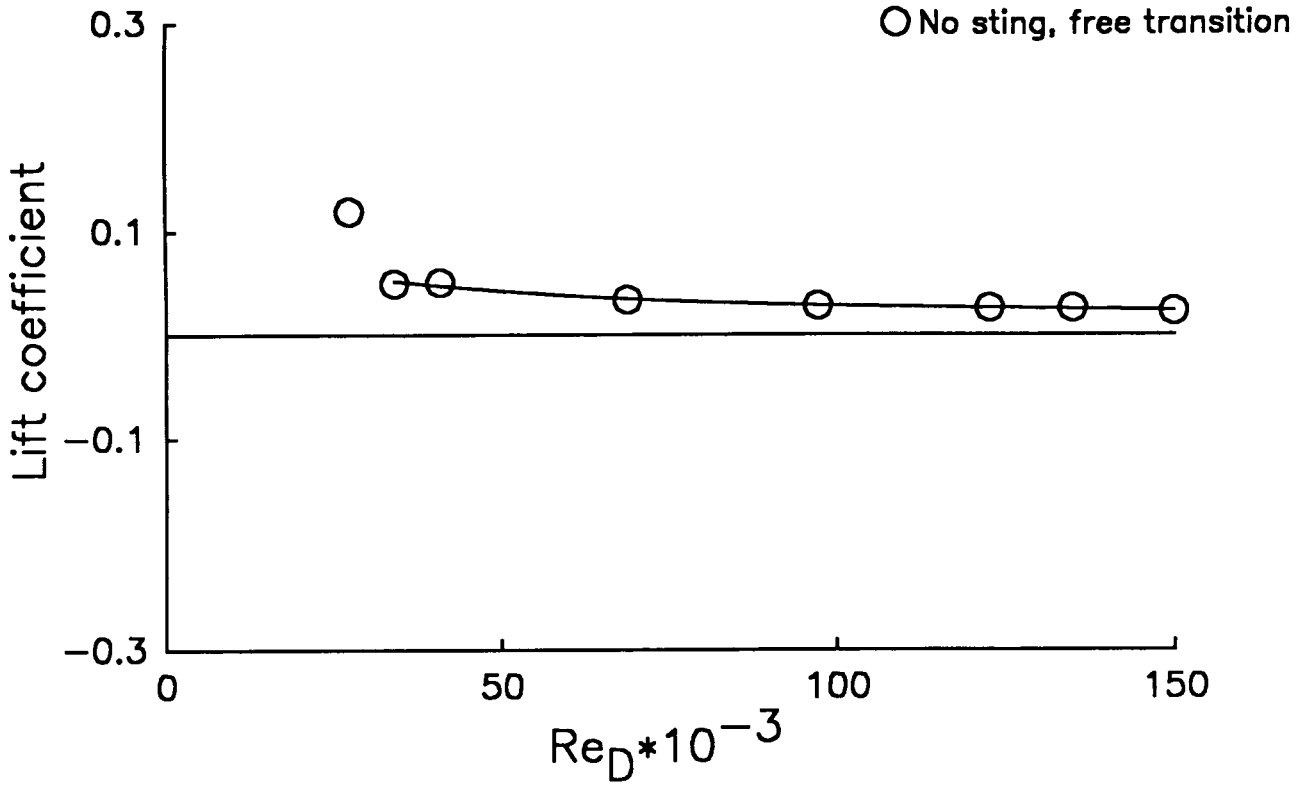


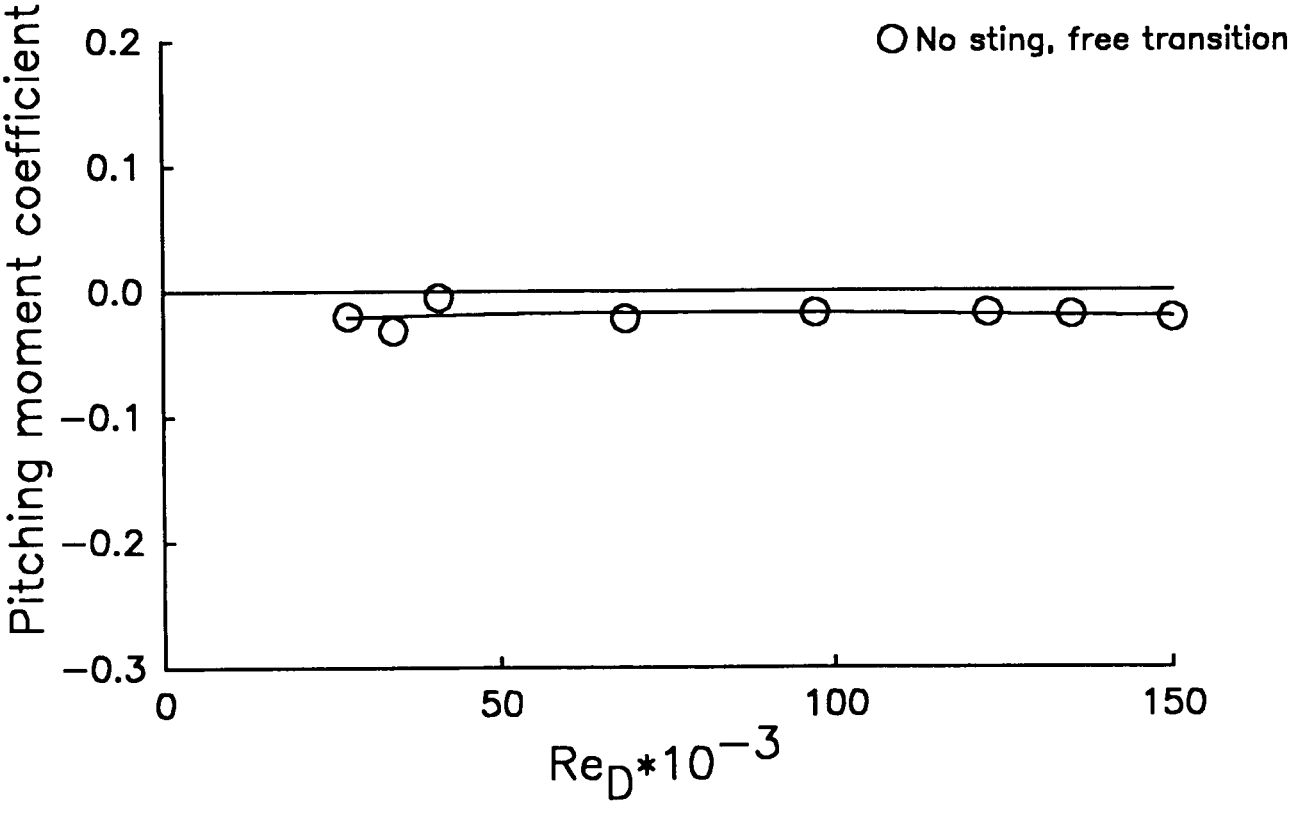


FIGURE 44 - Zero degree base: Lift Force and Pitching Moment

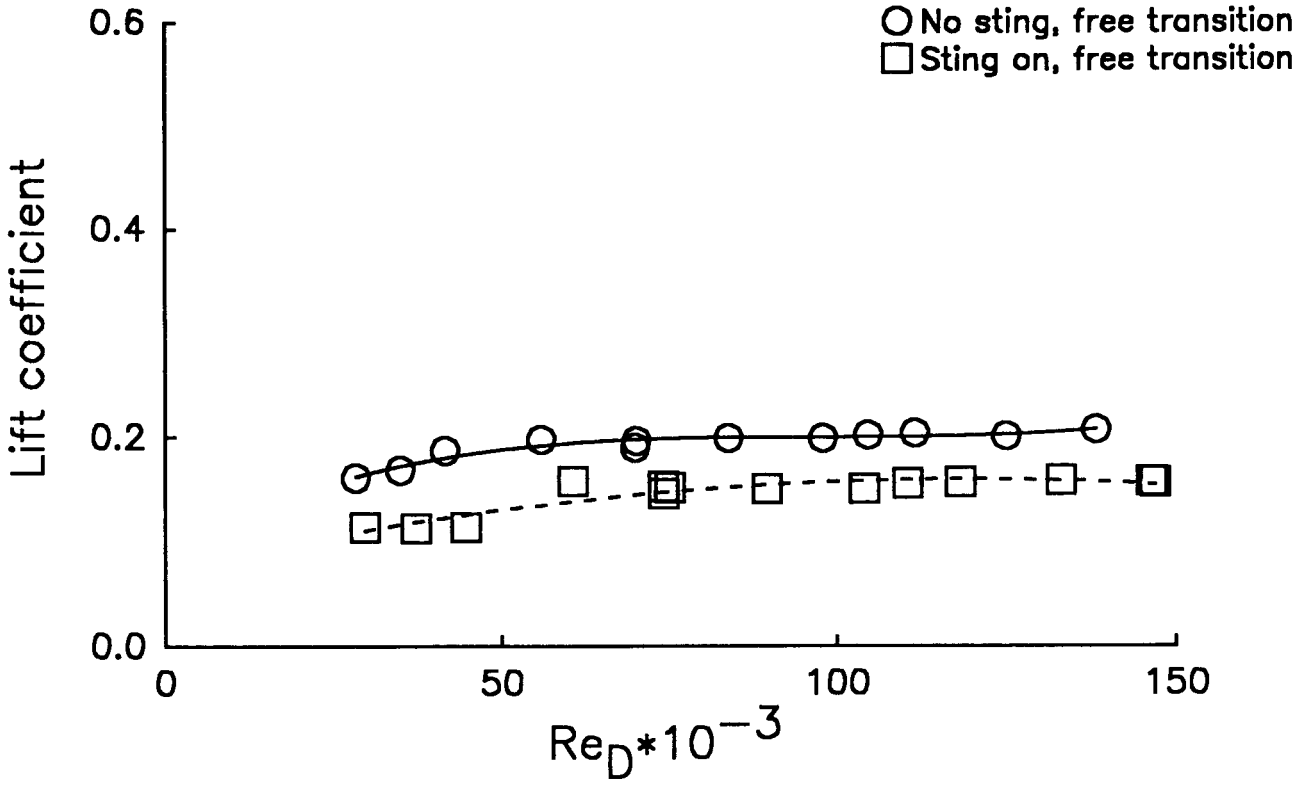


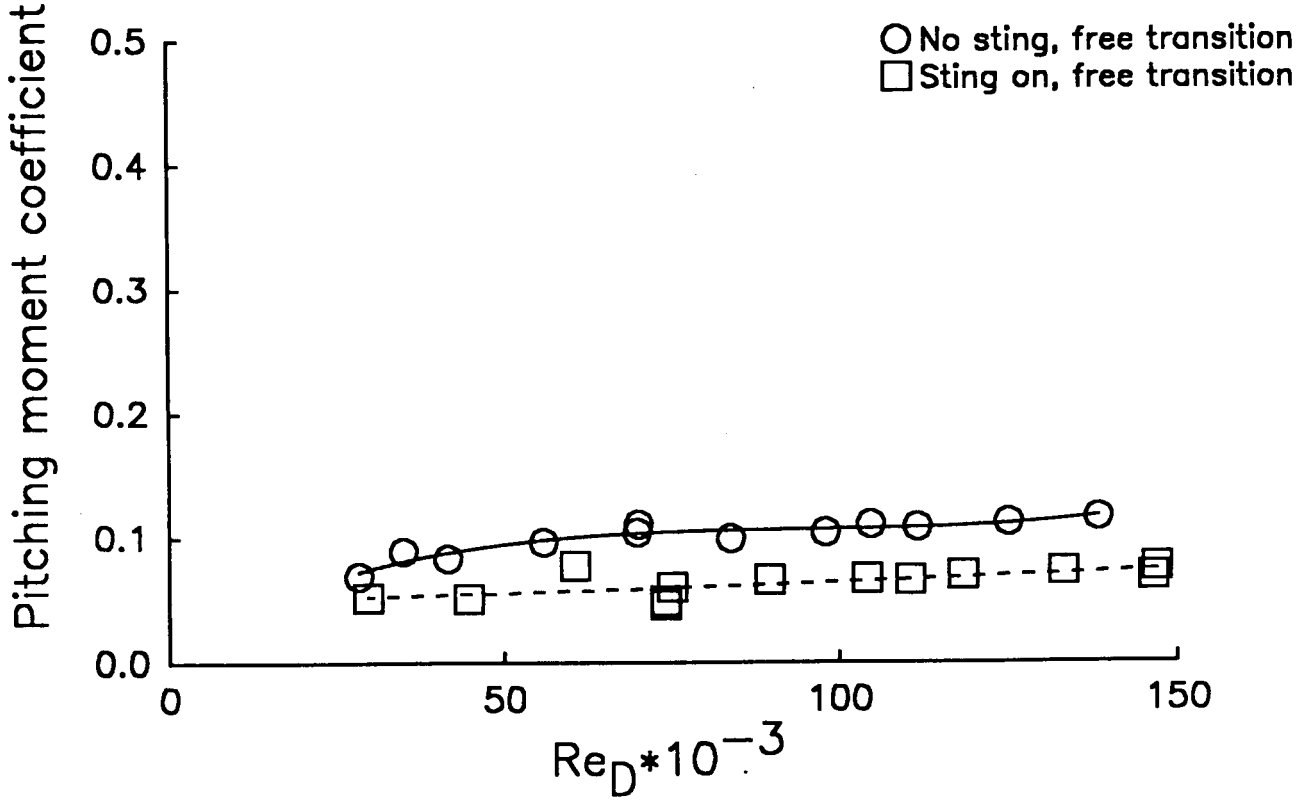


FIGURE 45 - 40 degree base: Lift Force and Pitching Moment

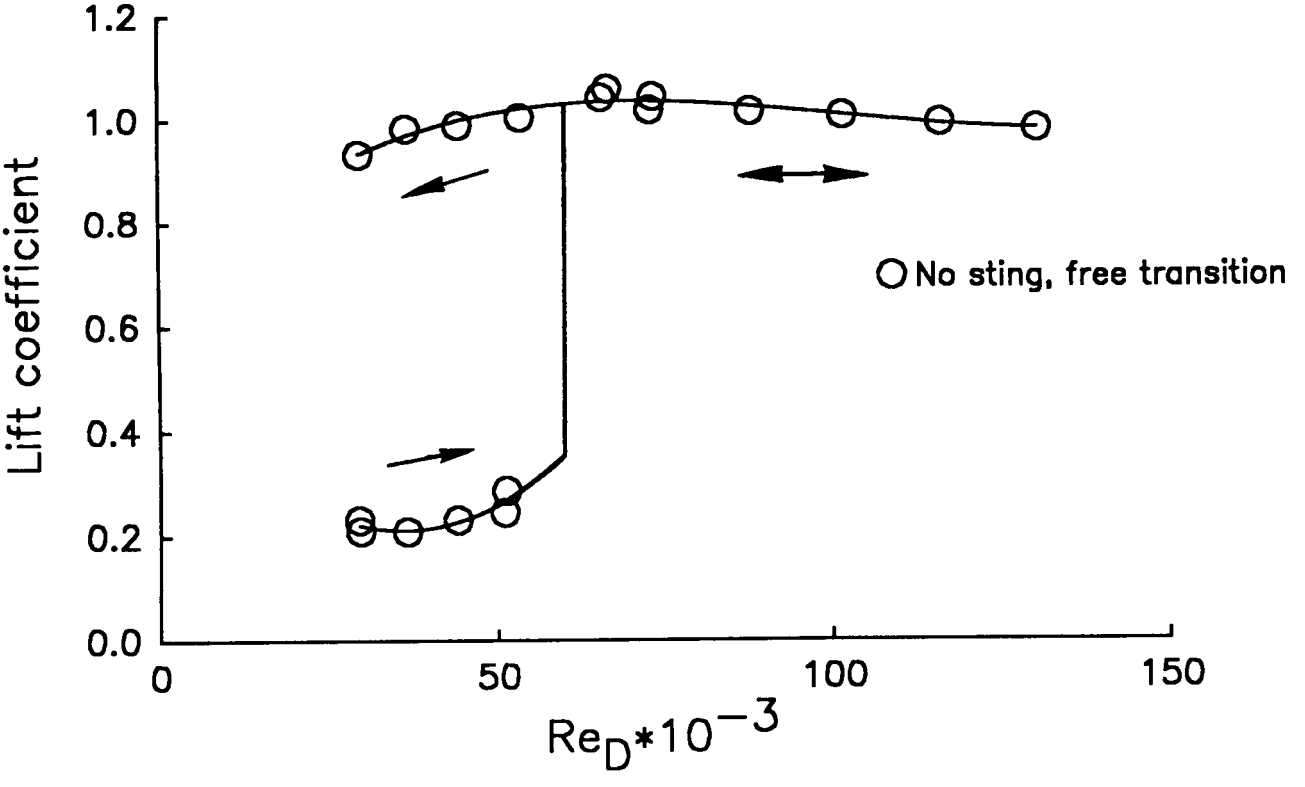


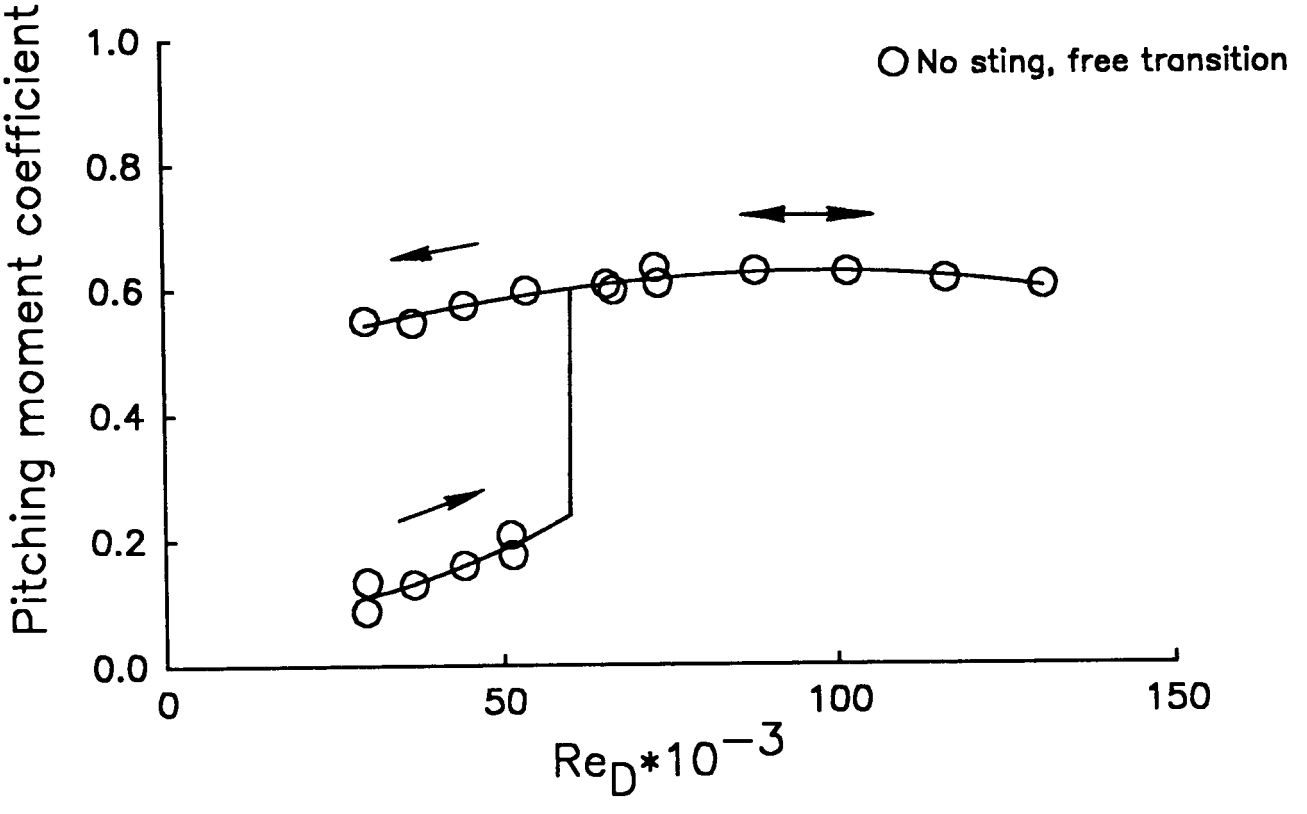


FIGURE 46 - 45 degree base: Lift Force and Pitching Moment

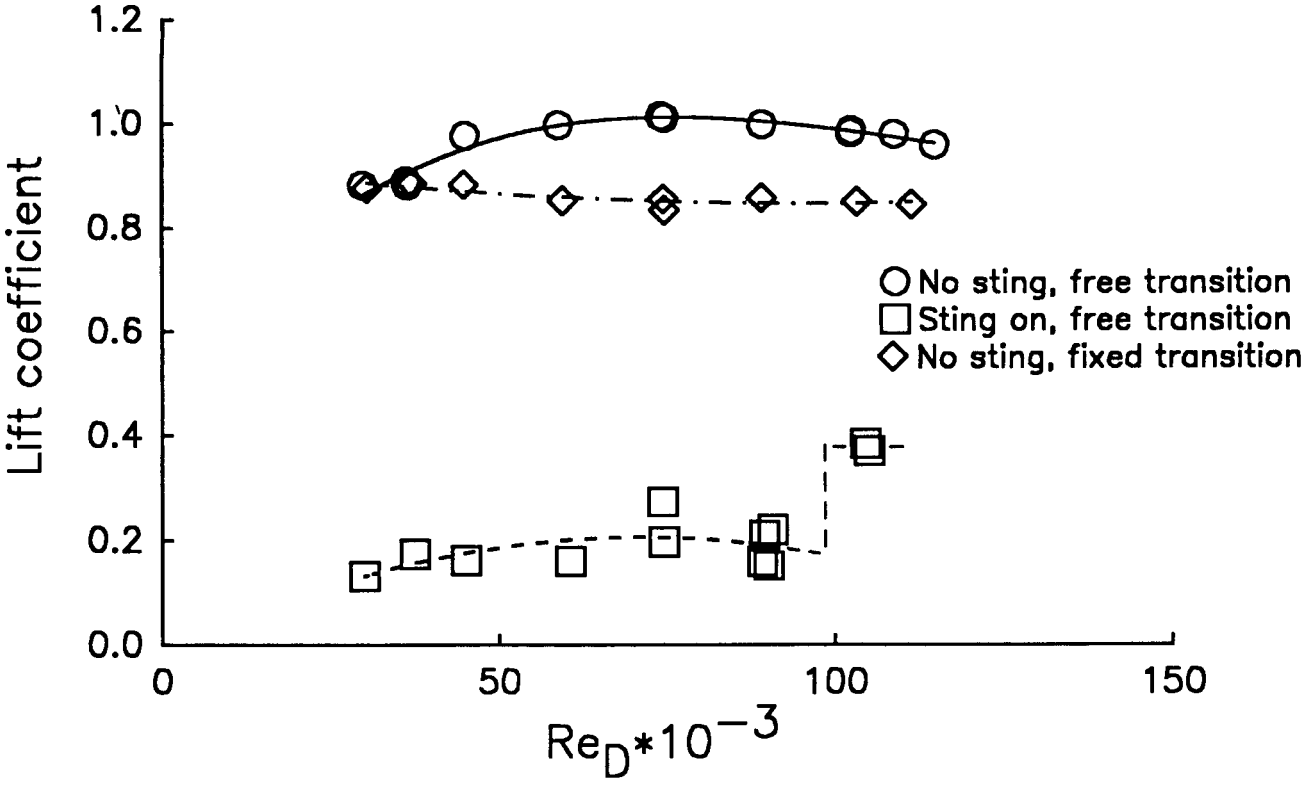


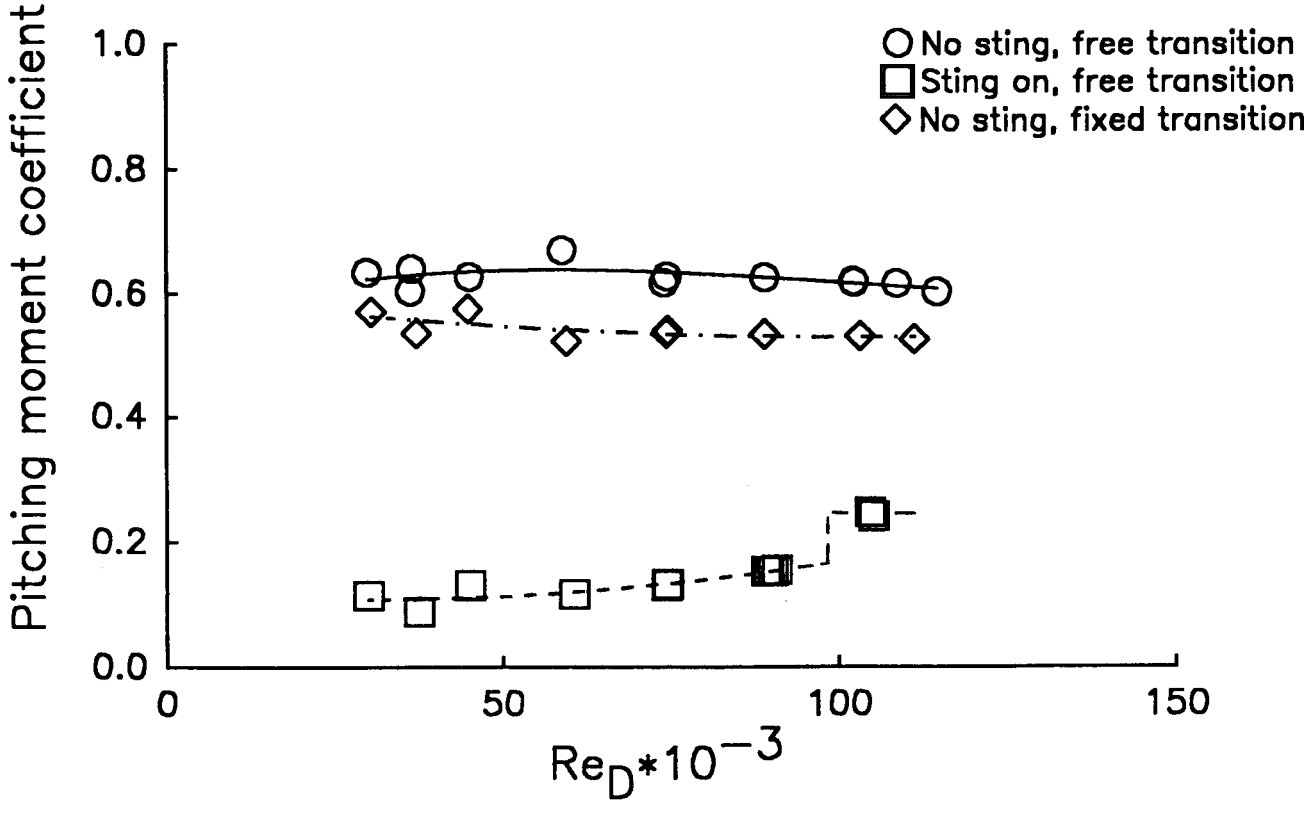


FIGURE 47 - 50 degree base: Lift Force and Pitching Moment

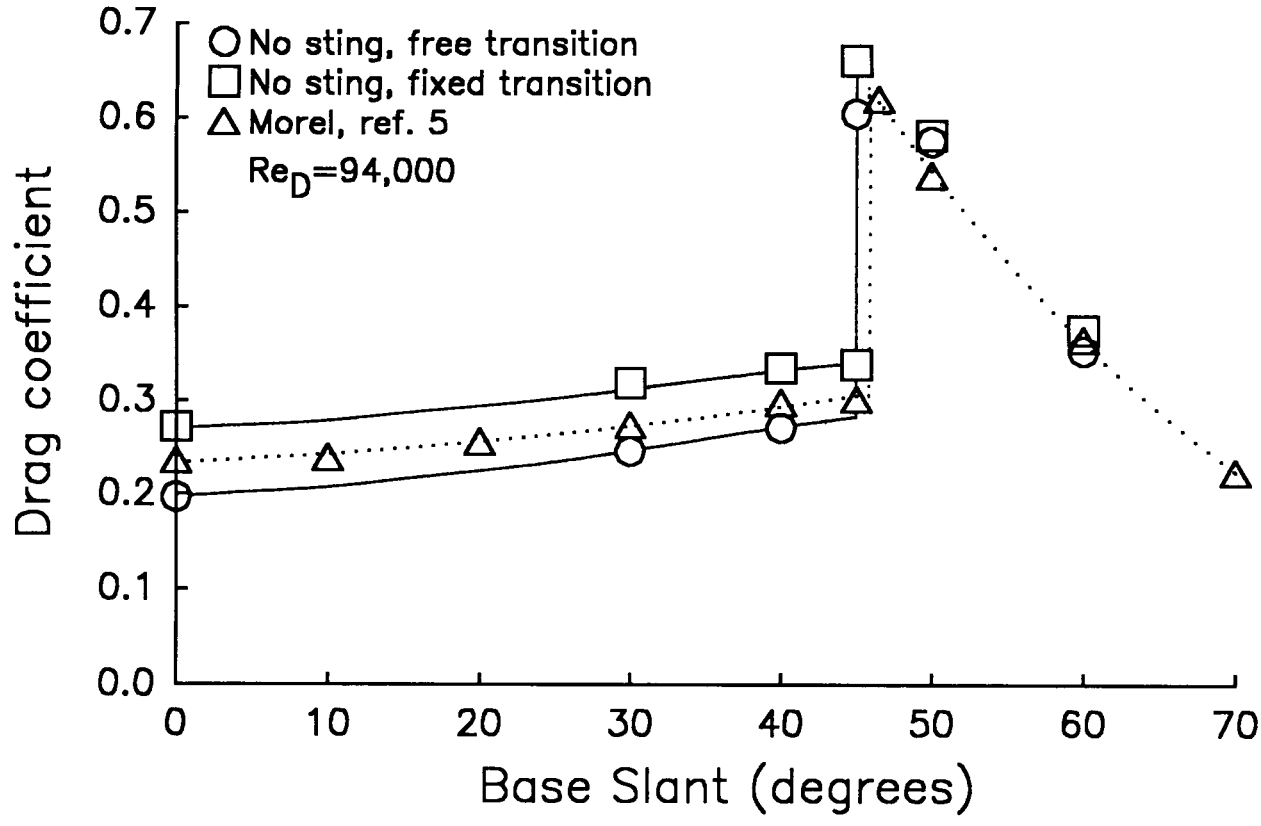


FIGURE 48 - Comparison of Interference-Free MSBS Data

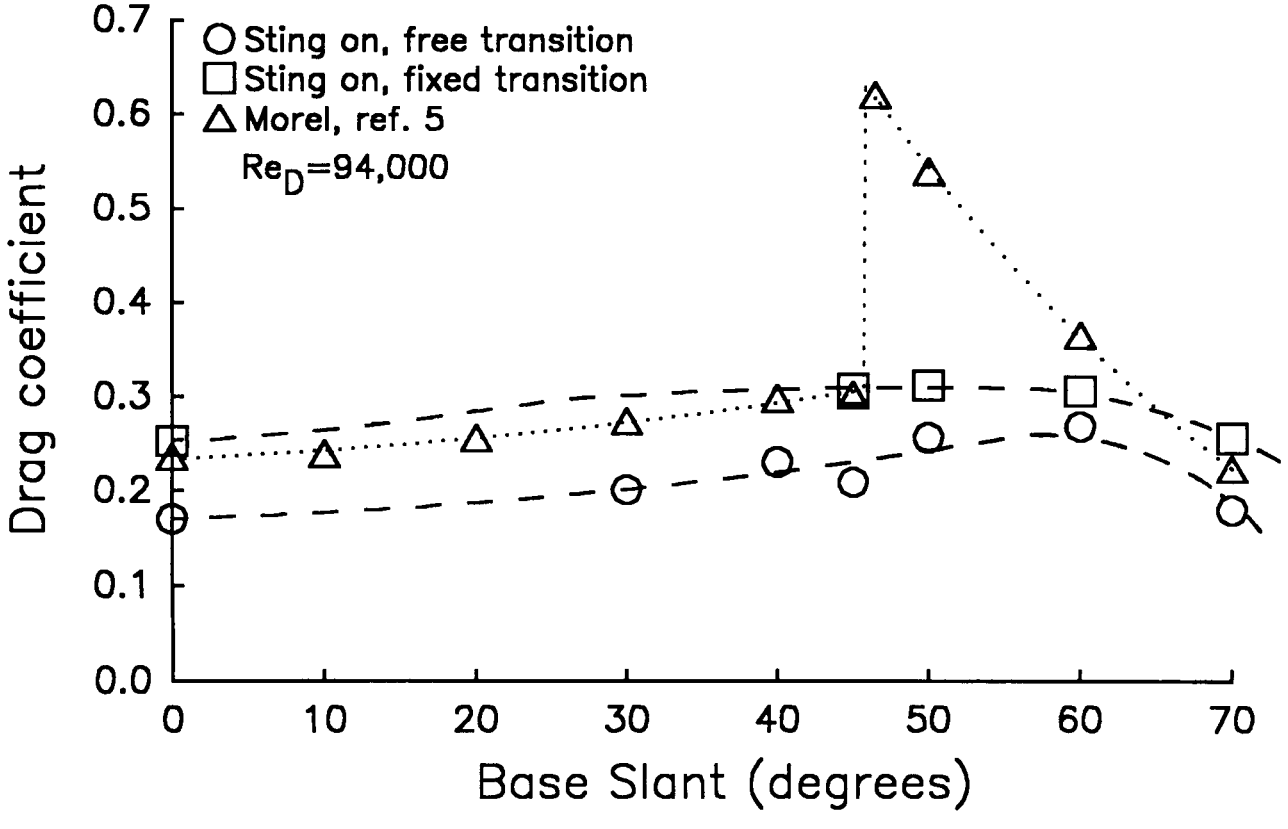


FIGURE 49 - Comparison of Sting-On MSBS Data

# 6. EXPERIMENTAL DIFFICULTIES

## 6.1 BOUNDARY LAYER TRIPPING AT LOW REYNOLDS NUMBERS

It was found that No.60 grit was too fine to ensure proper tripping of the boundary layer at the lower Reynolds's numbers. This is illustrated in Figures 50 and 51, where data from several base slants has been assembled. This is presented as some indication of the sensitivity of the MSBS as a drag measurement tool.

## 6.2 ROLL OSCILLATIONS

The 13 inch MSBS is not equipped with any form of active roll control. Models are generally constructed such that their magnetic and mass centers are offset by some small amount, resulting in weak passive roll stiffness. Models with the higher base slants exhibited a roll oscillation at higher tunnel speeds which is thought to be analogous to the classical slender wing rock phenomena [26]. That is to say, the pair of trailing vortices interact with each other to produce a periodic rolling moment. This phenomena prevented satisfactory measurements at higher speeds with the $50^{o}$ and $60^{o}$ bases. It is noted that under certain conditions, the roll oscillations diverged very rapidly, at other times, a limit cycle was observed.

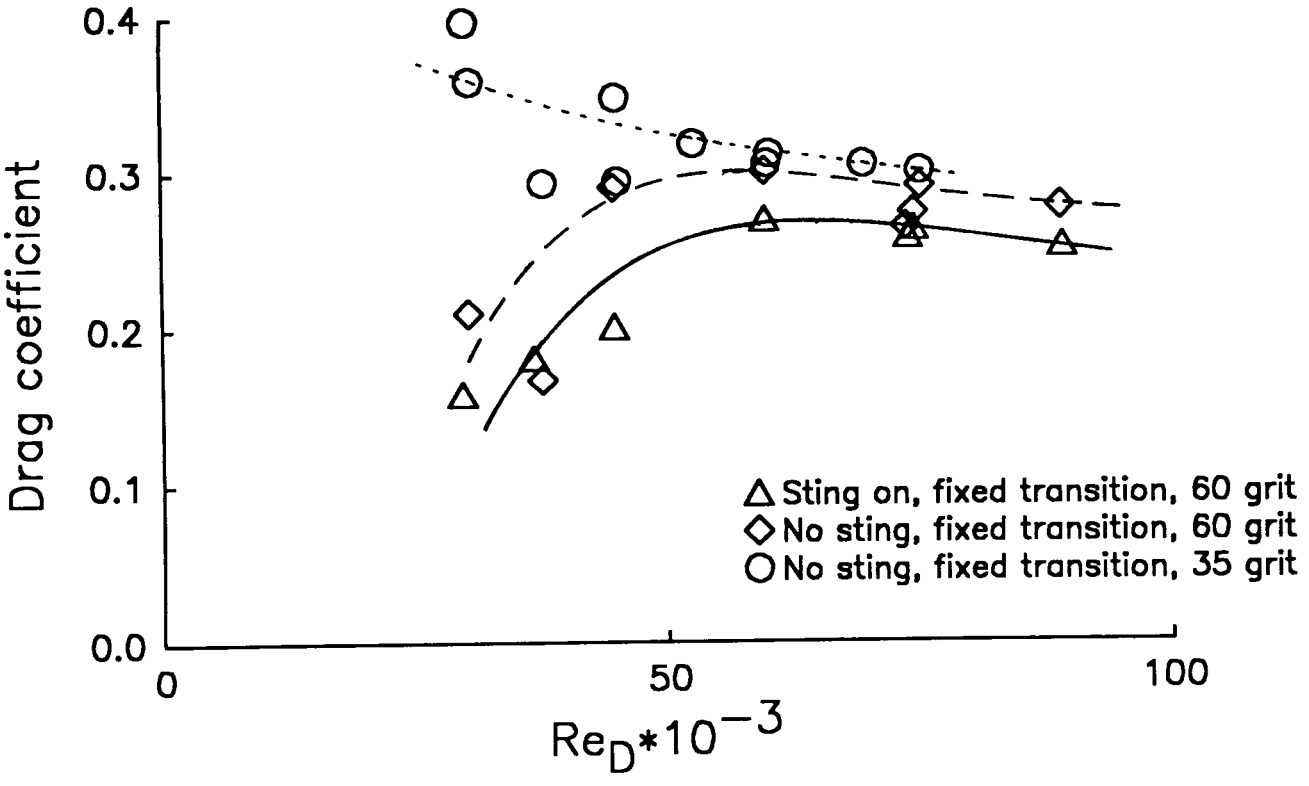


FIGURE 50 - Zero degree base: Drag Coefficients at Low Reynold's Numbers

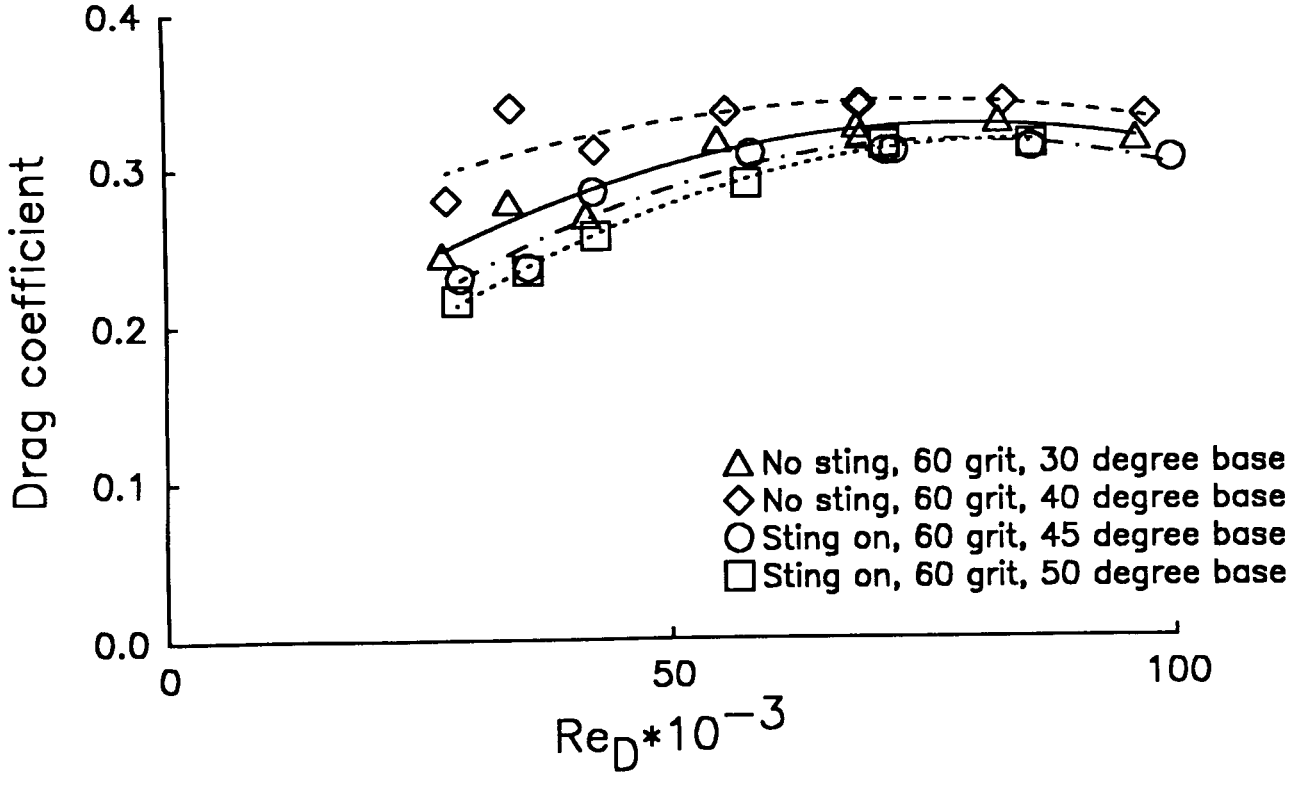


FIGURE 51 - Drag Coefficients at Low Reynold's Numbers

# 7. CONCLUSIONS

Sting interference is detectable for all geometries and under all conditions tested. The magnitudes of the interference can be extremely large. Entirely different wake structures can exist with and without the sting present.

Vortical wakes have been shown to be sensitive to the state of the oncoming boundary layer, with all areodynamic parameters consequently affected.

The 13 inch Magnetic Suspension and Balance System can be used for measurements of multiple aerodynamic components. This is despite the fact that the system's design is very poorly suited to this task (lack of electromagnet symmetry, freely magnetized iron cores) and despite many hardware problems.

REFERENCES


1. Carter, E.C.: Some Measurements of the Interference of a Sting Support on the Pressure Distribution on a Rear Fuselage and Tailplane at Subsonic Speeds. ARA Wind Tunnel Note No.67, 1967.
2. MacWilkinson, D. G.; Blackerby, W.T.; Paterson, J.H.: Correlation of Full-Scale Drag Predictions with Flight Measurements on the C-141A Aircraft - Phase II, Wind Tunnel Test, Analysis and Prediction Techniques. Volume 1 - Drag Predictions, Wind Tunnel Data Analysis and Correlation. NASA CR-2333, February 1974.
3. Clark, R.D.; Rosenstein, H.J.: Analytical and Experimental Methods Used to Resolve the Aerodynamic Results of Tests Conducted in Three Test Facilities. AGARD Conference on Aerodynamic Data Accuracy and Quality Requirements and Capabilities in Wind Tunnel Testing, CP-429. September-October 1987.
4. Carter, E.C.: Interference Effects of Model Support Systems. AGARD-R-601, April 1973.
5. Carlin, G.J.; Bevan, D.: Prediction of Subsonic Wind Tunnel Mounting System Interference. AIAA Journal of Aircraft, May 1987.
6. Pope, A.; Goin, K.L.: High Speed Wind Tunnel Testing. © Wiley 1965.
7. Lynch, F.T.; Patel, D.R.: Some Important New Instrumentation Needs and Testing Procedure Requirements for Testing in a Cryogenic Wind Tunnel such as NTF. AIAA 12th Aerodyunamic Testing Conference, March 1982.
8. Morel, T.: Effect of Base Slant on the Flow Patterns and Drag of Three-Dimensional Bodies with Blunt Ends. Symposium on Aerodynamic Drag Mechanisms of Bluff Bodies and Road Vehicles, September 1976. © Plenum Press 1978.
9. Xia, X.J.; Bearman, P.W.: An Experimental Investigation of the Wake of an Axisymmetric Body with a Slanted Base. Aeronautical Quarterly, February 1983.
10. Tanner, M.: Empirical Formulae for the Prediction of the Base Pressure of Missile Bodies at Subsoinc Velocities. European Space Agency TT-893, January 1985.
11. Lee, G.; Summers, J.L.: Effects of Sting Support Interference on the Drag of an Ogive-Cylinder Body with and without a Boattail at 0.6 to 1.4 Mach number. NACA RM-A57I09, December 1957.
12. Wolfe, W.P.; Oberkampf, W.L.: A Design Method for the Flow Field and Drag of Bodies of Revolution in Incompressible Flow. AIAA 9th Atmospheric Flight Mechanics Conference, August 1982.
13. Porteiro, J.L.F.; Page, R.H.; Przirembel, C.E.G.; Fletcher, L.S.: A Study of the Near Wake behind an Axisymmetric Body. 14th International Symposium on Space Technology and Science. 1984.
14. Maull, D.J.: The Drag of Slant-Based Bodies of Revolution. Aeronautical Journal, June 1980.
15. Alcorn, C.W.; Britcher, C.P.: An Experimental Investigation of the Aerodynamic Characteristics of

Slanted-Base Ogive-Cylinder Models using Magnetic Suspension Technology. AIAA 15th Aerodynamic Testing Conference, May 1988.

16. Alcorn, C.W.: An Experimental Investigation of the Aerodynamic Characteristics of Slanted-Base Ogive-Cylinders using Magnetic Suspension Technology. NASA CR-181708, November 1988.
17. Boyden, R.P.; Britcher, C.P.; Tcheng, P.: Status of Wind Tunnel Magnetic Suspension Research. SAE TP-851898, October 1985.
18. Tcheng, P.; Schott, T.D.: A five-component electro-optical positioning system. ICIASF '87 Record, June 1987.
19. Britcher, C.P.; Goodyer, M.J.; Eskins, J.; Parker, D.; Halford, R.J.: Digital Control of Wind Tunnel Magnetic Suspension and Balance Systems. ICIASF'87 Record, June 1987.
20. Johnson, W.G.Jr.; Dress, D. A.: The 13-Inch Magnetic Suspension and Balance System Wind Tunnel. NASA TM-4090, January 1989.
21. Tcheng, P.; Schott, T.D.: A Miniature Infra-red Pressure Telemetry System. 34th International Instrumentation Symposium, May 1988.
22. Batchelor, G.K.: Interference on Wings, Bodies and Airscrews in a Closed Octagonal Section. Report ACA-5, March 1944.
23. Garner, H.C.; Rogers, E.W.E.; Acum, W.E.A.; Maskell, E.C.: Subsonic Wind Tunnel Wall Corrections. AGARDograph 109, October 1966.
24. Dress, D.A.: Drag measurements on a laminar-flow body of revolution in the 13-inch Magnetic Suspension and Balance System. NASA TP-2895, April 1989.
25. Johnson, J.L.; Grafton, S.B.; Yip, L.P.: Experimental investigation of the effect of vortex bursting on the high angle-of-attack lateral/directional stability characteristics of highly swept wings. AIAA 11th Aerodynamic Testing Conference, March 1980.
26. Konstadinopoulos, P.; Mook, D.T.; Nayfel, A.H.: Subsonic wing rock of slender delta wings. AIAA 23rd Aerospace Sciences Meeting, January 1985.

Acknowledgements

This work was supported by NASA Langley Research Center under Grant NAG-1-716, Richmond P. Boyden, Technical Monitor. The authors would like to express appreciation for assistance given by David Dress of the High Reynolds Number Aerodynamics Branch, with pressure instrumentation and data acquisition; also Timothy Schott and Paul Roberts of the Instrument Research Division, with pressure telemetry and sting contact circuitry respectively.

# Appendix A

Model Construction Details

Additional details of pressure model may be found in Reference 16)

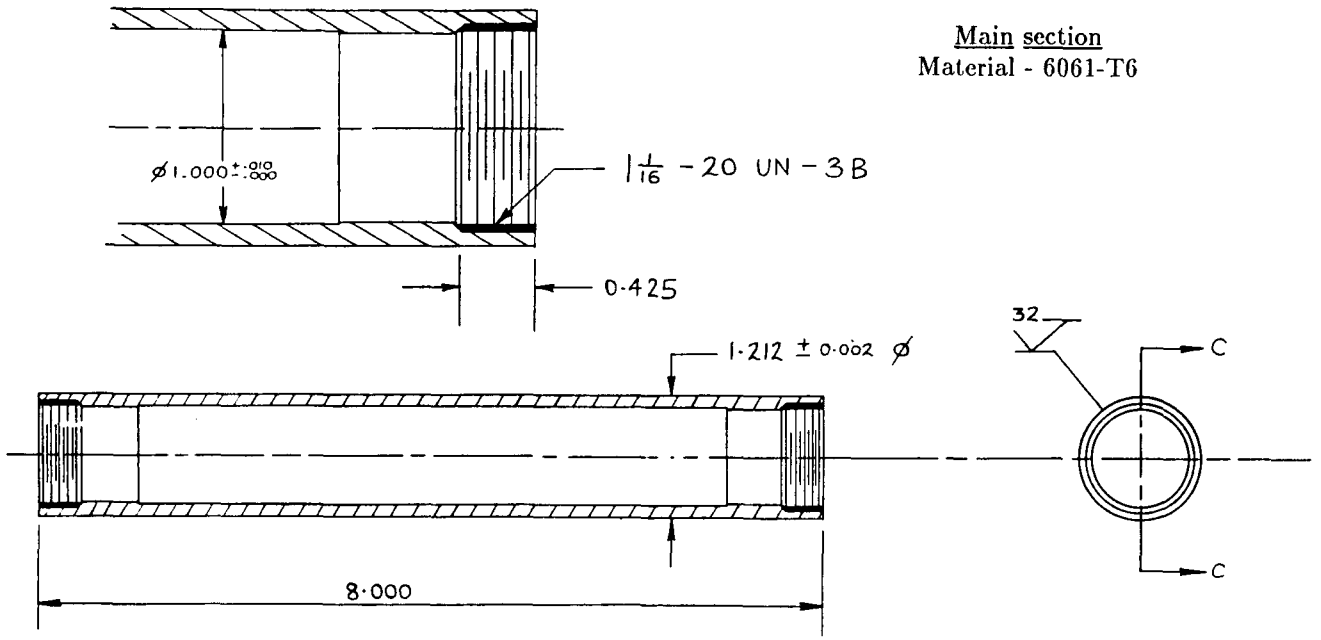


Main section
Material - 6061-T6

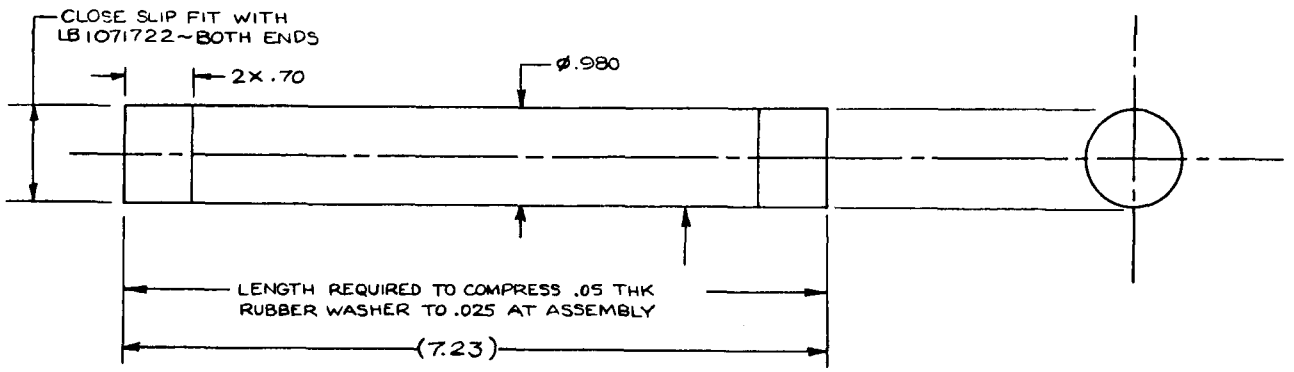


Magnetic core
Material - Magneform C

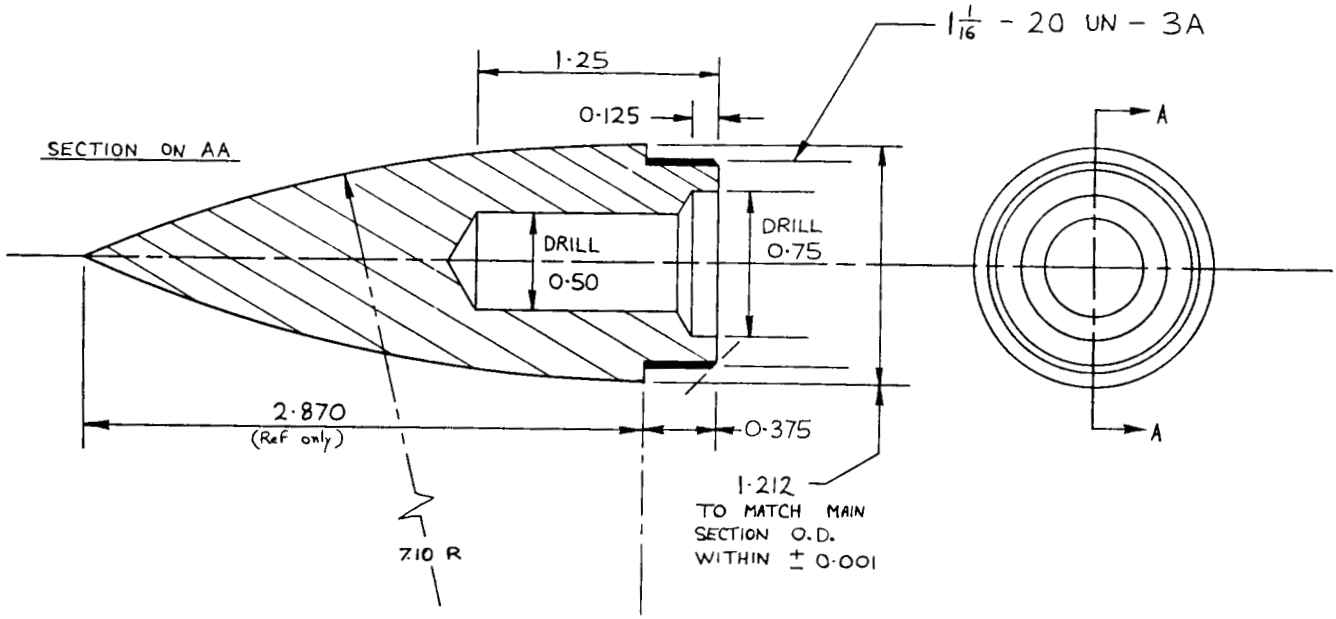


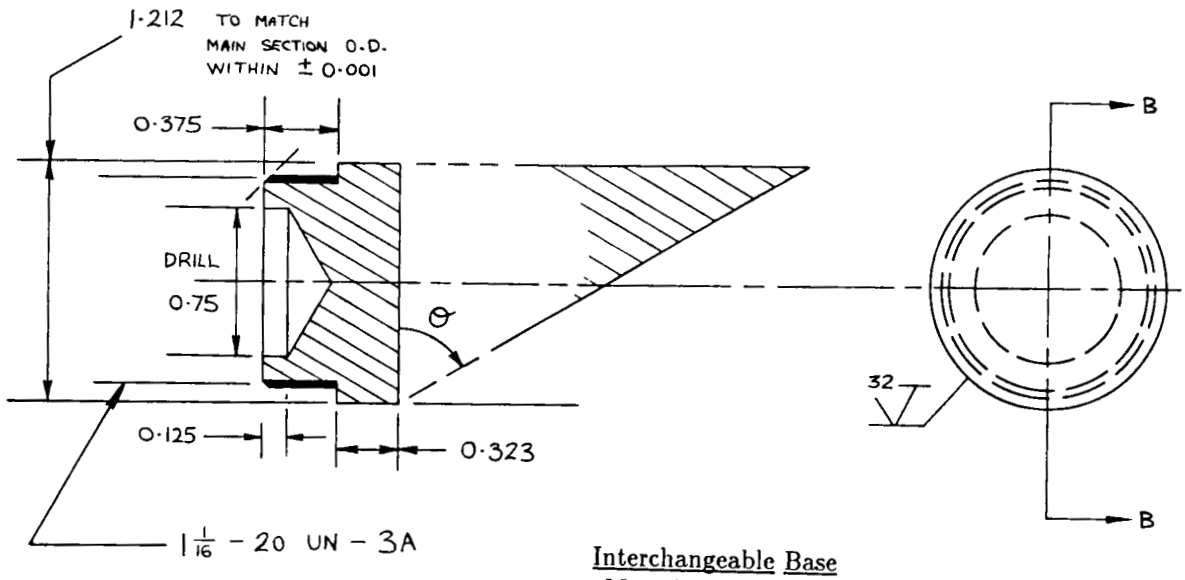


Interchangeable Base
Material - 6061-T6

# Appendix B

Plates

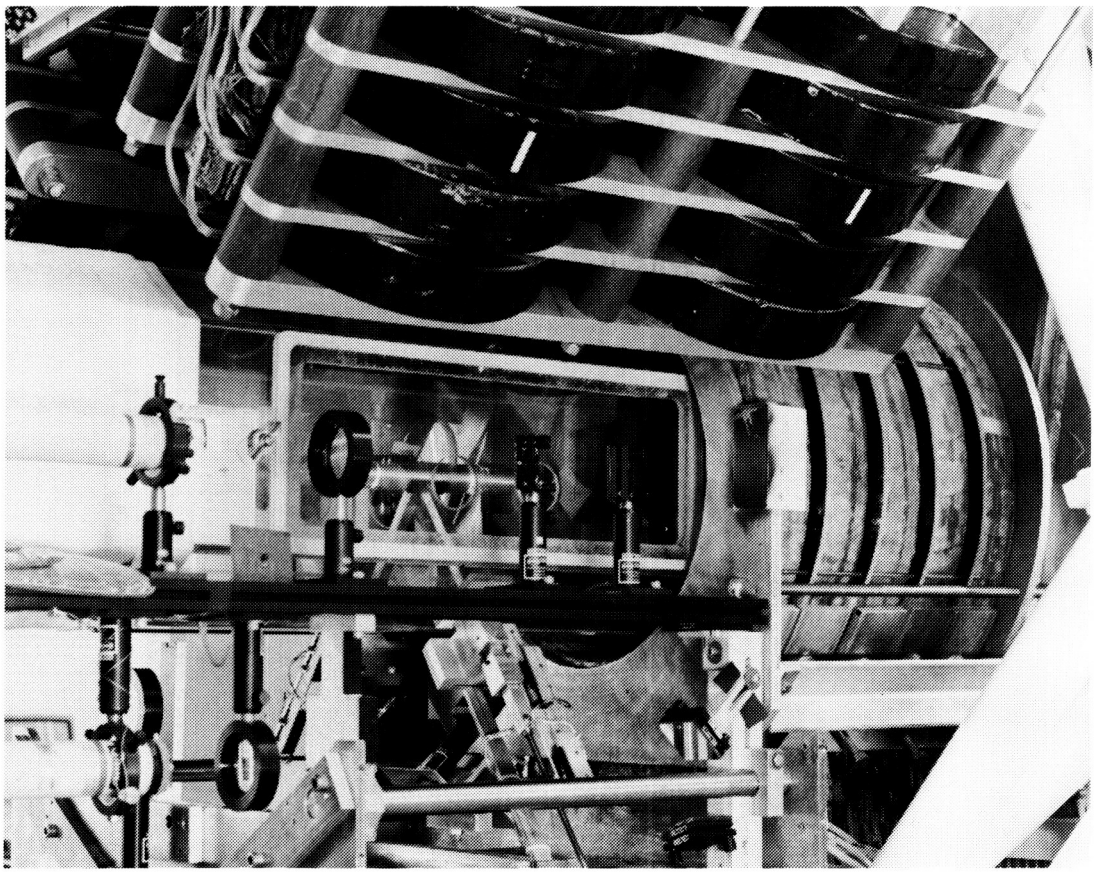

PLATE A - General View of MSBS

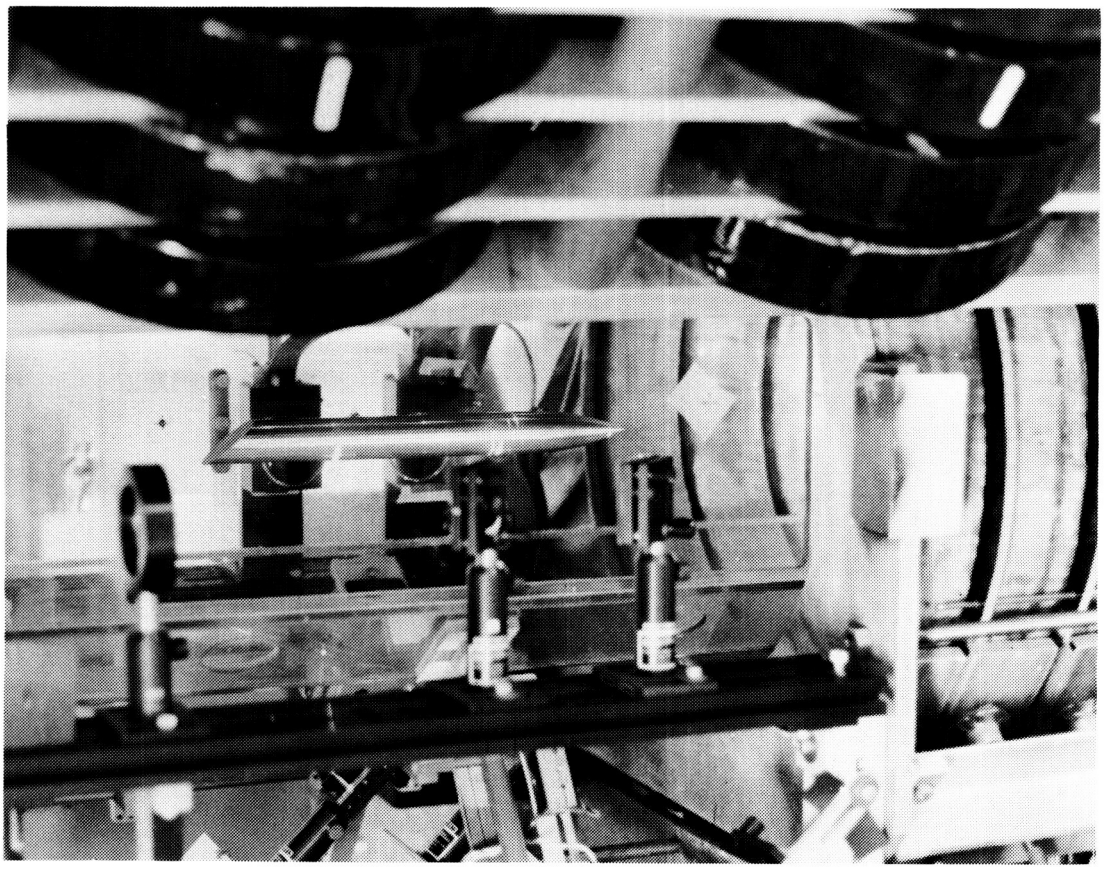

PLATE B - Close-up of Test Section with Slanted-Base Model in Suspension

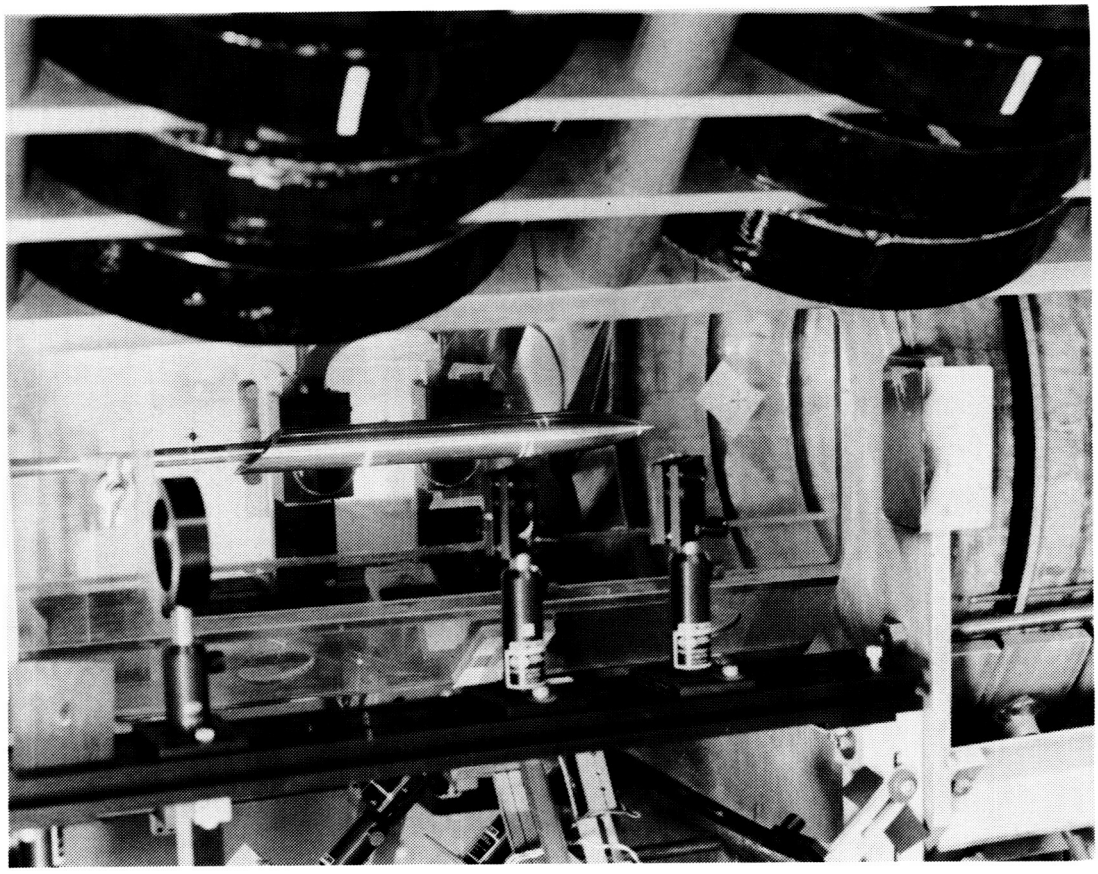

PLATE C - Slanted-Base Model with Dummy Sting Installed

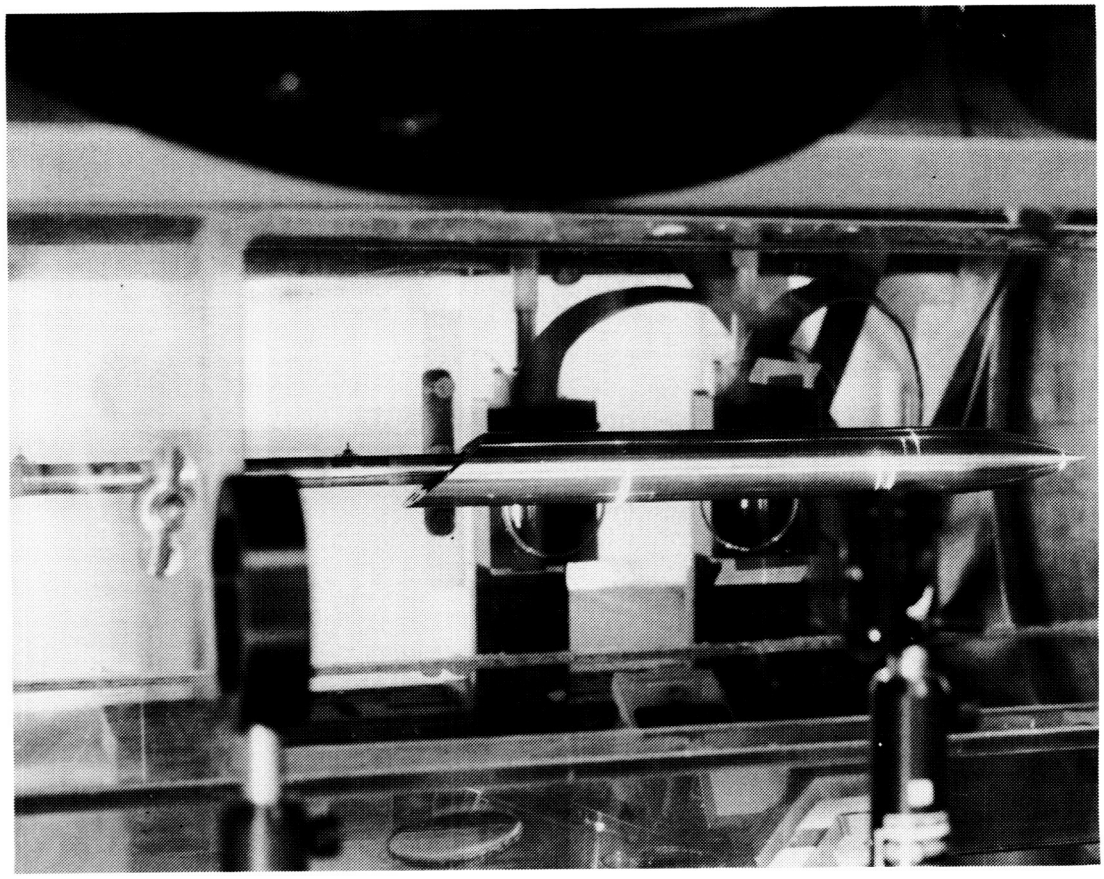

PLATE D - Close-up showing Sting Entry into Suspended Model

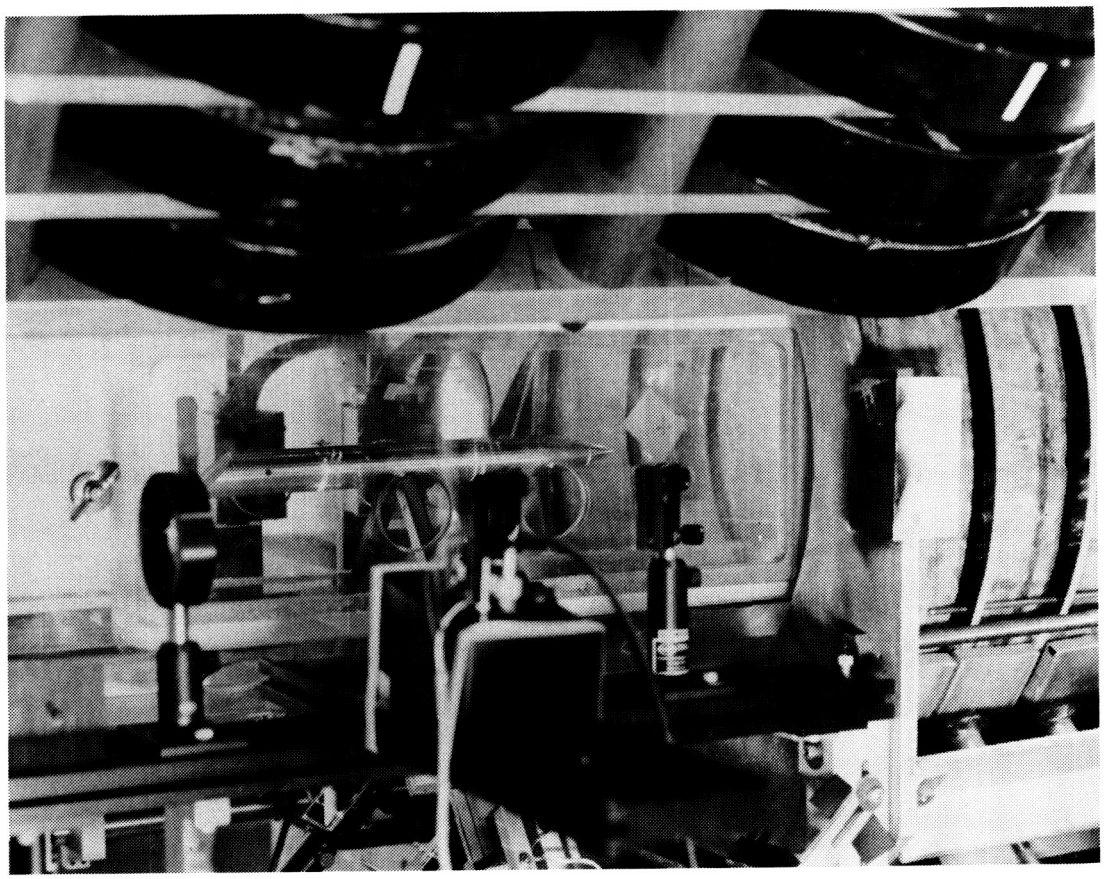

PLATE E - Set-up for Base Pressure Telemetry

NASA
National Aeronautics and Space Administration

# Report Documentation Page

| 1. Report No. | 2. Government Accession No. | 3. Recipient's Catalog No. |
|---|---|---|
| NASA CR-4299 | | |

**4. Title and Subtitle**

Subsonic Sting Interference on the Aerodynamic Characteristics of a Family of Slanted-Base Ogive-Cylinders

**5. Report Date**

June 1990

**6. Performing Organization Code**

**7. Author(s)**

Colin P. Britcher, Charles W. Alcorn, and W. Allen Kilgore

**8. Performing Organization Report No.**

**10. Work Unit No.**

505-61-91-03

**9. Performing Organization Name and Address**

Old Dominion University
Department of Mechanical Engineering and Mechanics
Norfolk, VA 23508

**11. Contract or Grant No.**

NAG1-716

**13. Type of Report and Period Covered**

Contractor Report

**12. Sponsoring Agency Name and Address**

National Aeronautics and Space Administration
Langley Research Center
Hampton, VA 23665-5225

**14. Sponsoring Agency Code**

**15. Supplementary Notes**

Principal Investigator: Dr. Colin P. Britcher
Langley Technical Monitor: Richmond P. Boyden

**16. Abstract**

Support interference-free drag, lift, and pitching moment measurements on a range of of slanted-base ogive-cylinders have been made using the NASA Langley 13-inch Magnetic Suspension and Balance System. Typical test Mach numbers were in the range 0.04 to 0.2. Drag results are shown to be in broad agreement with previous tests with this configuration. Measurements were repeated with a dummy sting support installed in the wind tunnel. Significant support interferences were found at all test conditions and are quantified. Further comparison is made between interference-free base pressures, obtained using remote telemetry, and sting cavity pressures.

| 17. Key Words (Suggested by Author(s)) | 18. Distribution Statement |
|---|---|
| Ogive-Cylinders<br>Slanted Base<br>Magnetic Suspension | Unclassified-Unlimited<br>Subject Category: 02,09 |

| 19. Security Classif. (of this report) | 20. Security Classif. (of this page) | 21. No. of pages | 22. Price |
|---|---|---|---|
| Unclassified | Unclassified | 76 | A05 |

NASA FORM 1626 OCT 86

For sale by the National Technical Information Service, Springfield, Virginia 22161-2171

NASA-Langley, 1990